

EUROPEAN SPACE AGENCY

ESRIN/Contract No. 18746/05/I-LG



AQUIFEREX

Optical and Radar Campaign

Final Report



DATE: December 11, 2007

GENERAL

Distribution

Organisation	Copies	Name
ESA-ESRIN	1	R. Bianchi
DLR/HR	1	A. Moreira
DLR/HR	1	R. Horn
DLR/HR	1	I. Hajsek
DLR/HR	1	R. Scheiber
LMU/gtco	1	W. Mauser
LMU/gtco	1	N. Oppelt
ITC	1	M. Lubczynsky

Contributing authors

Author	Sections
Rolf Scheiber (DLR-HR)	Introduction / E-SAR Data Processing
Ralf Horn (DLR-HR)	E-SAR Data Acquisition
Natascha Oppelt (gtco, LMU)	AVIS, Ground measurements, GIS
Irena Hajsek (DLR-HR)	Scientific Radar Data Evaluation

Reference Documents

- [1] - *Technical Assistance for the Development of the Airborne Radar & Imaging Spectrometer AQUIFEREX Campaign* – Statement of work, ESA-ESRIN, EOEP-DUEP-EOPS-SW-04-0007, 2005
- [2] - *Technical Assistance for the Development of the Airborne Radar & Imaging Spectrometer AQUIFEREX Campaign* – DLR/gtco Proposal, 2005
- [3] - *Experiment Plan - AQUIFEREX Optical and Radar Campaign*, DLR/gtco/LMU, October, 2005
- [4] – *Data Acquisition Report - AQUIFEREX Optical and Radar Campaign*, DLR/gtco/LMU, December, 2005
- [5] – *Ground Measurement Report- AQUIFEREX Optical and Radar Campaign*, DLR/gtco/LMU, March, 2006

Document Change Control

Verify that this is the correct revision before use. Check the document server for the latest version. Distributed hardcopies of documents are not automatically updated. In case of uncertainty contact the person who released the document or the documentation manager.

Issue	Rev.	Date	Pages	Changes	Status
0	1	25.11.2006	all		draft
0	2	11.05.2007	all	Section 5,6 & 7 updated	open

CONTENTS

1	INTRODUCTION	6
1.1	CONSOLIDATED AQUIFER PROTOTYPE AREAS.....	6
2	AQUIFEREX TEST SITES	7
2.1	TEST SITES OVERVIEW	7
2.2	DETAILED DESCRIPTION OF TEST SITES.....	8
	<i>Test Site Ben Gardane</i>	<i>8</i>
	<i>Test Site Gabes</i>	<i>10</i>
3	DATA ACQUISITION	12
3.1	AIRBORNE DATA SENSORS.....	12
	<i>E-SAR Description.....</i>	<i>12</i>
	<i>AVIS Description.....</i>	<i>14</i>
3.2	GENERAL WEATHER OBSERVATIONS	15
3.3	AIRBORNE DATA ACQUISITIONS	15
	<i>GPS master station installation and positioning</i>	<i>16</i>
	<i>Flight mission planning for test site coverage.....</i>	<i>17</i>
	<i>Ben Gardane</i>	<i>18</i>
	<i>Gabes (first flight)</i>	<i>20</i>
	<i>Gabes (second flight).....</i>	<i>22</i>
3.4	AVIS DATA ACQUISITION DETAILS	23
3.5	GENERAL DESCRIPTION OF GROUND MEASUREMENTS.....	24
	<i>Gravimetric Soil Moisture Measurements.....</i>	<i>24</i>
	<i>Volumetric Soil Moisture Measurements</i>	<i>25</i>
	<i>Field Spectrometer Measurements.....</i>	<i>25</i>
	<i>Vegetation Sampling.....</i>	<i>28</i>
	<i>Leaf Area Measurements</i>	<i>29</i>
	<i>Land Cover Mapping</i>	<i>30</i>
	<i>Soil Roughness Measurements.....</i>	<i>30</i>
3.6	GROUND MEASUREMENTS - BEN GARDANE	31
	<i>Measurement Overview Ben Gardane</i>	<i>31</i>
	<i>Radar reflectors</i>	<i>32</i>
	<i>Contributions of ITC to soil moisture.....</i>	<i>34</i>
	<i>Further contributions of ITC.....</i>	<i>35</i>
3.7	GROUND MEASUREMENTS - GABES	36
	<i>Measurement Schedule Gabes</i>	<i>36</i>

<i>Radar reflectors</i>	37
<i>Contributions of ITC to soil moisture</i>	38
<i>Further contributions of ITC</i>	39
4 DATA PROCESSING	39
4.1 E-SAR DATA PROCESSING	39
<i>E-SAR data processing has been performed as follows:</i>	39
<i>Digital Elevation Models</i>	40
<i>Geocoded Terrain Corrected Data</i>	41
<i>Implementation of Adaptive Receiver Gain Control</i>	42
<i>Radiometric characteristics</i>	43
<i>Repeat-Pass Interferometric Processing</i>	44
4.2 AVIS DATA PROCESSING	46
4.3 VALIDATION OF THE AVIS DATA	47
<i>Validation Using Field Spectrometer Data</i>	47
<i>Validation Using Overlapping Areas</i>	50
4.4 GROUND MEASUREMENTS GIS (ARCGIS)	51
4.4.1 <i>General Information:</i>	53
4.4.2 <i>Image data</i>	53
4.4.3 <i>Ground measurements</i>	54
4.5 GROUND MEASUREMENTS GIS (ARCEXPLORER).....	54
5 SCIENTIFIC RADAR DATA ANALYSIS	55
6 SUMMARY & CONCLUSIONS	75
7 ANNEX 1: AIRBORNE RADAR DATA SUMMARY	78
8 ANNEX 2: AIRBORNE AVIS DATA SUMMARY	82
9 ANNEX 3: SPACEBORNE DATA SUMMARY	83
10 CONTACTS	85

1 INTRODUCTION

1.1 Consolidated Aquifer Prototype Areas

The coarse geographic position of the “AquiferEx” test sites has been already identified within Phase 1 of ESA’s ongoing “Aquifer” project. (for details on “Aquifer” see <http://www2.gaf.de/aquifer>)

Within “Aquifer” project *Areas of Interest* (Aoi) are defined in lullemeden (trans-boundary aquifer between Mali, Niger and Nigeria) and SASS (trans-boundary aquifer between Algeria, Tunisia and Libya). Within these Aoi *Prototype areas* (PA) were identified for the generation of remote sensing based products by “Aquifer” project partners and local service providers. Only within these PA, the selection of test sites for the “AquiferEx” airborne campaign has been considered.

ESA, GAF and DLR have agreed on selecting test sites within the SASS prototype areas due to limitations in budget and better local infrastructure, compared to lullemeden area. The selection of two test sites within two different prototype areas, both in reach from the same airport, determined the choice of Tunisia as the country where the airborne campaign should take place.

As AquiferEx is in support of information product generation based on satellite data, harmonization of satellite data acquisition was performed among Aquifer and AquiferEx project partners to facilitate comparison of information retrieval possibilities for the airborne (high resolution) and space-borne cases. Related spaceborne acquisitions from ENVISAT, ERS, and CHRIS are summarized in the Appendix.

Data acquired by the AquiferEx airborne campaign will be used by the Aquifer project team for the development and validation of the Aquifer science products (e.g. refined land use map). However, first evaluation of radar data with respect to soil moisture and land use/land cover classification is foreseen within this project.

2 AQUIFEREX TEST SITES

2.1 Test Sites Overview

Two test sites have been selected for the airborne AquiferEx campaign. Both are located in Tunisia and are within the Djeffara sub-aquifer of the SASS aquifer (“Système d’Aquiferes du Sahara Septentrional”), which is a trans-boundary aquifer shared by Algeria, Tunisia, and Libya. The test site selection is in accordance with the objectives of the ongoing “Aquifer” project of ESA. Within “Aquifer”, several prototype areas were selected, two of them being located in Tunisia: PA3 Gabes and PA4 Ben Gardane. Within each of them, the precise location of a test-site for “AquiferEx” has been defined. This was an iterative process performed as part of a consolidation meeting in Tunis, July, 2005 by representatives of User’s organisations (OSS and DGRE), Aquifer project responsables (GAF and ESA) as well as DLR. Subsequently, the final AquiferEx test site coordinates were approved by CNT.

Table 2.1: Coordinates (WGS-84) for test site in Ben Gardane PA.

Ben Gardane	degree E	N	decimal E	N
N- Ouest	10° 57' 49.79'	33° 15' 01.29"	10.96383056	33.25035833
N- Est	11° 00' 37.49"	33° 15' 28.47"	11.01041389	33.25790833
S- Est	11° 02' 25.84"	33° 03' 29.02"	11.04051111	33.05806111
S- Ouest	10° 59' 35.64"	33° 03' 04.71"	10.99323333	33.05130833

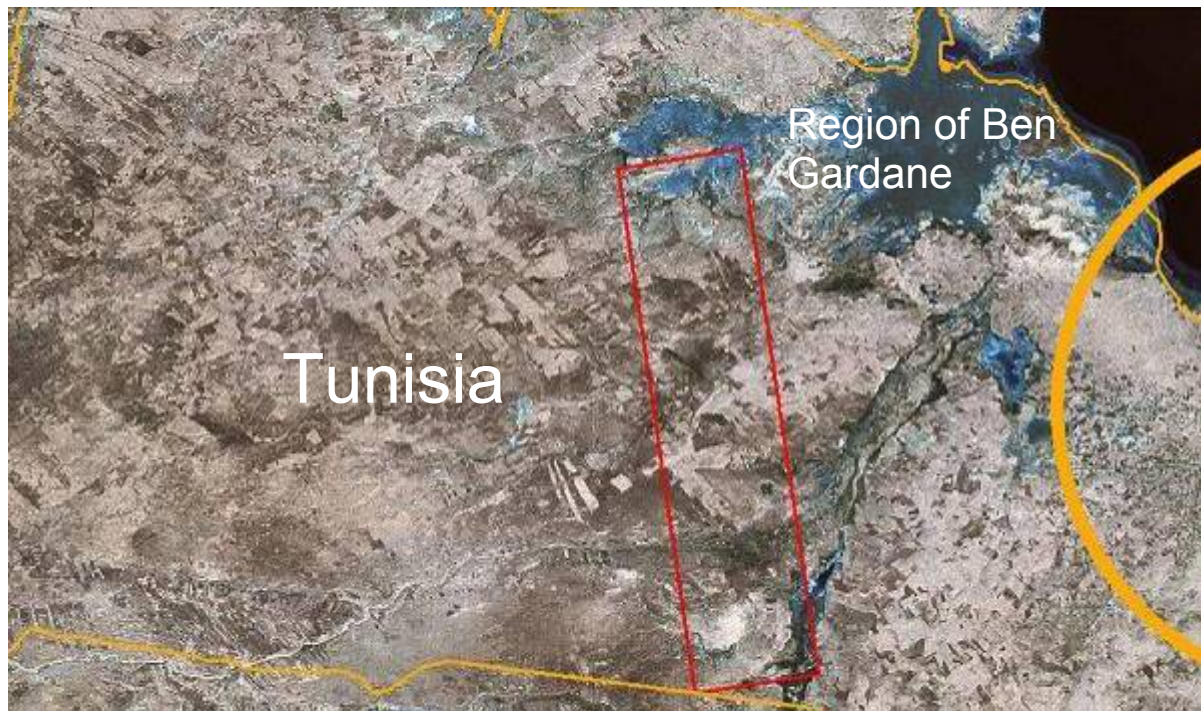


Figure 2-11: Location of Ben Gardane test site on LandsatTM (image provided by Aquifer project GAF/VISTA)

Table 2.2: Coordinates (WGS-84) for test site in Gabes PA.

Gabes	degree E	N	decimal E	N
N- Ouest	09° 51' 12.24"	33° 54' 41.40"	09.8534	33.9115
N- Est	10° 04' 06.24"	33° 57' 42.84"	10.0684	33.9619
S- Est	10° 05' 37.32"	33° 55' 13.44"	10.0937	33.9204
S- Ouest	09° 52' 55.56"	33° 52' 28.20"	09.8821	33.8745

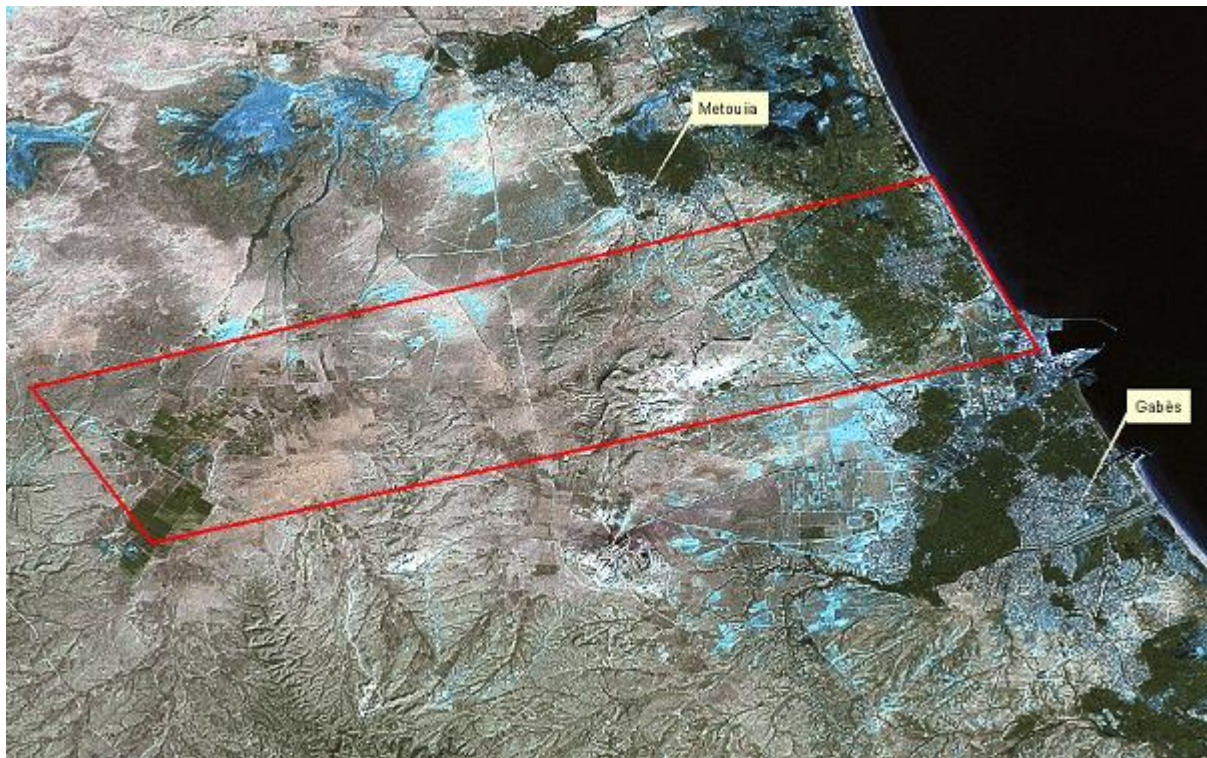


Figure 2.2: Location of Gabes test site on LandsatTM (image provided by Aquifer project GAF/VISTA)

The coordinates are given in Table 2.1 and 2.2. They are also marked in Figure 2.2 and Fig. 2.3. The basis is LandsatTM data from 1999.

2.2 Detailed Description of Test Sites

Information provided in this section is based on a pre-campaign test site visit performed by DLR/gtc representatives in Tunisia by end of August 2005. During the visit, different locations have been visited based on the Landsat maps provided by "Aquifer" project. For documentation purposes photographs and GPS measurements were taken.

Test Site Ben Gardane

Important characteristics and facilities for the planning of the ground truth activities for Ben Gardane test site are summarized below.

- ◇ Ben Gardane is a very representative example for the south Tunisian environment!

- ◇ The size of the area of Ben Gardane is about 50 000 ha. It can be roughly divided into 4 parts:
 - N: Salt lake and saline soil area, no cultivation of crops
 - Centre N: Saline, no crops, olive tree plantings
 - Centre S: Episodic river, trees and shrub land along dry river bed, eventually small plots of cereals along river
 - S: Mainly pasture
- ◇ If there is enough precipitation during summer and autumn about 27 000 ha are cultivated in November (21 000 ha barley, 6 000 ha wheat)
- ◇ The major problem in this region is that the sea water is invading into the aquifer



Soil covered with salt

erosion. In the last decades a lot of effort was undertaken to cope with that problem: Trees were planted and walls were made up of stone and soil to prevent aeolian soil transport (see also photograph).

- ◇ The heavy wind erosion, the high salinity of the ground water and therefore of the soil in combination with the low precipitation leads to desertification.
- ◇ There is only one road in this area and only few unsealed roads. Ground truth measurements are nearly impossible in the northern part near the salt lake.
- ◇ Dominant soil type is sand. Gypsum occurs overall the area as well as clay. Stony!
- ◇ Sand blocking vegetation leads to hilly patches overall the area. Waste deposits overall the area (see photographs)!
- ◇ Areas in the central part are vegetated with olive tree plantings, during winter cereals might be cultivated between the trees.

(the sahelian aquifer extends over Tunisia, Algeria and Libya; this aquifer was used to be under high pressure so sea water could not invade. During the last decades the pressure within the aquifer was reduced due to massive extraction of ground water for industrial and agricultural purposes leading to an invasion of salty sea water into the ground water). A salt lake borders the test site in the north. The ground water level falls from 3m in the south to 7m in the north. The static layer is near the surface. The average content of salt in the ground water can be rated at 5-6 g/l.

- ◇ Another problem in Ben Gardane is wind



II Wall for the protection against aeolian erosion



Irrigation practice: Water is pumped from wells via channels into the field plots



Plantings of pimento



Pimento plant

- ◇ Field plots 2-3 m x 20 m
- ◇ Alfalfa is patchy even when tall, different phenological stages of the plots
- ◇ Between fields some small apple trees can be found, many wild bushes with different sizes (see photograph)



Patchy structure of alfalfa



Alfalfa fields with wild vegetation

3 DATA ACQUISITION

In the frame of the AquiferEx-project the data acquisition campaign was performed in southern Tunisia in the time period November, 7 to 14. 2005. Successful measurement flights were conducted over Ben Gardane test site on November, 9 and over Gabés area on November, 11 and 12. In parallel a variety of ground measurements were performed on both test sites.

The objective of the proposed “AquiferEx” project is to build up a data base of multi-frequency and multi-polarisation radar (SAR) data as well as hyperspectral data suitable for the development and validation of science products to be performed by the project team of ESA’s “Aquifer” project and supposed to meet the user needs related to water management in African countries.

This section summarizes all data acquisitions performed during this campaign and gives a first assessment on data quality. All the details on the performed AquiferEx data acquisition can be found in the AquiferEx Data Acquisition Report.

3.1 Airborne Data Sensors

E-SAR Description

DLR-HR operates the experimental multi-frequency, multi-polarisation Synthetic Aperture Radar (SAR) system E-SAR onboard a Do228 aircraft (Figure 2.1). E-SAR features across track SAR interferometry capabilities at X-band (VV polarisation). Single channel operation in X-band with VV and HH polarisations switched from pass to pass. The E-SAR C-band acquires data either in single channel mode (VV, HH polarisations, pass to pass) or in dual-channel mode with combinations of VV/VH and HH/HV polarisations switched from pass to pass. Fully polarimetric data acquisition is possible in L- and P-bands only. The SAR processing ground segment, adapted to E-SAR data at DLR-HR, includes operational modules for DEM generation and geo-coding amongst others. The data products fulfil high quality standards in terms of calibration and geometric accuracy. Aircraft navigation and SAR motion compensation are based on a modern combined DGPS/INS system. Thus the sensor is positioned with highest precision.

The aircraft Do 228 is operated by DLR’s Flight Facility Oberpfaffenhofen (DLR-FB). DLR-FB is contributing full maintenance of the aircraft, pilots and aircraft engineers. The standard aircrew consists of pilot-in-command, co-pilot and aircraft engineer. The mission team is completed by two E-SAR radar engineers (one of them having the responsibility for the technical execution of any E-SAR data acquisition flight) and one AVIS operator (responsible for the AVIS operation).



Figure 3-1: DLR's DO228, the E-SAR operation platform

Tab. 3.1: E-SAR Technical Parameters

RF-Band	X-Band	C-Band	L-Band	P-Band
RF-centre frequency	9.6 GHz	5.3 GHz	1.3 GHz	350 MHz
Transmit peak power	2.5 kW	750 W	400 W	1000 W
Receiver noise figure	4.0 dB	4.0 dB	8.5 dB	6.0 dB
Antenna gain	17.5 dB	17 dB	15 dB	10 dB
Azimuth beamwidth	17°	17°	18°	30°
Elevation beamwidth	30°	33°	35°	40°
Antenna Polarisation	H and V	H and V	H and V	H and V
Aquisition Mode	single pol	dual pol	quad pol.	quad pol.
IF-centre frequency	300 MHz	300 MHz	300 MHz	300 MHz
Max. Signal bandwidth	100 MHz	100 MHz	100 MHz	100 MHz

AVIS Description

The AVIS sensor is the hyperspectral sensor to be operated for the AquiferEx project. The prototype of AVIS (Airborne Visible / near Infrared imaging Spectrometer) was designed and built in 1998 at the chair for geography and remote sensing of the University of Munich (LMU). The concept of AVIS was the development of a cost-effective system for environmental monitoring purposes. Currently the second and third generation of this system - AVIS-2 and AVIS-3 – are being operated. For AquiferEx the AVIS-2 sensor was operated due to better SNR performance.

AVIS-2 consists of the following components:

Camera Unit:

Camera (Vosskühler C1020)

Spectrograph (Im Inspector V9enhanced)

Lens (Schneider Cinegon)

Navigation and Storage Unit:

PC

14bit Frame-Grabber (Matrox)

differential GPS (AfuSoft Raven)

Inertial Navigation System (IMAR GmbH)

Standard-Camera Mount

AVIS-2 is a push broom scanner that operates in the visible and near infrared spectral domain with a number of 64 bands.

A photograph of AVIS-2, which is given in Figure 2.2, points up the compactness of the system. The system was developed mainly for the application on small aircrafts such as Do-27 or Piper. AVIS-2 can also be operated on an ultra-light aircraft. Therefore the concept is directed to a manageable size and weight (see Table 3.2). The implementation of an inertial navigation system enables the geo-rectification of data acquired on platforms which are relatively unstable such as small aircrafts.



Figure 3-2: Photograph of AVIS-2. The sensor unit is on the left and the storage unit on the right hand side.

Table 3.2: AVIS-2 parameters

The specifications of AVIS-2 are as follows:

Number of bands	64
Spectral range [nm]	480 – 880
Spectral resolution [nm]	9
Radiometric resolution [bit]	14
Spatial resolution [m]	6 (altitude 3000m above ground)
FOV [rad]/ aperture angle [°]	1.1 / 56
IFOV [mrad]	2.2
Weight camera unit (kg)	30
Weight PC unit (kg)	20
Size camera unit [cm]	56 x 44 x 18
Size PC unit [cm]	56 x 44 x 18

The AVIS system is currently configured to fit the camera mount of a Do-27 aircraft or an ultra-light. Therefore it was necessary to construct a new frame to fit the sensor into the Do-228 camera mount. This modification process was completed successfully and a first test flight with AVIS-2 was performed on October, 24, 2005.

The data acquisition process was performed by an additional operator on board. It was planned very carefully in order to assure a proper configuration of AVIS and an optimal interplay with the DLR sensor equipment.

3.2 General Weather Observations

The time window for the data acquisition campaign in southern Tunisia was scheduled in the “rainy” season to allow the mapping of developing agricultural crops in semi-arid areas. However, good weather conditions were a pre-condition to perform successful flight with the AVIS sensor. In this sense, the AquiferEx campaign was lucky as rain events took place only 2-3 days prior to the first measurement flight and in the night between the second and third flight.

Local weather observations are summarised in a table below, to later allow interpretation of airborne data. Temperature range was in the order of 25-30 deg during daytime and around 15 deg during night.

Date	Observation
Sunday, November 6	Strong rainfalls (on Djerba airport but also in the test-sites). Some rain water pools could still be seen three days after.
Monday, November 7	Some clouds, mostly sunny, no rain
Tuesday, November 8	Sunny, no clouds
Wednesday, November 9 (flight at Ben Gardane)	Sunny, few cirrus clouds above flight level
Thursday, November 10	Sunny, no clouds
Friday, November 11 (flight 1 at Gabes)	10:00 AM: mostly sunny at clear sky. Some altostratus patches. Cumulus from northern horizon approaching the test-site.
Saturday, November 12 (flight 2 at Gabes)	4:00-5:00 AM: strong rain in the coast (Gabes oasis area, eastern part of testsite). In the western part only some rain drops for 2-3 minutes. 11:00 AM: additional rainfalls in the eastern part; no rain in the west. Rain limit is mountain area in the centre of the test site. 2:00 PM: partly sunny; 40-60% cloudy

3.3 Airborne Data acquisitions

The AQUIFEREX data acquisition flights took place in Tunisia in the period from November 9 to November 11, 2005. In parallel to the flights the GPS master receiver station was set up and operated by DLR-HR on the premises of the Djerba airport with the permission of the airport authority.

The following tasks were carried out by and with participation of the aircrew (DLR-FB, DLR-HR, GTCO):

- November 8, 2005: Briefing. Preparation of the measurement flights at the airport. Functional check of E-SAR and AVIS. Selection of GPS master receiver station location and system check.
- November 9, 2005: First measurement flight overhead Ben Gardane. Operation of the GPS station. E-SAR data transcription for Survey processing. GPS and IMU data pre-processing. AVIS data check.
- November 10, 2005: Operation of the GPS station parallel to the work in the field near Gabes. Survey processing of the radar data.
- November 11, 2005: Second measurement flight overhead Gabes. Operation of the GPS station. E-SAR data transcription for Survey processing. Survey processing of the radar data. GPS and IMU data pre-processing. AVIS data check.
- November 12, 2005: Additional third measurement flight overhead Gabes. Operation of the GPS station. E-SAR data transcription for Survey processing. Survey processing of the radar data. Acquisition of GPS reference data of the EUREF station 'LAMP' on Lampedusa. Static DGPS processing of CR and GPS master station positions. Kinematic DGPS and IMU data processing. AVIS data check.
- November 13, 2005: Preparation of the material to be send by airfreight. De-briefing.

GPS master station installation and positioning

The GPS master station named 'DTTJ' was set up on the premises of Djerba airport close to the DLR aircraft between the general aviation parking area and the runway. The distance was approx. 20m north of the plane. The two photographs (Figure 2.1) show the DLR GPS station of type Ashtech (Thales) Z-Surveyor.



Figure 3-3: The DLR GPS master station on Djerba airport premises

The geographical position of the phase centre of the GPS antenna was measured with respect to the position of the EUREF GPS reference station 'LAMP' which is located on the island Lampedusa at a distance of 246km. The result was cross-checked with data of the IGS station 'NOT1' which is located in the City of Noto on Sicily. The reference data was obtained via internet. The static DGPS processing was carried out using Waypoint's GrafNet software.

Project: REF_DTTJ_09112005
 Program: GrafNet Version 7.50.2117
 Profile: Geographic
 Source: Traverse

Datum: WGS84, (processing datum)
 Control IDs: LAMP

Station	Latitude (+/-D M S)	Longitude (+/-D M S)	H-Ellipsoide (m)
DTTJ	N 33 52 28.88465	E 10 46 29.61185	40.118
LAMP (Reference)	N 35 29 59.17200	E 12 36 20.37600	57.789

Flight mission planning for test site coverage

For the selected test sites the following E-SAR and AVIS operations as listed in Table 3.1 below shall be performed.

Table 3.1: Sensor operations to be performed

E-SAR			
Pol-InSAR	L-band	2 passes	quad pol. (master & slave)
InSAR	X-band	1 pass	single pol. (vv)
PolSAR	C-band	2 passes	dual pol. (hh & hv, vv & vh)
AVIS			
		2 passes	ascending
		1 pass	descending

A total number of 5x4 passes is required for each test site. For L-band 2 passes are considered to allow for Pol-InSAR evaluation, for C-band also two passes are chosen to acquire the full set of available polarisations, but without interferometric observables. In X-band one polarisation amplitude image can be obtained in VV along with a high resolution digital elevation model (DEM) from single pass SAR interferometry. The repeat pass baselines for L-band are chosen correspondingly to the expected crop height on ground. For Gabés test site the baselines are 20m for the northern strip and 60m for the southern strip. If time permits, a second baseline (third pass) should be flown (20m for southern and 60m for northern strip). For Ben Gardane test-site the baseline should be 0m.

Because the complete area to be covered is larger than the radar and hyperspectral swath, a flight strategy as shown in Figure 3.4 is adopted.

AVIS Swaths of 2.8 x 20 km each (50 deg at 3000 m)

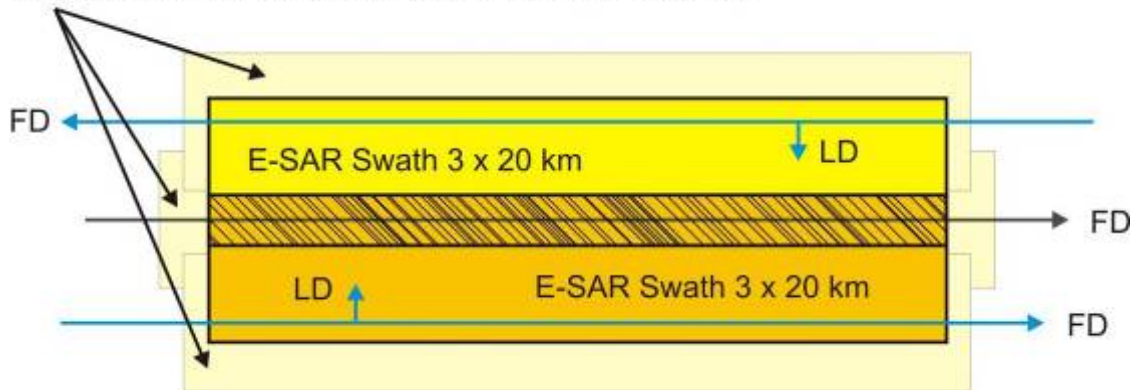


Figure 3-4 Coverage of a test site by E-SAR and AVIS

E-SAR covers a swath of 3 x 20km² in one pass. For an area of 5 x 20km² two passes have to be flown such that the individual ground swaths overlap by about 1km. Due to overall flight time limitations in a single flight carried out under IFR the data have to be acquired with opposite look directions (LD).

The AVIS coverage is 2.8 x 20km² (50deg aperture, altitude 3000m above ground). To cover the area of 5 x 20km² three passes are required. The individual swaths overlap by 30%.

Area covered with E-SAR: 5 x 20km² (2 swaths, overlap ~1km)
 Coverage with AVIS: 6.8 x 20km² (3 swaths, overlap ~0.8km)

Ben Gardane

Date of flight: 09.11.2005

System start-up: 10:32h (UTC)

System shut-down: 13:51h (UTC)

Table 2.3: Airborne data takes overhead area 'Ben Gardane' (all times UTC)

Pass	Line	Sensor	Mode	Hdg [°]	Time (start) [hh:mm]	Time (stop) [hh:mm]
A	11	AVIS		172	11:07	11:13
B	(-)12	AVIS		352	11:20	11:26
C	10	AVIS		172	11:31	11:37
1	7	E-SAR	C-vh/vv	352	11:43	11:48
2	4	E-SAR	C-vh/vv	172	11:54	11:59
3	7	E-SAR	C-hv/hh	352	12:10	12:15
4	4	E-SAR	C-hv/hh	172	12:22	12:27
5	7	E-SAR	L-pm (master)	352	12:32	12:36
6	4	E-SAR	L-pm (master)	172	12:41	12:45
7	7	E-SAR	L-pm (0m base)	352	12:51	12:55
8	4	E-SAR	L-pm (0m base)	172	13:00	13:04
9	3	E-SAR	X-vv-xti (full base)	352	13:11	13:15
10	6	E-SAR	X-vv-xti (full base)	172	13:20	13:25

Flight altitude: 10000ft GALT (GPS altitude, fixed), corresponding to FL95!

Two flight levels were blocked: FL90 and FL100. The available flight time was just sufficient to complete the nominal measurement programme. The optional L-band repeat pass data set could not be obtained!

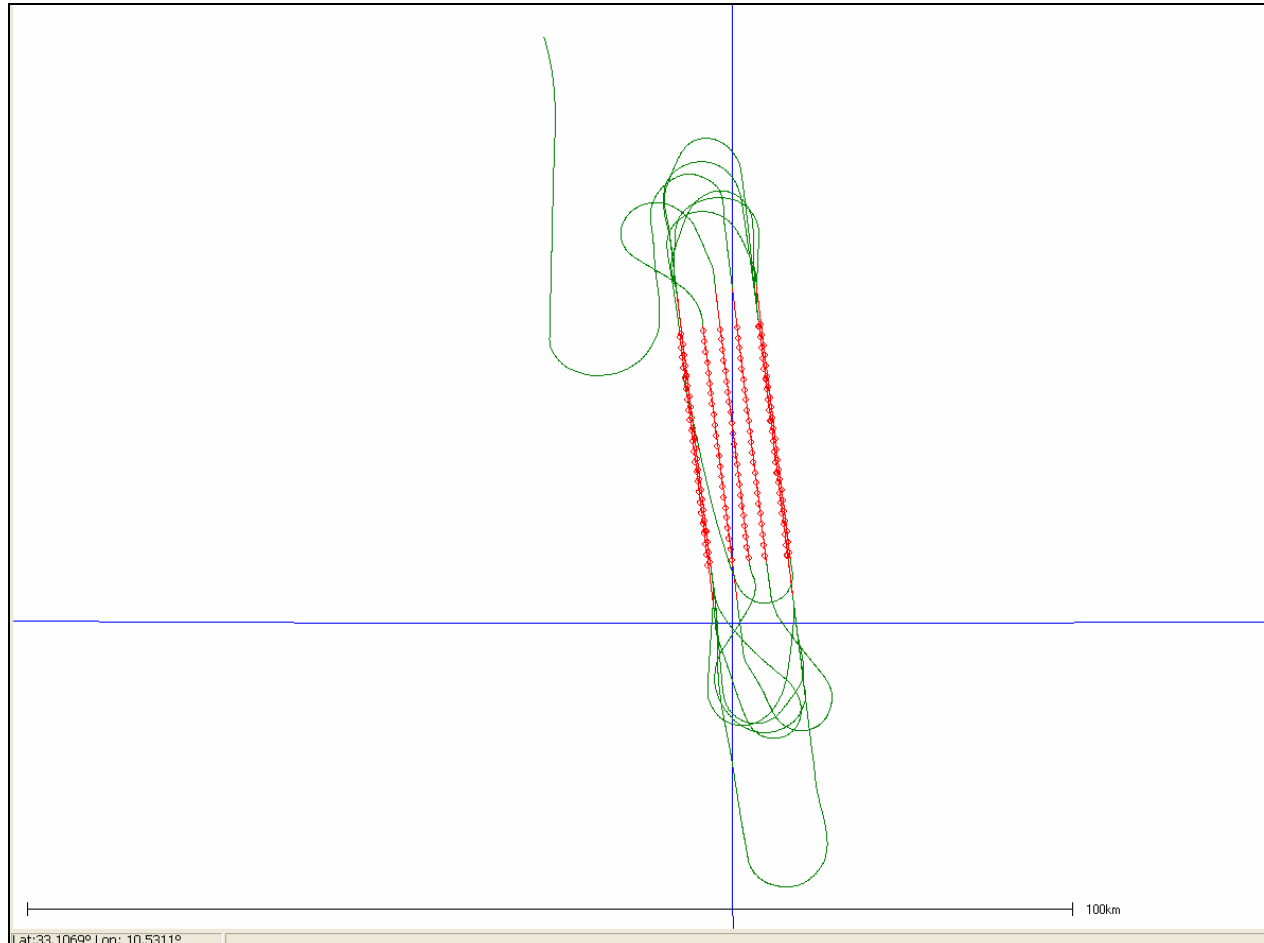


Figure 3-5: Actual flight pattern during data acquisition overhead area 'Ben Gardane'

Observations:

The flight was under supervision by ATC in Tunis. The lacking radar control and an inexperienced air traffic controller caused delays in flight in the order of 10 to 15 minutes in total. The weather conditions were very good during AVIS operation. A few cirrus clouds above flight level and some haze below were observed. Later during radar data acquisition cumulus clouds developed below flight level. Weather conditions are known of the weather station in Djerba (listed below). For the atmospheric correction of the AVIS data radiosonde data will be requested from Lampedusa.

Weather conditions during AVIS acquisition as measured in Djerba (data source: www.wetter.com)

Nov 9	11:00 (Time UTC)	11:30 (Time UTC)
Temperature [°C]	23.8	24.0
Pressure [hPa]	1023.2	1022.8
Rel. Humidity [%]	54	50
Visibility [km]	10	10

Low radar backscatter signal levels were observed at all wavelengths during flight which are caused by the dry and overall very homogeneous land surface. Data quality in cross-pol channels may be affected!

Gabes (first flight)

Date of flight: 11.11.2005

System start-up: 09:53h (UTC)

System shut-down: 12:59h (UTC)

Table 2.4: Airborne data takes overhead area 'Gabes' (all times UTC)

Pass	Line	Sensor	Mode	Hdg [°]	Time (start) [hh:mm]	Time (stop) [hh:mm]
A	(-)12	AVIS		74	10:32	10:37
B	11	AVIS		254	10:43	10:48
C	(-)10	AVIS		74	10:55	11:00
1	4	E-SAR	C-vh/vv	254	11:06	11:10
2	8	E-SAR	C-vh/vv	74	11:15	11:20
3	4	E-SAR	C-vh/vv	254	11:25	11:29
4	8	E-SAR	C-hv/hh	74	11:34	11:38
5	4	E-SAR	C-hv/hh	254	11:43	11:48
6	8	E-SAR	L-pm (Master)	74	11:53	11:58
7	4	E-SAR	L-pm (Master)	254	12:03	12:07
8	9	E-SAR	L-pm (60m base)	74	12:12	12:16
9	5	E-SAR	L-pm (15m base)	254	12:22	12:26
10	8	E-SAR	L-pm (Master)	74	12:31	12:35

Flight altitude: 10700ft GALT (FL100, barometric), according to ATC requirements for the area!

The available flight time was not sufficient to complete the nominal measurement programme. The acquisition in mode X-xti had to be cancelled because of lacking flight time! The strong variation in radar backscatter levels along track required repeated overpasses in C- and L-bands!

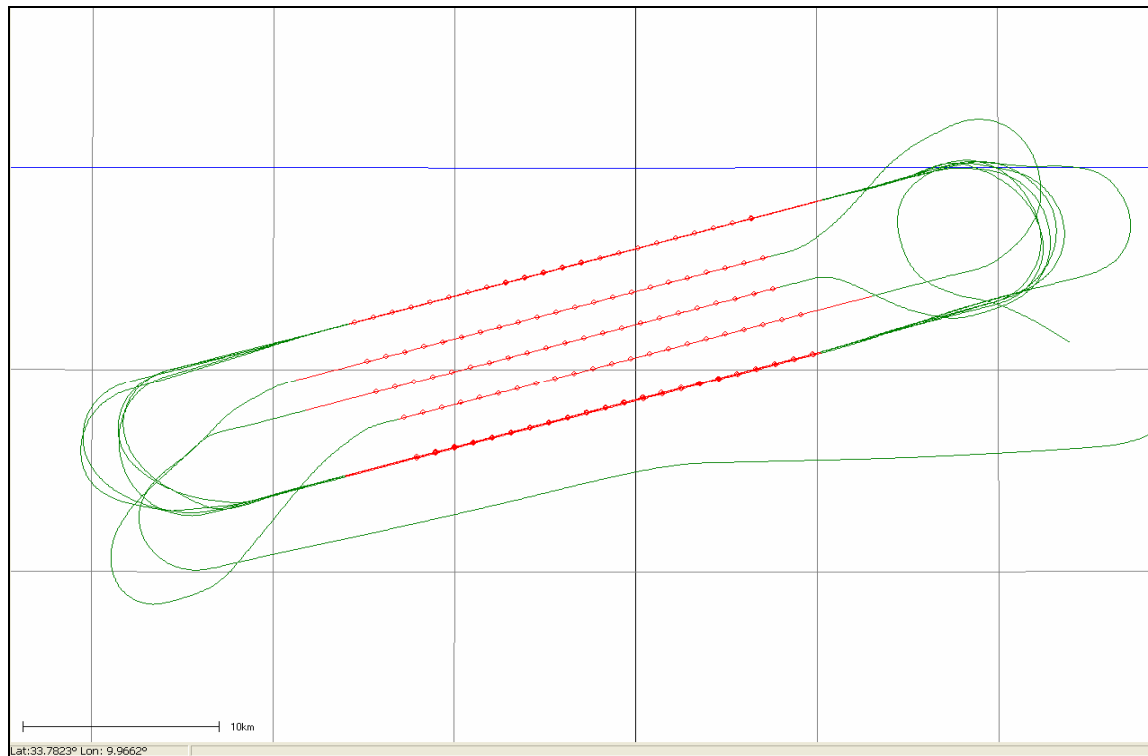


Figure 3-6: Actual flight pattern during data acquisition overhead area 'Gabes' on Nov-11, 2005

Observations:

The flight was under supervision by ATC in Tunis. No delays due to ATC intervention occurred. The weather conditions during AVIS operation were not optimum. Cumulus clouds (2/8 coverage) below flight level caused shadows in the test area. About 20% of the AVIS data is affected by clouds. Later during radar data acquisition the cumulus partly developed to cumulus nimbus and caused light turbulence locally.

Weather conditions during AVIS acquisition as measured in Djerba (data source: www.wetter.com)

Nov 11	10:30 (Time UTC)	11:00 (Time UTC)
Temperature [°C]	24.3	24.5
Pressure [hPa]	1025.8	1025.5
Rel. Humidity [%]	60	59
Visibility [km]	15	15

A strong variation in radar backscatter signal levels was observed at all wavelengths during flight which was caused by various types of land cover (urban area, oasis, agriculture, desert, mountainous area) along track. Data quality may be affected locally by saturation or by low signal levels! To obtain best possible data quality overpasses were repeated! Radar receiver gain setting had to be changed along track at waypoints. The settings were registered in the flight protocol sheet for offline adjustment during SAR processing!

Pass 1, C-vh/vv, probably has poor quality due to the variation of backscatter levels and not optimum setting of receiver gain. Pass 5, C-hv/hh, suffers from saturation over urban area near the coast. Pass 6, L-pm, probably suffers from low signal levels along the first quarter of track 8. The measurement was repeated with Pass 10. Passes 6 and 10 may also be considered as 0m baseline pair for Pol-InSAR!

Gabes (second flight)

Date of flight: 12.11.2005

System start-up: 12:46h (UTC)

System shut-down: 15:04h (UTC)

Table 2.5: Airborne data takes overhead area 'Gabes' (all times UTC)

Pass	Line	Sensor	Mode	Hdg [°]	Time (start) [hh:mm]	Time (stop) [hh:mm]
1	7	E-SAR	X-vv-xti (full base)	254	13:31	13:35
2	3	E-SAR	X-vv-xti (full base)	74	13:41	13:46
3	7	E-SAR	X-vv-xti (full base)	254	13:51	13:56
A	10	AVIS		74	14:03	14:08
4	4	E-SAR	C-hv/hh	254	14:15	14:20
5	8	E-SAR	L-pm (master)	74	14:25	14:30
6	4	E-SAR	L-pm (master)	254	14:35	14:39
7	14	E-SAR	L-pm (15m base)	74	14:44	14:48

Flight altitude: 10465ft GALT (FL100, barometric), according to ATC requirements for the area!

The flight was not foreseen originally, but due to the difficulties the day before required to complete the measurement programme for the area 'Gabes'. The missing X-xti data were acquired plus extra passes in L- and C-bands for reason of detecting and analysing changes in the area during 24 hours. The duration of the flight was limited by the local weather situation. A heavy cumulus nimbus developed in the test area!

Observations:

The flight was under supervision by ATC in Tunis. The beginning of the measurements got delayed by approx. 10 – 15 min because of the air traffic controllers in Tunis not being informed in time about this third flight by the CAA. The CAA had given DLR the permission to fly earlier.

The weather conditions during AVIS operation again were not optimum. Cumulus clouds (3-4/8 coverage) below flight level caused shadows in the test area. Only the central line was flown to fill gaps in the data. During radar data acquisition in L- and C-bands after the AVIS pass a heavy cumulus nimbus had developed in the east part of the area which caused extreme local turbulence. This forced DLR to stop the operation in the area and return to Djerba.

Weather conditions during AVIS acquisition as measured in Djerba (data source: www.wetter.com)

Nov 12	14:00 (Time UTC)
Temperature [°C]	22.4
Pressure [hPa]	1018.2
Rel. Humidity [%]	68
Visibility [km]	8

Again the radar receiver gain setting had to be changed along track at waypoints. The settings were registered in the flight protocol sheet for offline adjustment during SAR processing! It turned out that X-band showed less variation in signal level as anticipated.

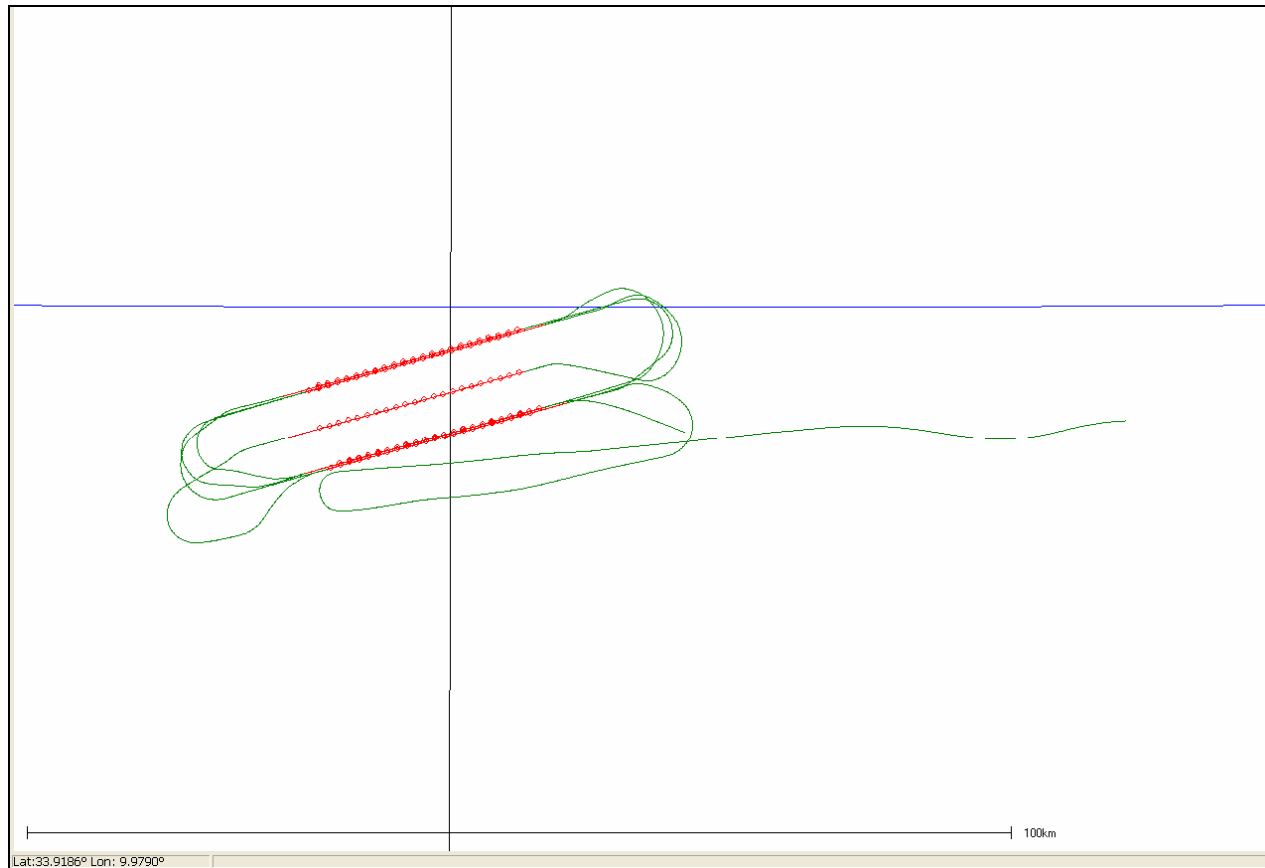


Figure 3-7: Actual flight pattern during data acquisition overhead area 'Gabés' on Nov-12, 2005

3.4 AVIS data acquisition details

AVIS-2 images were acquired on three dates, November 9, 11 and 12. Due to different weather and illumination conditions at the different dates, the integration time was changed to enable the highest possible signal to noise ratio (SNR) while preventing saturation (see *Table 3.2*). The SNR of the system at flight conditions is calculated according to Equation 1.

$$SNR = \frac{(DN_{saturation} - DN_{dark})}{\sigma_{dark}} \quad \text{Equation 3-1}$$

where DN = digital number and σ_{dark} = standard deviation of the dark current image.

Table 3.2: Flight conditions and AVIS settings at acquisitions during AquiferEx campaign

AVIS image stripe	Date [dd.mm.yyyy]	Aircraft speed [m/sec]	Cloud coverage [x/8]	Integration time [ms]	SNR [dB] at 550 nm
Ben Gardane 1	09.11.2005	80	0	18	64.0

Ben Gardane 2	09.11.2005	80	0	18	64.0
Ben Gardane 3	09.11.2005	80	0	18	64.0
Gabes 1	11.11.2005	80	2	26	65.5
Gabes 2	11.11.2005	80	2	26	65.5
Gabes 3	11.11.2005	80	2	26	65.5
Gabes 4	12.11.2005	75	4	32	65.5

The spatial resolution of airborne imagery can be different along an image line (across track) and along the movement of the aircraft (along track). Therefore both resolutions have to be calculated separately. The former is determined by the instantaneous field of view (IFOV) of the system and its altitude, the resulting spatial resolution on ground can be calculated according to Equation 2. The latter is determined by the sampling rate (SR) and the speed of the aircraft (v) (see Equation 3). The resulting spatial resolutions are shown in

$$R_{(across\ track)} = IFOV_{acrosstrack} \cdot h \quad \text{Equation 3.2}$$

$$R_{(along\ track)} = IFOV_{alongtrack} \cdot h \quad \text{Equation 1.3}$$

Table 3.1: Spatial resolutions and resampling of AVIS data

AVIS image stripe	Sampling rate [images/sec]	Altitude [m above ground]	Spatial resolution along track [m]	Spatial resolution across track [m]	Resampling [m]
Ben Gardane 1	16	3000	6	4.711	6
Ben Gardane 2	16	3000	6	4.711	6
Ben Gardane 3	16	3000	6	4.711	6
Gabes 1	16	3200	6.4	4.992	6
Gabes 2	16	3200	6.4	4.992	6
Gabes 3	16	3200	6.4	4.992	6
Gabes 4	16	3120	6.2	4.875	6

3.5 General Description of Ground Measurements

Gravimetric Soil Moisture Measurements

In total 41 and 39 gravimetric soil samplings were taken in the Ben Gardane and Gabes region respectively. The measurements were carried out during a time frame from 10 am to 2 pm (MEZ).

Measurement procedure

The gravimetric soil sampling was conducted using sample rings (Eijkelkamp) with a diameter of 53mm and a height of 40mm. The resulting soil samplings therefore are integral measurements for a soil volume of $V = r^2 \cdot \pi \cdot h = 88.25 \cdot 10^3 \text{ mm}^3$.

Most gravimetric measurements were conducted in 2 soil layers (0-4cm and 4-8cm). In the southernmost part of the test site Ben Gardane 3 layers (up to 12cm) were measured at two locations (water pool). Digital photographs were taken at the sampling locations. The soil samples were gathered using the sample rings which were placed in a cutting shoe to both

avoid any loosing of material and ensure the same volume of material to be measured. The soil material for every sampling was decanted into coated foil bags, labelled and stored. Thus any loss of material and water was prohibited and the number of samples could be increased.

The samples were brought to the lab, weighted, dried for approx. 24 hours at max. 105° C and were then weighted again. The water content (*wc*) in percent was calculated using Equation 4.

$$WC = \frac{(weight_{wet} - weight_{dry})}{(weight_{wet} - weight_{foilbag})} \cdot 100 \quad \text{Equation 3.2}$$

Volumetric Soil Moisture Measurements



Figure 3-8 TDR probe used for AquiferEx campaign

In total 75 volumetric measurements were conducted at 25 measurement points between 10 am and 2 pm in the test site Ben Gardane (MEZ).

In the test site Gabes a sum of 339 measurements was conducted at 113 different locations. 64 locations were measured at Nov 11 and 49 at Nov 12.

Measurement procedure

The volumetric soil moisture was measured using three TRIME FM 2-rod reflectance probes (see **Fehler! Verweisquelle konnte nicht gefunden werden.**). The rods with a length of 110mm are positioned at a distance of 20mm. The resolution of the TDR's is $\pm 2\text{vol}\%$ providing homogeneous, not swelling or shrinking soils. The effective penetration depth of the probe is about 15cm with the highest sensitivity in the immediate vicinity of the access tube. The sensitivity decreases exponentially with distance (TRIME FM User Manual)

To ensure the best performance, the basic alignment of the probes was carried out daily with the calibration set and special calibration sand.

To enable a higher representation three measurements were conducted at each sampling point by rotating the probe after each measurement. Three measurements were carried out providing means and standard deviations. If the soil was dense or hard auger probes were used to enable TDR measurements.

The measurements were conducted at bare soil and under different types of vegetation. No measurements were conducted in the southern part of the test site Ben Gardane because of the high salinity of the soils in this part of the test area that would have distorted the measurement.

Field Spectrometer Measurements

Field spectrometer measurements were carried out using a combination of OceanOptics instruments (www.oceanoptics.com). Three spectrometers with consecutive but overlapping ranges of sensitivity and different technical specifications were combined to produce a continuous reflectance spectrum from 440 to 1700 nanometres. The current setup reads as follows:

Table 2: Technical description of the detectors of the field spectrometer

Instrument	Detector	Lower Limit	Upper Limit	Bit depth	Sampling Rate
SD-2000 (Master)	Silicon	440nm	920nm	12-bit (Dynamic Range = 0 - 4096)	0.28-0.39nm
SD-2000 (Slave)	Silicon	510nm	980nm	12-bit (Dynamic Range = 0 - 4096)	0.27-0.38nm
NIR-512 (Master)	Indium-Gallium-Arsenide	870nm	1720nm	16-bit (Dynamic Range = 0 - 65536)	1.71-1.73nm

The radiation which is reflected by the target is gathered through a trifurcated optical fibre, equipped with three different inner diameters (also from OceanOptics), thus providing adjusted shares of energy as required by each detector. In the same time the design of the fibre makes sure that each detector is sampling the same target.

A panel of spektalon[®] supposed to reflect >98% of the incoming radiation between 350 and 1800nm was used as “white” reference.

According to the experiment plan, field spectrometer measurements were conducted at several locations within a time frame between 10am and 2pm (MEZ). In total 5 and 8 sampling points were measured in Ben Gardane and Gabes respectively.

Measurement procedure

Each measurement is performed following a strict procedure that is supposed to be the same for every target. After the tripod is placed near the location that is going to be measured, a dark current measurement is performed by completely closing the aperture of the optical fibre. After the dark current measurement the reference panel is put into the view of the probe. Now the incoming radiation with all its characteristics, determined by the travel of the sunlight through the atmosphere, is measured. When the dark current and the reference spectrum are taken, the target is measured. This process (dark-reference-target) has to be repeated for every measurement due to the fact that system noise is highly correlated with the operating temperature of the system and also because atmospheric conditions can change very rapidly in the field.

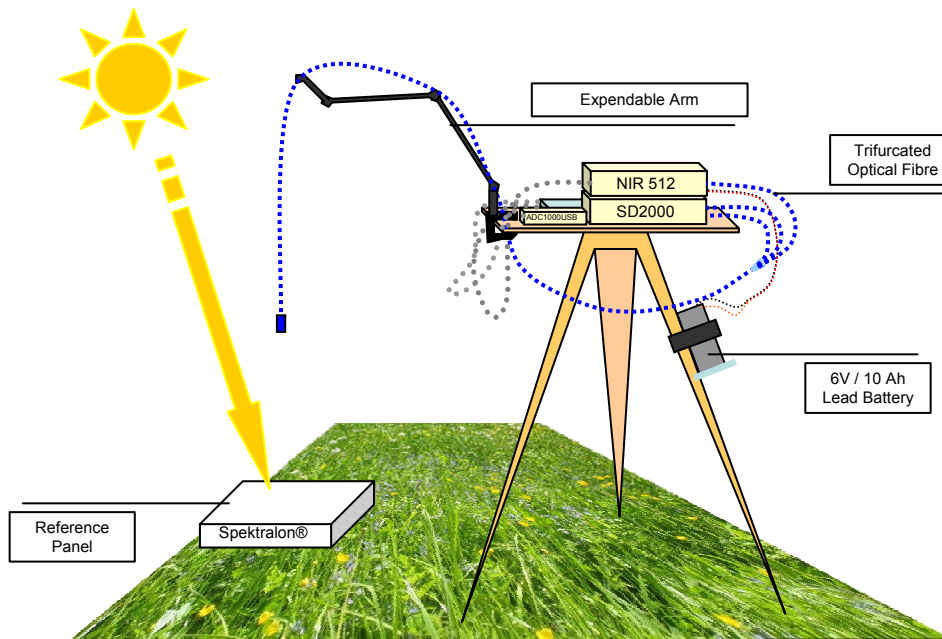


Figure 3-9 Field spectrometer measurements

Every target should be measured more than once to calculate an average reflectance spectrum with respect to the inhomogeneous surface.

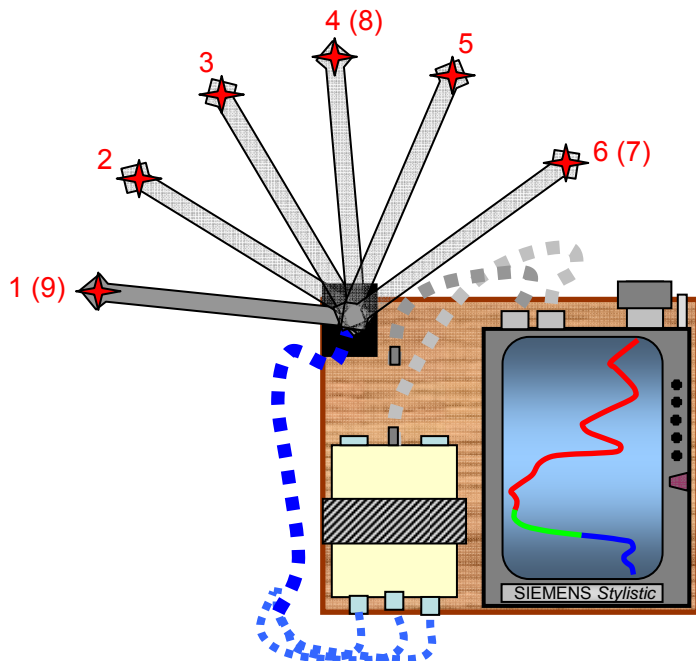


Figure 3 -10: Field spectrometer sampling pattern

Each measurement cycle would include six samples that should be taken in nearly a semi-circle shifting the position of the expendable arm from left to right. If possible three additional

samples should be stored while shifting the arm back to its home position (see [Figure 3 -10](#)). 50 single measurements were averaged to one spectrum for each position. The final result of each sampling point is the average of all the samples taken during the way through the pattern that provide enough quality to be used.

A perfect scenario would include nine times 50 spectra to be averaged for the final result. Real environmental conditions such as wind or changes in the atmosphere can easily disturb the measurement, so that often not all the samples provide reliable data and some of them had to be excluded.

A reflectance spectrum is calculated for each detector by comparing the signature of the incoming radiation with the signal caused by the reflection of the target, with respect to the electric noise of the system after the following equation.

$$\text{reflection}[\%] = \frac{(\text{Sample} - \text{DarkCurrent})}{(\text{reference} - \text{DarkCurrent})} \cdot 0.01 \quad \text{Equation 3.3}$$

Examples of field spectra are given in section 3.4.

Vegetation Sampling

No vegetation sampling was conducted at Ben Gardane due to the lack of cereals and/or vegetation with full soil coverage in the measurement areas.

Three vegetation samplings were measured in the test site Gabes. One carrot field as well as two fields of alfalfa (densely and sparse vegetated) were investigated. The vegetation sampling was not time critical, therefore the samples were taken the day before overflight.

Measurement procedure

One plot of 1/4m² was harvested at each field. This relatively small sampling area was due to the very small field sizes. A cardboard model resembling precisely a quarter of square metre was inserted at a randomly chosen section of the vegetation patch in question. All biomass encircled by the cardboard was cut and neatly removed. The removed biomass was separated into stem and leaf and packaged in a special plastic film that would be able to resist to the temperatures in the drying oven, while in the meantime would prevent the samples from losing water on their way to the laboratory.

Plant height was determined in two levels using folding rules. Therefore a set of about ten measurements was averaged for the leaf and for the sprout level.

Plant phenology was determined using the BBCH code (FederalBiologicalInstitute-FederalBureauOfSpecies-CHemicalIndustry) that classifies the growth stage of different crops into a decimal code from 0 (sowing) to 99 (ripeness, harvested). Phenological descriptions specially adapted for root and stem vegetables were used to classify the carrot measurement. For the alfalfa measurements a different code ranging from 0 (early vegetative) to 9 (ripe seed pod) had to be applied since alfalfa belongs to the category of nitrogen fixing plants. The codes for the estimation of the phenological stages are attached in Annex 1.

After the samples had been transported to the laboratory, the wet weight was determined by means of a laboratory scale. The samples then were inserted into a drying oven running at 105° C. After 24 hours of drying time the samples were removed from the oven and weighed again on the laboratory scale.

The wet weight was determined for each sample according to Equation 6).

$$WetWeight[kg / m^2] = \frac{WetSampleWeight[g] - FoilWeight[g] \cdot 4}{1000} \quad \text{Equation 3.4}$$

The dry weight was determined by Equation 7:

$$DryWeight[kg / m^2] = \frac{DrySampleWeight[g] - FoilWeight[g] \cdot 4}{1000} \quad \text{Equation 3.5}$$

The water content was calculated using Equation 8.

$$WaterContent[\%] = 100 - \left(\frac{WetWeight[kg / m^2] - DryWeight[kg / m^2]}{WetWeight[kg / m^2] \cdot 0.01} \right) \quad \text{Equation 3.6}$$

Leaf Area Measurements

No vegetation sampling was conducted at Ben Gardane due to the lack of cereals and/or vegetation with full soil coverage in the measurement areas. According to that no LAI measurements were carried out.

Four different land cover types were measured in the test site Gabes. For each sampling point four measurements were conducted. In the protocol both mean and standard deviation are listed. Two sampling points were measured in one field leading to a sum of eight sampling points.

Leaf area measurements are not time critical, therefore the measurements were carried out at Nov. 10 and 12 in the afternoon.

Measurement procedure

The Leaf Area measurements were carried out using a LI-COR LAI 2000 instrument. The measurements itself have to be conducted under diffuse light conditions. Therefore the measurements were conducted at dawn or dusk, while under clouded sky the measurements can also be done during the day.

The measuring technique combines a measurement of sky brightness above the canopy with measurements beneath the canopy while the sensor is viewing skywards. In practice, four below measurements are taken to achieve a suitable spatial average for the corresponding sampling point. To exclude the effect of the operator and the shadow he is casting during the measurements, the LAI-2000 was operated using the 180° azimuth view. Below and above canopy measurements were carried out at the same height with the same azimuth direction.

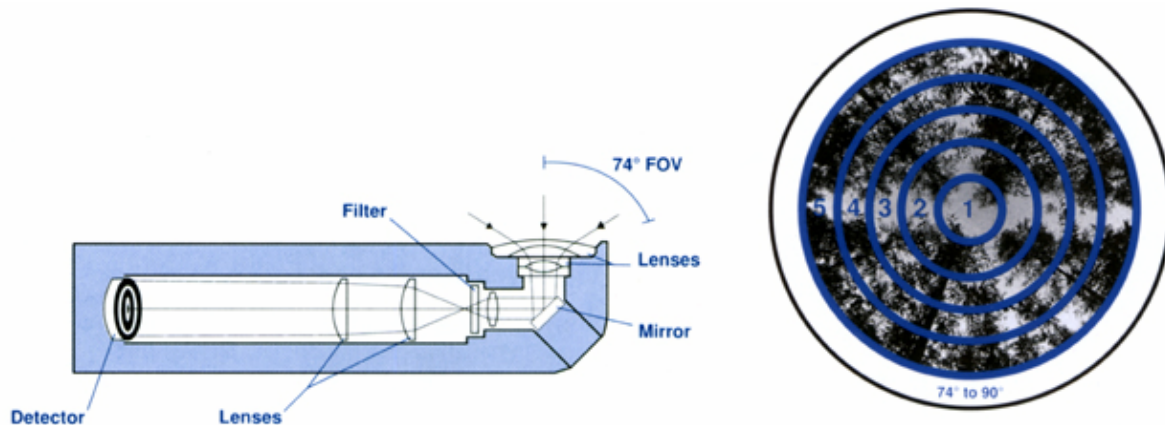


Figure 3-11: Principle of LAI-2000 measurements with five silicon detectors, each corresponding to a different set of zenith angles

The LAI-2000 measurements are based on measurements of gap fraction at five zenith angles. The data that have to be supplied are the path lengths of view through the canopy at those five angles (see **Fehler! Verweisquelle konnte nicht gefunden werden.**). Therefore the LAI-2000 sensor has five concentric rings that make up a field of view extending from zenith (0°) to near the horizon (74°). If the sensor is viewing the sky, the 0° -detector is measuring the brightness straight overhead, while the 5th detector is measuring the brightness of a ring centred at 68° subtending 13° . Five values of canopy transmittance are calculated from these readings by dividing corresponding below and above pairs. From transmittance at all five zenith angles the LAI is calculated as output (for more details it is referred to LI-COR Biosciences, LAI-2000 Plant Canopy Analyzer, Operating Manual, Lincoln, USA, 1992).

The resulting LAI values are means and standard deviations of one measurement cycle (one above and four below canopy).

Land Cover Mapping

Land cover mapping was achieved for different locations at Ben Gardane and Gabes. The land use protocols provide calibration and validation data for the land cover classification. The land cover mapping is not time critical, therefore it was done both the day before the ESAR/AVIS data acquisition and in the morning/evening of the overflight.

Measurement procedure

The land cover mapping included a photographic documentation combined with a GPS positioning of the mapped area. The position of the mapping team member was pinpointed by GPS measurements (GARMIN GPS eTreck Venture). From this position photographs were taken in 4 different azimuth angles (normally north, east, south and west). The corresponding land cover was described for each photograph.

Soil Roughness Measurements

In total eleven measurements at six locations were carried out using a stereo photography technique in the test site Ben Gardane. Twelve measurements were conducted at five locations in Gabes.

The soil roughness was derived from vertical stereo photography. Stereo-pairs were acquired in two different heights (140 and 175 cm above ground), except for two sampling points where only one height was measured.

Measurement procedure

The photographs were recorded with a digital camera (Olympus: Model C-7070). In order to take vertical stereo photos from the soil, an iron T-shaped bar mounted on a tripod was used (see Fehler! Verweisquelle konnte nicht gefunden werden.).

To avoid errors due to different interior orientations of diverse camera types, only one camera was used. The pairs of shots were taken in two different heights. One with the camera mounted face downward on the right and one looking directly down from the left end of the T-bar, using the width of the rack as a base line. The images are oriented parallel and/or rectangular to the flight direction of ESAR.

The photographs were processed with software called LPS (the Leica Photogrammetry Suite Version 8.7). A digital terrain model was calculated for a part the overlapping range of the stereo pair undisturbed by mounting gear or folding rule. The method is based on correlation and cross-correlation techniques, a procedure that requires a dependable set of ground control points. The relative height of the resulting DTM corresponds to the parallax displacement. The triangulation accuracy is given by a RMS value (RMS Tri in the GIS). The resulting digital terrain model was calculated to meet a ground resolution of 0.3 cm. The root mean square of the DTM corresponds to the soil roughness of a defined area (80 x 50 cm) of the ground.

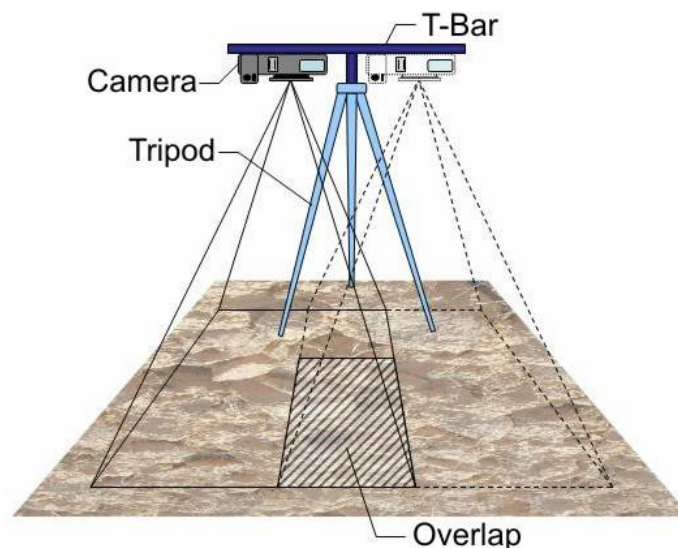


Figure 3-12: Experimental setup for soil roughness measurements

3.6 Ground Measurements - Ben Gardane

Measurement Overview Ben Gardane

The time critical measurements were conducted within a time frame between 10 am and 2 pm of the date of overflight. The land cover mapping was carried out the day before overflight as well as outside the time window of the E-SAR/AVIS acquisition day.

Time	Spectra-team	LAI-team	Soil-team	DLR-team	ITC-team
Team members	gtco + guide	gtco + guide	gtco + DLR + guide	dlr + DLR + guide	ITC + TUDelft +guide
Day before	Survey of test site/sampling points, Land cover mapping, Corner				
8:30-10:00	Land cover	Land cover	Land cover	Corner & GPS	Sap flow/moisture
10:00-12:00	Spectrometer	Moisture	Roughness	Moisture	Sap flow/moisture
12:00-14:00	Spectrometer	Moisture	Roughness	Moisture	Moisture
14:00-15:00	Spectrometer	Land cover	Laboratory	Moisture	Sap flow/moisture
15:00-16:00	Laboratory	Land cover	Laboratory	Moisture	Sap flow/moisture
16:00-17:00	Laboratory	Land cover	Laboratory	Corner & GPS	Sap flow/moisture
Day after			Laboratory		Laboratory

Measurements points for and borders of Ben Gardane test site are visualized in the following GPS-map.

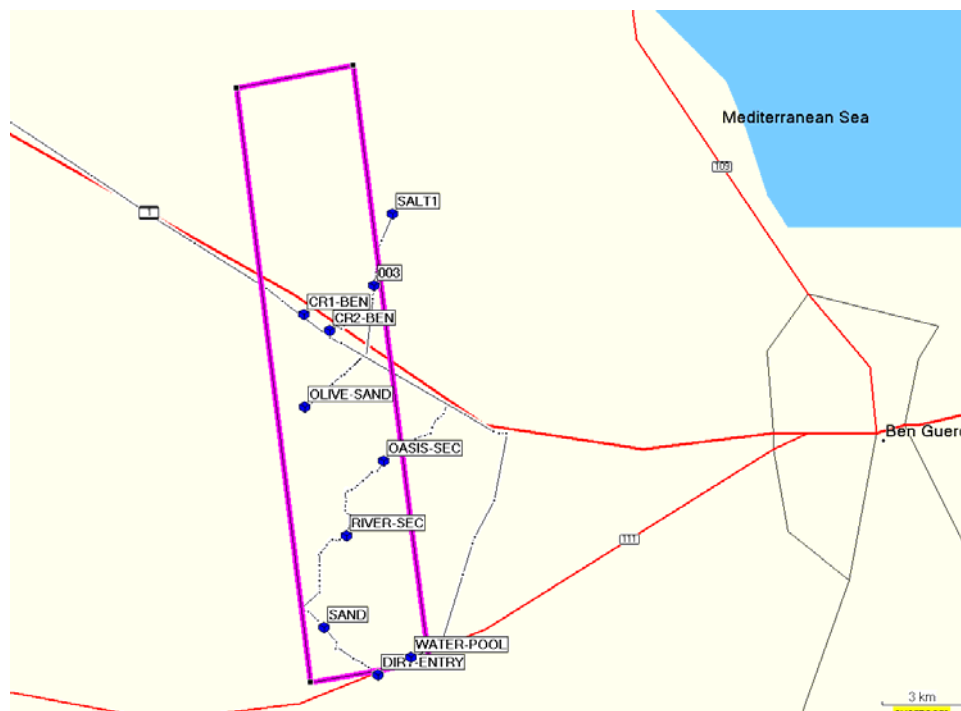


Figure 3-13: GPS waypoints 'Ben Gardane' for orientation and allocation of ground measurements

Radar reflectors

The swath wide of the E-SAR sensor is approximately 3km. Two passes are necessary to cover the whole test site of 5km width. Due to flight time limitations the data is recorded with opposite look directions. Therefore for the two look directions separate radar reflectors (corner reflectors) had to be installed. For each swath two radar reflectors were mounted, one at each border of the swath. Since the center of the test area is in the overlap of the two swaths, two corner reflectors with opposite look directions could be positioned there at the same spot. Therefore it was possible to get by with three

corner reflector spots CR1-BEN, CR2-BEN, and CR3-BEN, which reduced the effort to guard the reflectors during the mission. The foldable corner reflectors have an edge length of 90cm. Extensions to 150cm edge length were mounted to the corner reflectors in the centre of the test area.



Figure 3-14: Radar reflector locations in the Ben Gardane test site (LandsatTM image provided by Aquifer project GAF/VISTA)



Figure 3-15: Radar reflector at location CR2-BEN

Name	Location	Size	Azimuth	Elevation (Spirit level)	Direction of sight	Position Latitude	Position Longitude
BE11	CR1-BEN	90cm	352°	5°	82°	33° 10,926' N	10° 58,704' E
BE12	CR2-BEN	150cm	352°	20°	82°	33° 10,168' N	11° 00,168' E
BE21	CR2-BEN	150cm	172°	20°	262°	33° 10,263' N	11° 00,228' E
BE22	CR3-BEN	90cm	172°	5°	262°	33° 09,369' N	11° 01,245' E

Table 3.1: Radar reflector installation data for the Ben Gardane test site. Size: edge length from centre corner to vertex. Azimuth: parallel to flight direction. Elevation: inclination of the base plate. Direction of sight: line of sight of the reflector. Position: approximate position (WGS84)

All positions of the radar reflectors were measured with high precision using a geodetic GPS system. For the best possible position accuracy, the positions of two other GPS stations were used to create a network: The official Lampedusa GPS station and a second GPS receiver from DLR which was operated at Djerba airport.

During the measurement flights the network of three GPS stations was also used for differential GPS measurements of the aircraft position. Therefore the GPS receiver in the field was placed at a reference point for the complete mission duration.

The record interval of the GPS receivers was 10s for the measurements of the radar reflector positions and 0.5s at the reference point.

Name	Location	Position Latitude	Position Longitude
BE01	CR2-BEN	33° 10,232' N	11° 00,195' E

Table 3.2: GPS reference station in the Ben Gardane test site. Position: approximate position (WGS84)

Contributions of ITC to soil moisture

19 gravimetric soil moisture probes were taken by ITC-team.

Volumetric moisture measurements were taken at 68 points using hydra-probes (65 points on a transect in olive plantation with spacing of 20-25 m and 3 in high salinity part in the southern part of the test-site, see Fig. 3.6 and 3.7). Every value is the average of three readings within the foot print of the GPR (see below).

Every record of the hydra-probe has the following parameters:

- Volumetric soil moisture
- Temperature
- Salinity

In addition hydra-probe logging was also performed. Every record has the same previously mentioned parameters. The measurements were taken every half an hour from

- November the 8th 17:00 GMT until
- 17:00 GMT of November the 9th

Ground penetrating radar (GPR) measurements were also taken at the same locations from a height of some tens of centimetres. The GPR data were acquired at 301 operating frequencies in the frequency range 800-2500 MHz (frequency step of about 5.67 MHz). However, only the range from 902-2092 MHz will be considered for analyzing the data (higher quality and information content of the data in that range). Derived entities are surface dielectric permittivity and correlated water content:

Measurements were taken on:

- (1) 68 geo-referenced points on soil,
- (2) 2 points on the road
- (3) 3 points on the concrete platform.

For each GPR measurement on soil, one gravimetric sample has been taken and 3 Hydro-probe measurements were performed in the antenna footprint. The purpose of the GPR measurements is to bridge the scale gap between the ground truth measurements and the airborne and spaceborne measurements.



Figure 3.6: Location of ITC measurements within Gabes test site (marked in black on LandsatTM image)

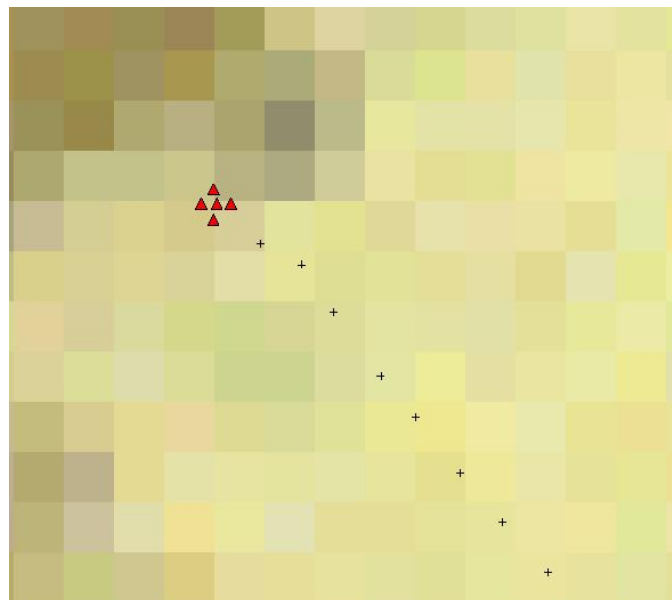


Figure 3.7: Experiment Setup for GPR measurements (up). Zoom of Landsat Image with indications of measurements points (down)

Further contributions of ITC

In addition to soil moisture probing also measurements on olive trees have been performed. In particular

24 hours of automatic records of sap flow velocities in olive trees with Thermal Dissipation Probes have been recorded at a logging interval of 30min. This was achieved by increment borer sampling of tree stems.

In addition TDR/GPR measurements in tree stems for investigation of conductive xylem area and trunk electromagnetic properties were also performed.

3.7 Ground Measurements - Gabes

Measurement Schedule Gabes

ESAR/AVIS data were acquired on 11th and 12th November respectively. Therefore time critical measurements have been carried out twice.

Time	Spectra-team	LAI-team	Soil-team	DLR-team	ITC-team
Team members	gtco + guide	gtco + guide	gtco + guide	DLR + guide	ITC + TUDelft +guide
Day before	Survey of test site/sampling points & Vegetation sampling, LAI, corner				
7:30-8:30		LAI		Corner & GPS	
8:30-10:00	Land cover	Land cover	Corner	Corner & GPS	Sap flow/moisture
10:00-12:00	Spectrometer	Moisture	Soil roughness	Moisture	Sap flow/moisture
12:00-14:00	Spectrometer	Moisture	Soil roughness	Moisture	Moisture
14:00-15:00	Laboratory	Land cover	Soil roughness	Moisture	Sap flow/moisture
15:00-16:00	Laboratory	Land cover	Laboratory	Moisture	Sap flow/moisture
16:00-17:00	Laboratory	Land cover	Laboratory	Corner & GPS	Sap flow/moisture
Day after					
8:30-10:00	Land cover	Land cover	Land cover	Corner & GPS	Moisture
10:00-12:00	Spectrometer	Moisture	Roughness	Moisture	Moisture
12:00-14:00	Spectrometer	Moisture	Roughness	Moisture	Moisture
14:00-15:00	Laboratory	LAI	Laboratory	Moisture	Moisture
15:00-16:00	Laboratory		Laboratory	Corner & GPS	Laboratory

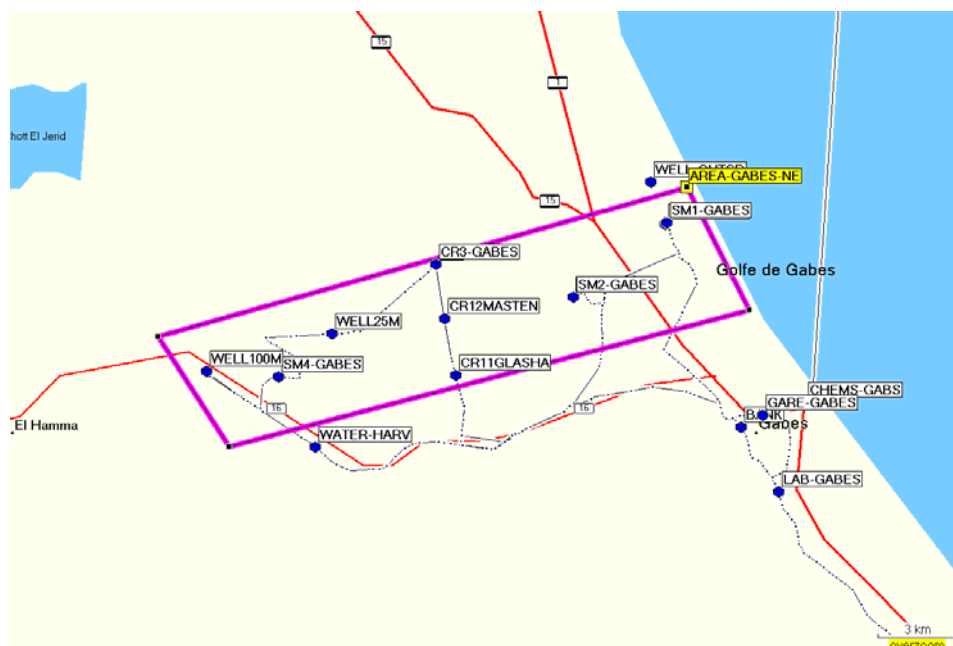
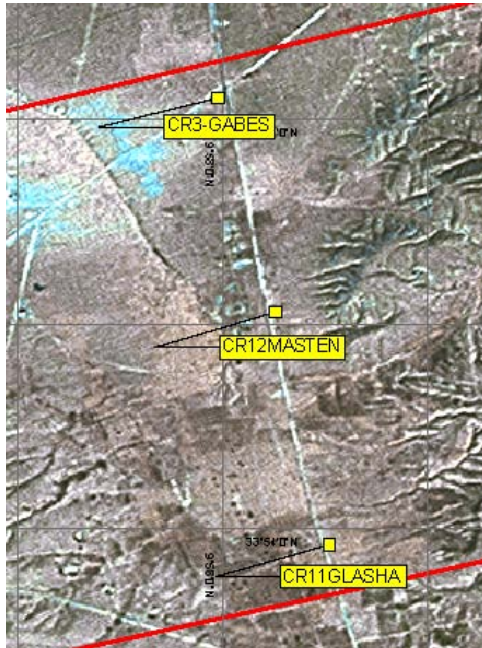


Figure 3-16: GPS waypoints ‘Gabes’ for orientation and allocation of ground measurements

Radar reflectors



The placement of the radar reflectors was similar as at the Ben Gardane test site, except that at the centre of the test area one 90cm reflector and one 150cm reflector was placed. The reason for this was that in each swath two reflectors of similar size are visible.

The two reflectors at CR12MASTEN were installed on 10.11.2005, the day before the flight. Additionally the second 150cm reflector was assembled at CR12Masten. The reflectors were guarded during the night. At the next day the 150cm reflector was brought to CR11GLASHA and installed there. At CR3-GABES the fourth reflector was placed.

Since another flight was planned for the next day, the 150cm reflector was brought back to CR12MASTEN in the evening where it and the other two reflectors were guarded another night.

Figure 3-17: Radar reflector locations in the Gabes test site (LandsatTM image provided by Aquifer project GAF/VISTA)

Name	Location	Size	Azimuth	Elevation (Spirit level)	Direction of sight	Position Latitude	Position Longitude
GA11	CR11GLASHA	150cm	254°	5°	344°	33° 53,950' N	9° 58,479' E
GA12	CR12MASTEN	150cm	254°	20°	344°	33° 55,080' N	9° 58,136' E
GA21	CR12MASTEN	90cm	74°	20°	164°	33° 55,090' N	9° 58,098' E
GA22	CR3-GABES	90cm	74°	5°	164°	33° 56,138' N	9° 58,013' E

Table 3.3: Radar reflector installation data for the Gabes test site. Size: edge length from center corner to vertex. Azimuth: parallel to flight direction. Elevation: inclination of the base plate. Direction of sight: line of sight of the reflector. Position: approximate position (WGS84)

Since there were two flight days at the Gabes test site, there had to be two reference point measurements. There is no need that the same spot is used so the GPS system was placed at the most suitable place. At 11.11.2005 this was at CR11GLASHA, at 12.11.2005 at CR12MASTEN.

As at the Ben Gardane test site, the record interval of the GPS receivers was 10s for the measurements of the radar reflector positions and 0.5s at the reference point.

Name	Location	Position Latitude	Position Longitude
GA01	CR11GLASHA	33° 53,940' N	9° 58,484' E
GA02	CR12MASTEN	33° 55,070' N	9° 58,132' E

Table 3.4: GPS reference station at the Gabès test site. Position: approximate position (WGS84)

Contributions of ITC to soil moisture

A total of 36 Gravimetric soil moisture samples were taken by ITC-team during first Gabes flight (November, 11). Volumetric moisture measurements were taken at the same 36 points using hydra-probes. Every value is the average of three readings within the foot print of the GPR (see below). Measurements were taken in 17 nearby plots (different moisture conditions due to irrigation practice), 1-4 measurements per plot (see Figure 3.13).

Every record of the hydra-probe has the following parameters:

- Volumetric soil moisture
- Temperature
- Salinity

In addition hydra-probe logging was also performed for short time. Every record has the same previously mentioned parameters. The measurements were taken every half an hour from

- November the 11th 10:00 GMT until 13:30 GMT of same day

GPR measurements of surface dielectric permittivity and correlated water content were taken in the irrigated perimeter: 36 geo-referenced points on soil. For each GPR measurement, one gravimetric sample has been taken and 3 Hydro-probe measurements were performed in the antenna footprint.

On second Gabès flight (November, 12) 73 hydra probe samples for volumetric soil moisture were taken on the locations indicated in Figure 3.14.



Figure 3-18: Location of ITC measurements within Gabes test site (marked on LandsatTM image). First Gabès flight on

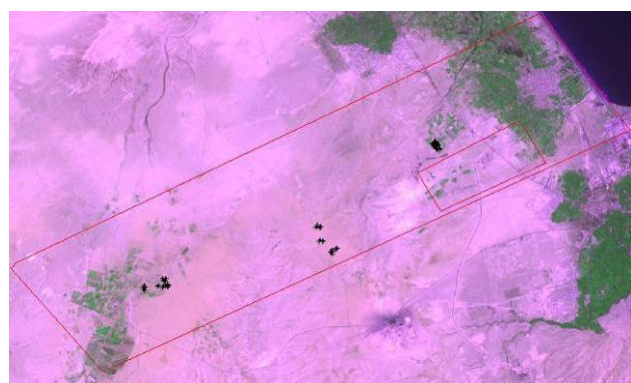


Figure 3-19: Location of ITC measurements within Gabès test site (marked on LandsatTM image). Second Gabes flight on November, 12.

November, 11.

Further contributions of ITC

Also in Gabes area TDR/GPR measurements in tree stems/canopies for investigation of conductive xylem area have been and trunk electromagnetic properties. Increment borer sampling of tree stems has been performed. These measurements were taken only during first Gabes flight on November, 11.

4 DATA PROCESSING

This sections describes the adopted processing strategy for AquiferEx data and provides examples for both test sites.

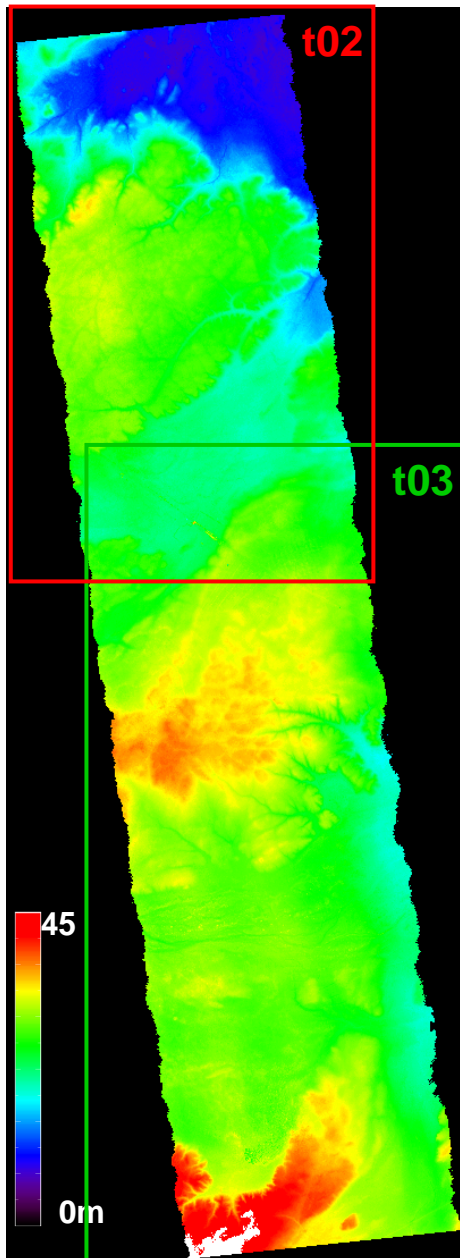
4.1 E-SAR data processing

E-SAR data processing has been performed as follows:

- Navigation data processing:
 - kinematic differential GPS processing, using reference station described in section 2
 - fusion of inertial and GPS data using AeroControl SW.
- precise Corner reflector position estimation
- DEM generation as mosaic of 2 swaths
- DEM segmentation for input to geocoding

For each segment of 10-15km length the radar data were focussed and geocoded on a 2m grid (UTM-zone32 projection on WGS-84 ellipsoid). The azimuth resolution of the radar data was set to 4m (4.5m in L-band) @ 5 effective looks. Slant range resolution is 2m corresponding to 2.5 to 4m on ground.

In addition repeat-pass interferometric processing has been performed for the parallel L-band tracks. This includes residual motion compensation, co-registration of master and slaves, as well as interferometric phase and coherence estimates. For the first GABES flight one repeat-pass interferometric C-band product has been generated in addition (only for the south-west segment), to provide a quasi-simultaneous quad-pol product.



Digital Elevation Models

Digital elevation models were computed from the single-pass SAR interferometry performed by the E-SAR X-band system.

Ben Gardane

The mosaic of the two swaths for Ben Gardane test site is shown in Fig. 3.1. Total size is 4.8km by 20 km. The two swaths are overlapping in far range. The relative accuracy in the overlapping area has been evaluated to +/- 2m. Absolute height accuracy is ensured by tiepointing to a Corner reflector.

As shown in Fig. 3.1 the DEM of Ben Gardane test site is segmented into a Northern and Southern part. Corner reflectors are located in the overlapping area. The two DEM segments were used for geocoding.

Gabès

The DEM for Gabès is shown in Fig. 3.2. Total size is 4.8km by 20 km. The two swaths are overlapping in far range. The relative accuracy in the overlapping area has been evaluated to +/- 2m. Absolute height accuracy is ensured by tiepointing to a Corner reflector.

As shown in Fig. 3.2 the DEM of Gabès test site is segmented into a Western and Eastern part. Corner reflectors are located in the overlapping area. The two DEM segments were used for geocoding.

The “t02” and “t03” relate to the last part of the radar data filename.

Figure 4.1: DEM of Ben Gardane test site

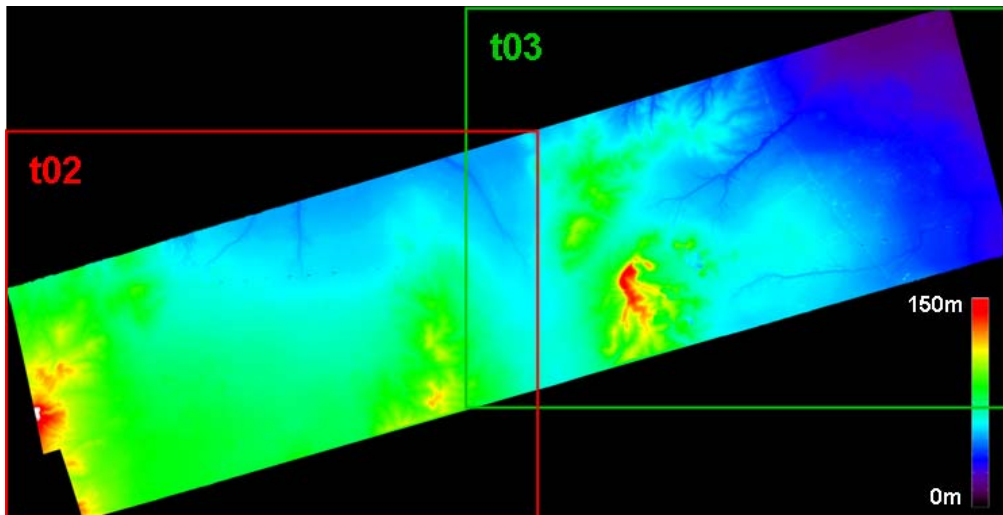


Figure 4.2: DEM of Gabès test site

Geocoded Terrain Corrected Data

The DEMs computed from the E-SAR data were used to generate geocoded terrain corrected (GTC) for each processed image data set. Each E-SAR flight strips was split into 2 overlapping segments to become more manageable. Opposite looking and overlapping images of the two flight directions were geocoded onto the same DEM-grid (see t02 and t03 rectangles in Fig. 4.1. and 4.2.)

For each image the associated incidence angle map is also provided to be used for radiometric compensation of incidence angle effects.

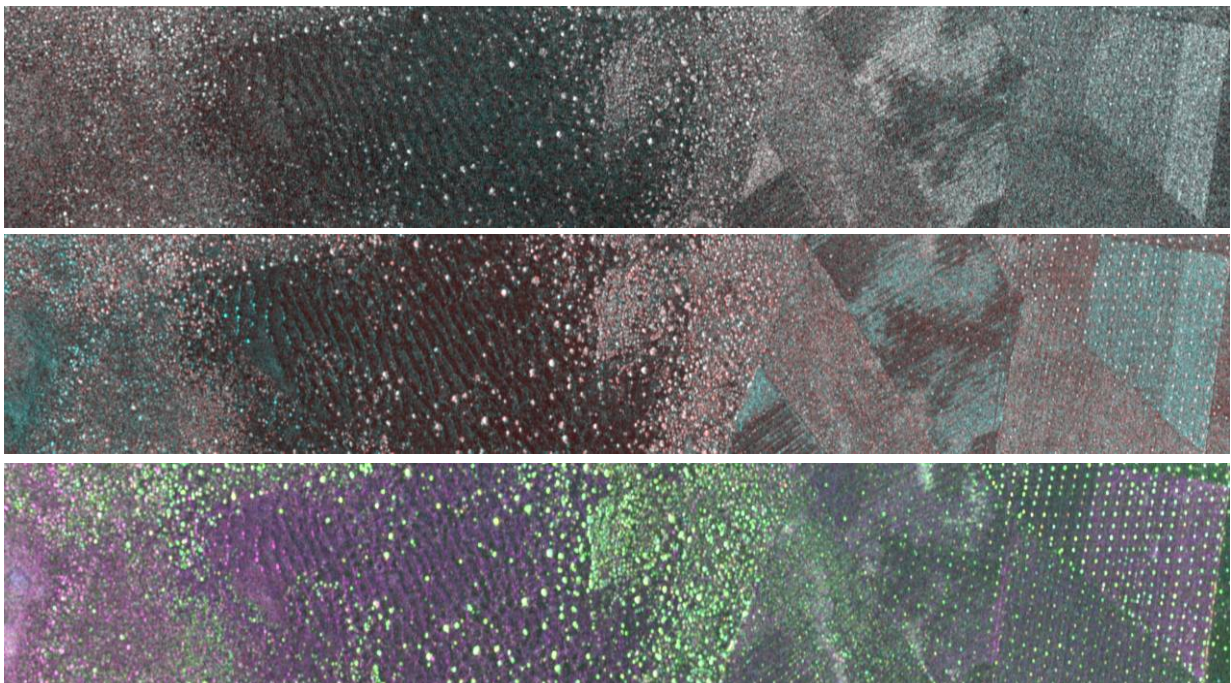


Figure 4.3: Typical radar signatures for Ben Gardane test site: X-band VV-polarisation (up), C-band dual polarisation (rgb=HV-VV-VV), and L-band quad-polarisation (rgb=HH-HV-VV)

Processed E-SAR data in different frequency bands (providing also single, dual and quad polarisation) are shown in Fig. 4.3 for Ben Gardane and in Fig. 4.4 for Gabès test sites. The size of the shown strips is in the order of 5km by 1km.

Note the typical olive plantations (with tree spacing in to order of 50m) in Ben Gardane and the small scaled irrigated field plots typical for parts of the Gabès test site.

For the complete list of available processed E-SAR image data products (RGI - radar geometry images including single look complex, GTC – geocoded terrain corrected data), see ANNEX 1.



Figure 4.4: Typical radar signatures for Gabès test site: X-band VV-polarisation (up), C-band dual polarisation (rgb=HV-VV-VV), and L-band quad-polarisation (rgb=HH-HV-VV)

Implementation of Adaptive Receiver Gain Control

Usually the E-SAR system's receiver gain is adjusted manually for each frequency band at test-site. The optimized setting is either determined during one first overpass of the scene to be imaged or (in homogeneous environment) is set taking into account the experience of the operator. Within the E-SAR system it is not foreseen to adapt the receiver gain during data acquisition.

During operation for Gabes test site in Tunisia, it turned out, that a constant receiver gain setting is strongly saturating the receiver in some parts of the scene (mountains, city of Gabès), whereas increased quantisation noise is present in low backscatter areas (arid, dry sand). Therefore it was decided to operate the system with adaptive receiver gain control (AGC). However, E-SAR does not allow the recording of the time and magnitude of AGC switching.

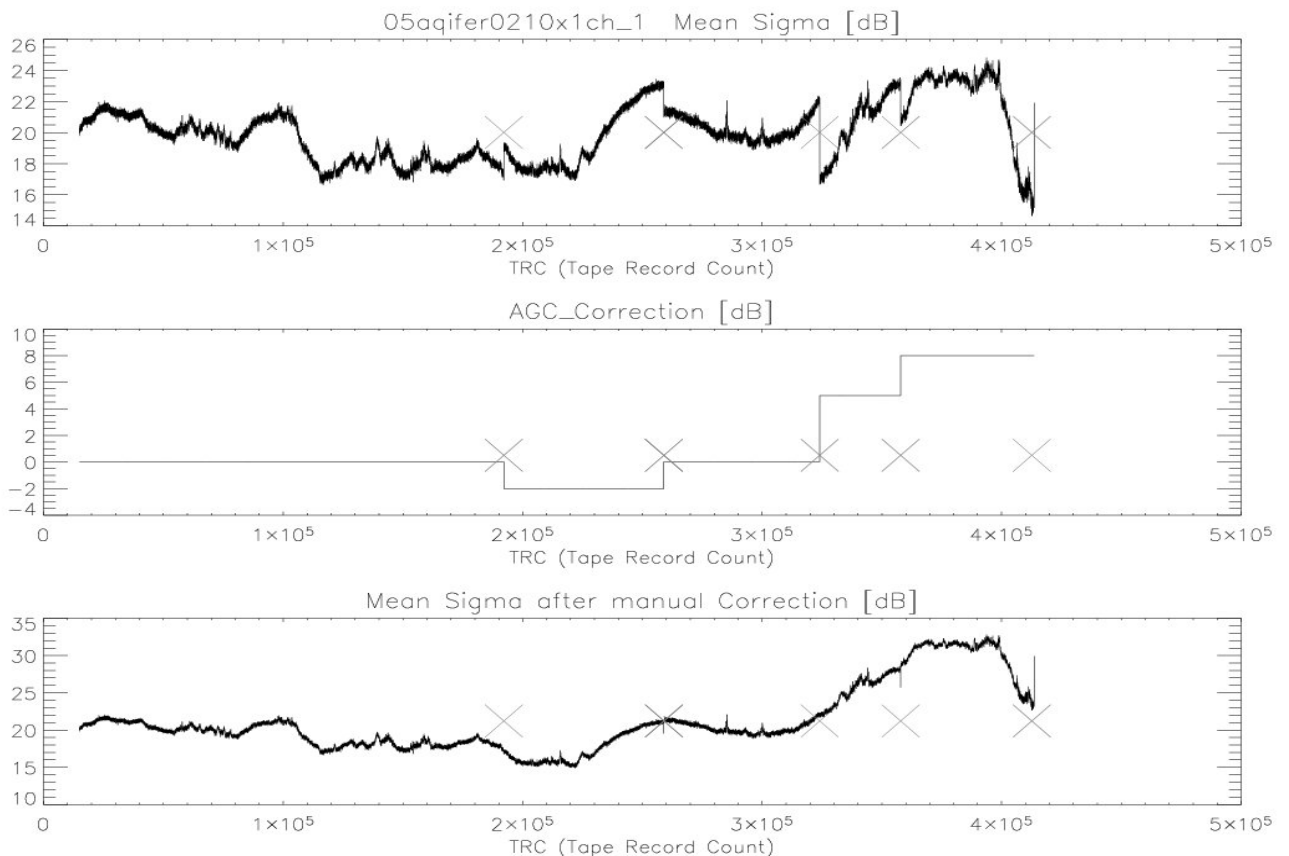


Figure 4.5: Automatic receiver Gain Control (AGC) implemented for Gabès data sets. Automatic retrieval of the variable settings is performed directly from the SAR raw data.

To retrieve the correct AGC sequence settings for SAR focussing, an automated procedure has been developed. Fig. 4.5 shows the results obtained for data set 0210 (L-band). Discontinuities were detected from the mean signal energy of the raw data and an AGC correction curve has been generated and cross-checked with the operators notes during data acquisition. The corrected mean signal energy profile is shown on the bottom. Note, that signal dynamics has been decreased by this adaptive procedure by ~10dB, thus keeping signal strength within the limitations of the ADC.

The adopted automatic AGC recovery approach from the SAR raw data proved very reliable. The only drawback is, that a constant calibration offset could not be retrieved automatically. It was found after processing and cross-checked with the radiometric response of the deployed corner reflectors. The list of AGC correction factors is also given in APPENDIX 1.

Radiometric characteristics

The radiometry of all AquiferEx radar data sets has been checked by examination of the radar cross section (RCS) of the deployed trihedral corner reflectors. Unfortunately, only one trihedral (out of two) is visible within each scene due to a mis-understanding of ground team and flight planning. Even worse, the visible corner reflectors are mis-pointing in elevation by 15-20 deg. However, examination of the data sets revealed that the RCS is stable, but at 1.5 to 4.0 dB below nominal values. This is reasonable taking into account that the mis-pointing is in the order of the 3dB width of the trihedral and that the absolute radiometric accuracy of E-SAR data is in the order of +/- 1-2dB.

For the Ben Gardane test site, which is quite homogeneous, the mean backscatter profiles along range have been obtained in terms of incidence angle corrected Sigma-Nought:

$$\gamma^0 = \sigma^0 / \cos\theta_i = \beta^0 \tan\theta_i$$

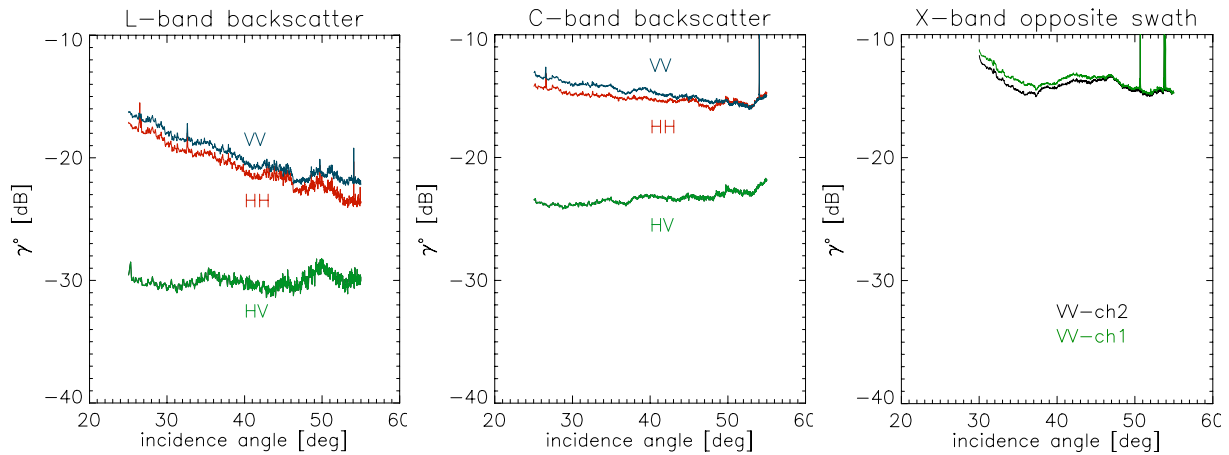


Figure 4.6: Range profiles of incidence angle corrected sigma nought for frequency bands L, C, and X and different polarisations.

The expected behaviour is confirmed, i.e. the lower the wavelength the higher the absorption in dry and sandy soil. Interesting to observe is the large change across incidence angle for co-polar L-band, as well as the low value for the cross-polarisations, which is close to the noise level. Note also, that the X-band (interferometric antennas) show stronger variation due to less accurate calibration (influence of aircraft fuselage distorts the antenna pattern). However, X-band is mainly operated for interferometric purposes of DEM generation, and there was no time allocation to operate also the radiometrically more accurate X-band horn antenna.

Repeat-Pass Interferometric Processing

For both test sites repeat pass interferometric processing has been performed using the additionally required L-band tracks. Repeat pass interferometric processing is possible because of precise navigation of the Do-228 aircraft operating the E-SAR system and because of the highly accurate residual motion error correction implemented for the repeat-pass interferometric processing chain.

Fig. 4.7 shows the tracks flown in L-band for Gabès test site (look direction from south) on the two days of data acquisition. Note the precision of aircraft navigation for the 0m and -60m horizontal baselines.

The tracks flown on the second day are offset in altitude by 75m because of air traffic control (ATC) restrictions. There are also increasingly more turbulences on the second day as can be seen from the the 0307 (yellow) -20m horizontal baseline track. In fact data acquisition was finished with this track.

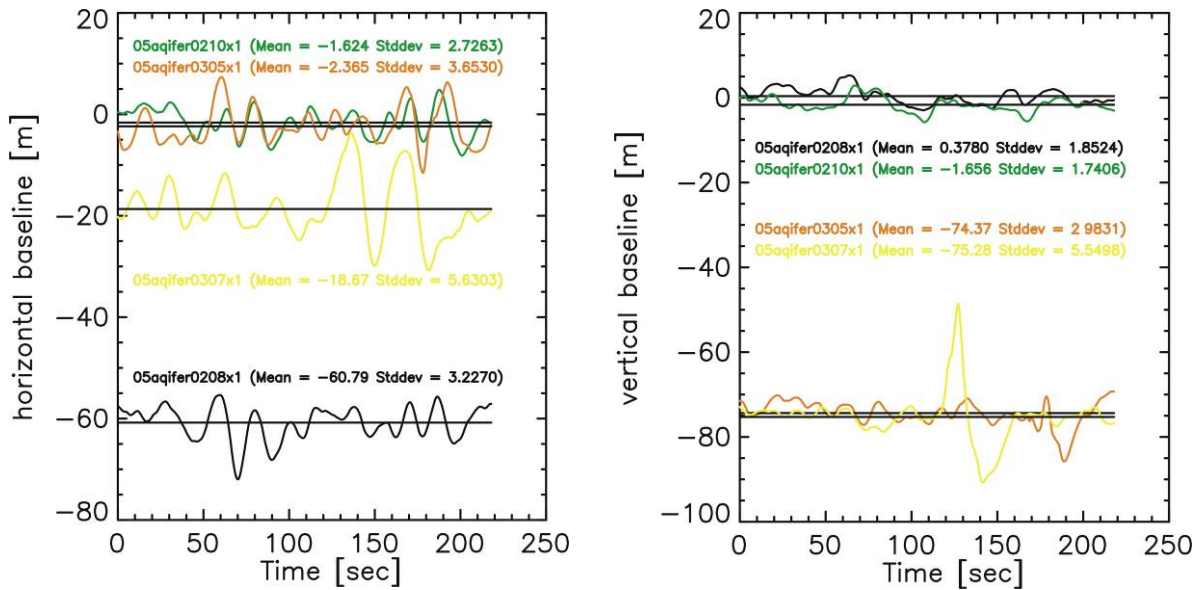


Figure 4.7: L-band Baselines flown for the Gabès test site on the two days (look direction from south). Turbulences occurred for last flow track 0307 and flight altitude offset of 75m between the two days.

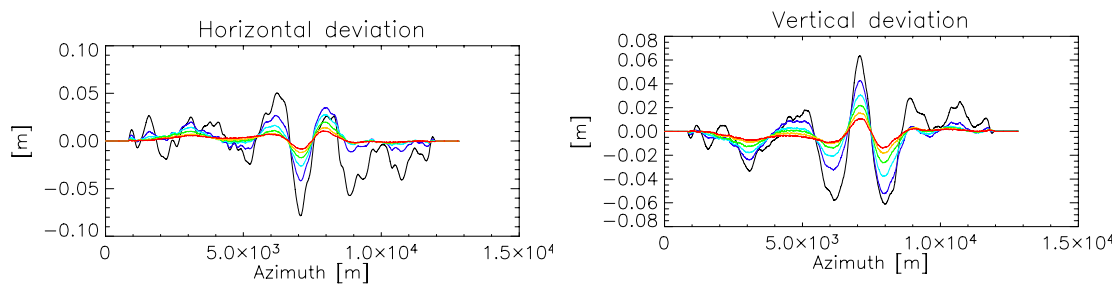


Figure 4.8: Residual motion errors estimated from interferometric repeat-pass data sets. The relative accuracy is in the order of millimetres.

Figure 4.8 presents the evaluation of the residual motion errors for data takes 0206 and 0208. Precise estimation of residual motion errors (track deviations) in the order of few millimeters is reached within 2-3 iterations. The compensation of these residual errors within the processing is mandatory. Otherwise coherence loss and high phase errors are observed, making the data useless for Pol-InSAR evaluations.

An example of repeat-pass interferometric phase and coherence is given below in Fig. 4.9. It relates to the same 60m baseline (tracks 0206 with 0208).

Figure 4.8: L-band polarimetric composite (rgb=HH-HV-VV), interferometric phase and coherence (HH) for Gabès SE segment.

4.2 AVIS data processing

The processing of the AVIS data was conducted as followed:

- ◇ Dark current correction
- ◇ Flatfield correction (homogeneity of the camera CCD)
- ◇ Spectral resampling: The data were resampled to a spectral sampling rate corresponding to the spectral resolution. This enabled the reduction of the huge amount of data as well as an increase of the SNR without any loss of spectral information. The averaging was done assuming a Gaussian-shaped response function represented by the different weights for the adjacent bands. An oxygen-fitting algorithm was added to the resampling procedure to correct any wavelength shifts that may have occurred.

Atmospheric correction and reflection calibration were calculated using a radiation transfer model based on MODTRAN. The resulting data finally are spectral reflectances [%]. Input data for the atmospheric correction are listed in Table 4.

Table 3: *Input parameters for the atmospheric correction of the AVIS data*

Date	Visibility on ground [km]	Water vapour factor
Nov 9	40	1.1
Nov 11	40	1.1
Nov 12	40	1.1

These data are validated using the field spectrometer data acquired during the ground truth campaign, which are described in more detail in section 4.3.

- ◇ Geometric correction: The position of each pixel is calculated using the data of the GPS (time, altitude, position) and the inertial navigation unit (roll, pitch, yaw). If necessary, the image data are fine tuned after the standard correction using ground control points. The resulting data fit well with the ESAR data, which is shown in Figure 4.9.



Figure 4.9: Overlap of geometrically corrected AVIS and ESAR data

4.3 Validation of the AVIS data

The AVIS data were validated using field spectrometer data gathered during the ground truth campaign. The comparison of reflectance spectra in overlapping areas of different flight stripes is another technique that will also be described.

Validation Using Field Spectrometer Data

The comparison of AVIS reflectance spectra and field spectrometer data was conducted and showed good results, although considering a spatial integral measurement of AVIS in comparison to a number of point measurements can be problematic. **Figure 4.10** shows vegetated canopies at the test site Gabes, which were monitored with AVIS and the field spectrometer. The photographs illustrate the difficulties when the spatial integral of AVIS spectra should be compared directly with field spectrometer point measurements in this landscape. The sparser the vegetation the more differences may occur, which can also be observed during one measurement cycle of the field spectrometer (measurement procedure is described in section 3.5).

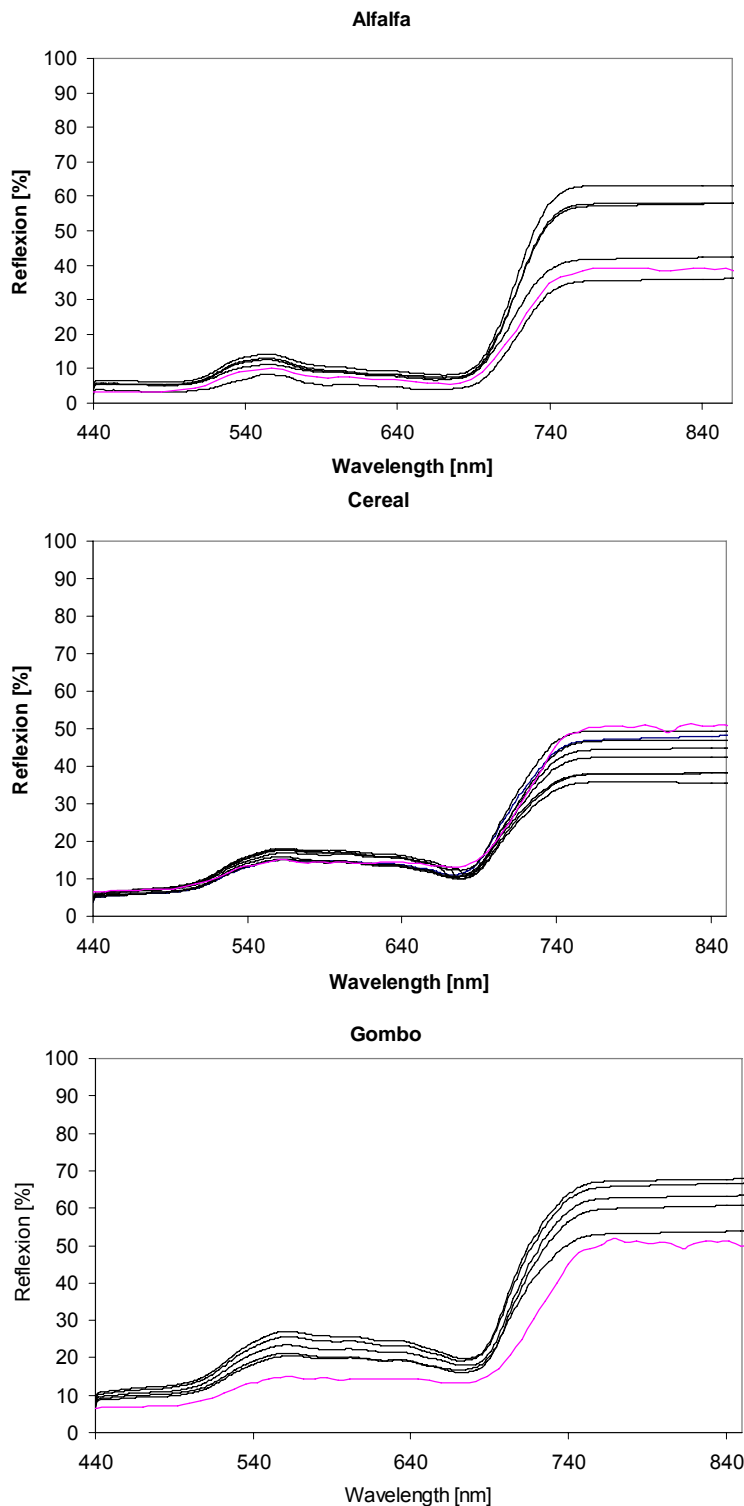


Figure 4.10: Comparison of AVIS reflectance spectra and field spectrometer data for vegetation canopies with different density at the test site Gabes (Alfalfa at SM-2, Cereal at SM-2 and Gombo at SM-4). The data were acquired on November 11. The black lines represent field spectrometer data, the purple lines AVIS spectra.

Taking into consideration the great heterogeneity on ground (as shown in **Figure 4.11**), the spectra show good consistency at sparsely vegetated or not vegetated areas.

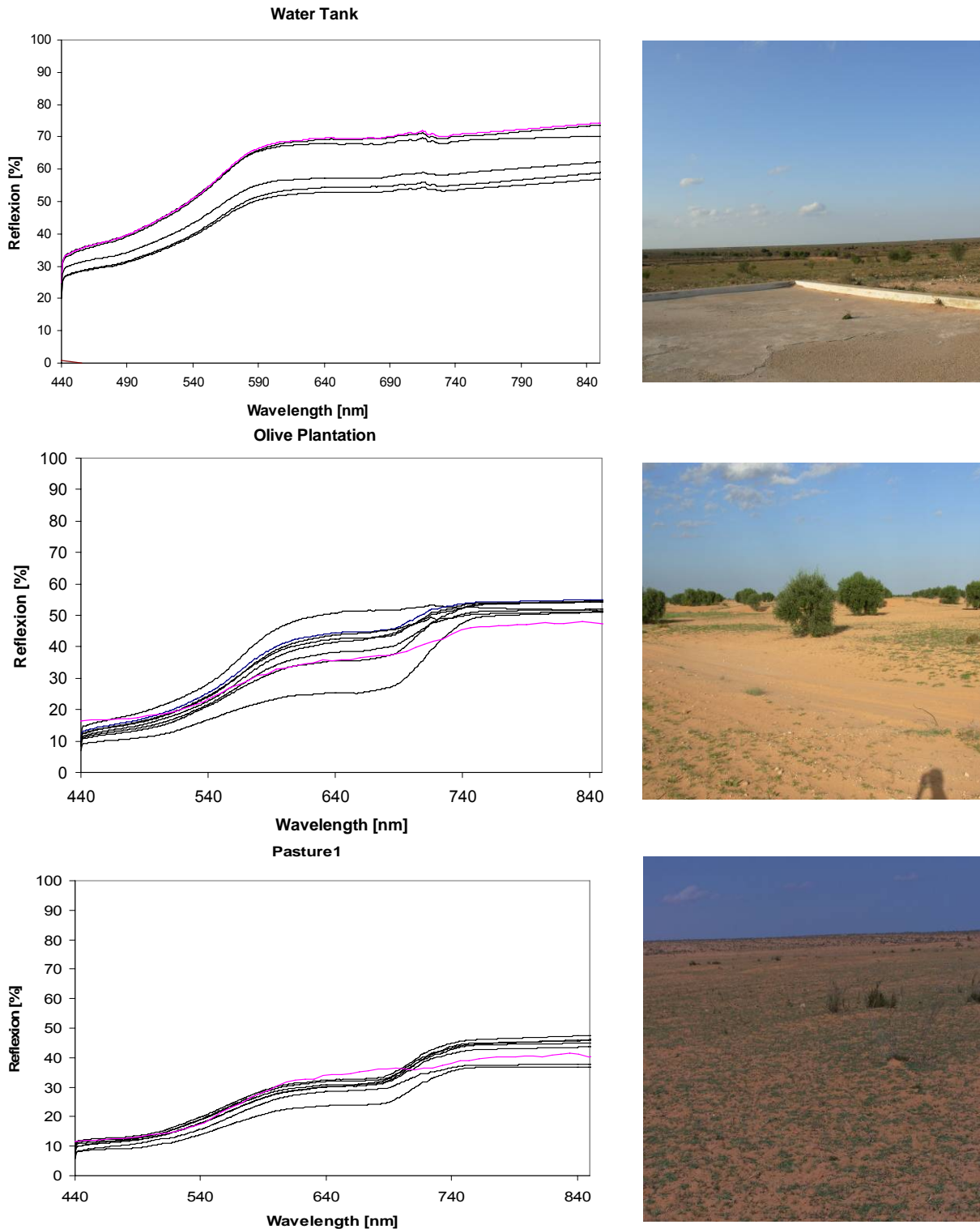


Figure 4.11: Comparison of AVIS reflectance spectra and field spectrometer data for sparsely or not vegetated areas at the test site Ben Gardane (Water tank at CR-2, Olive planting at CR2-2 and pasture near water pool). The data were acquired on November 9. The black lines represent field spectrometer data, the purple lines AVIS spectra.

Validation Using Overlapping Areas

The review of overlapping AVIS image stripes can only be shown exemplary. **Figure 4.12** and 4.13 present some comparisons of individual spectra. The use of individual pixels is due to the great heterogeneity of the landscape with very few homogeneous targets. The results show a good agreement between the different flight stripes. Deviations can be observed especially in the near infrared at vegetated areas which can be explained by angle (brdf) effects.

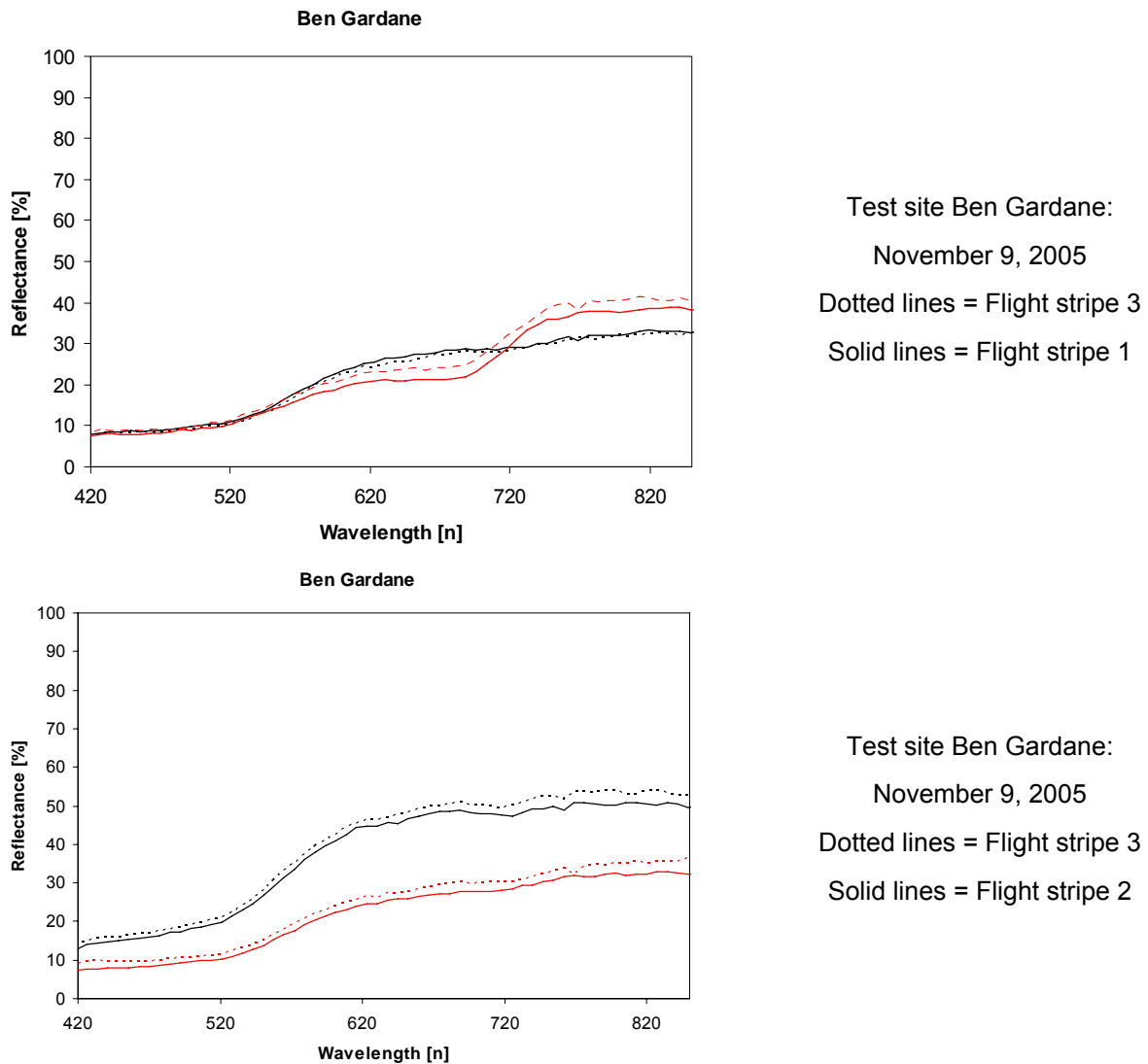


Figure 4.12: Comparison of spectra of different flight stripes for the test site Ben Gardane

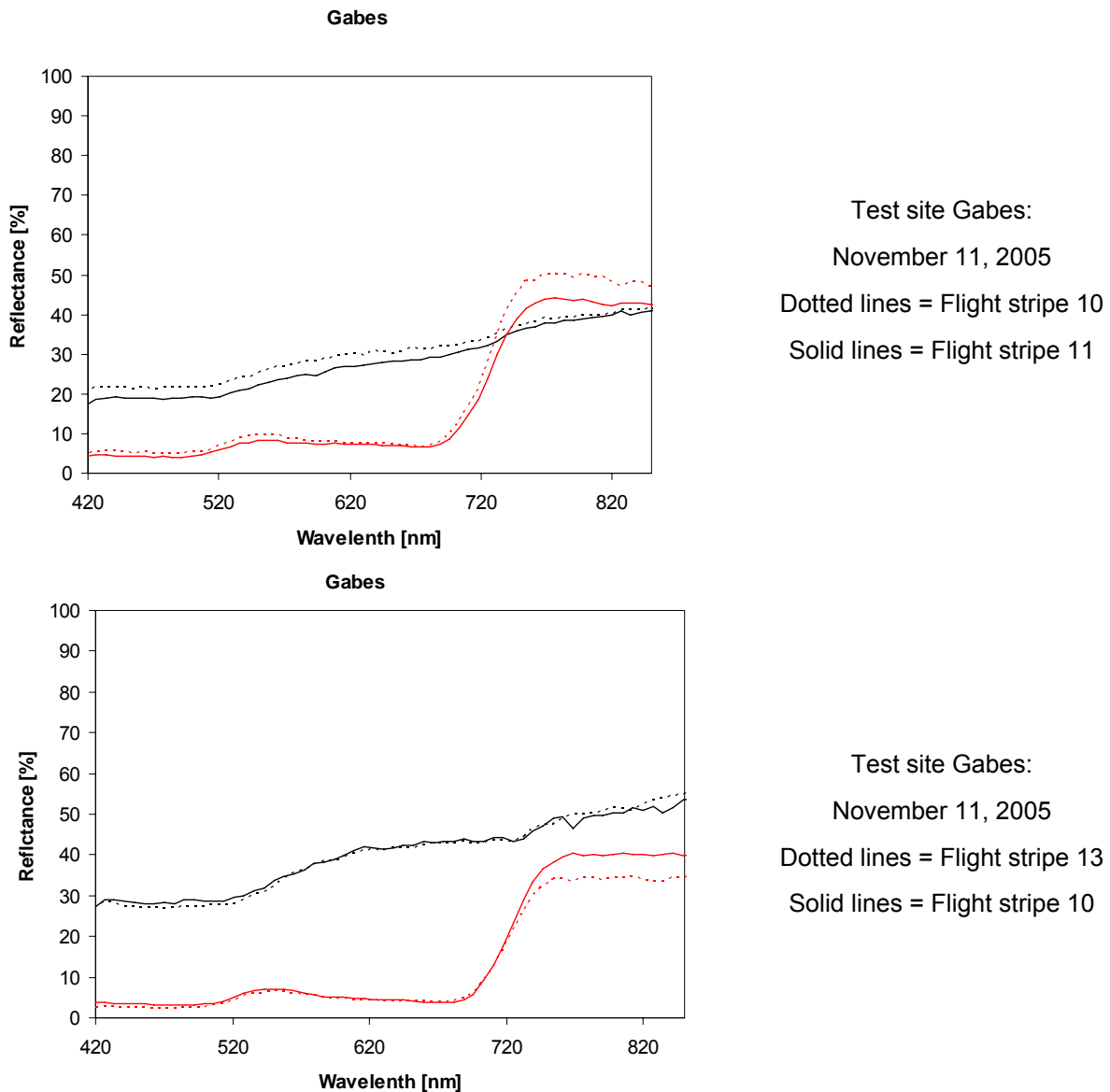


Figure 4.13: Comparison of spectra of different flight stripes for the test site Gabes

4.4 Ground measurements GIS (ArcGIS)

CHRIS, AVIS and Radar quicklooks form the basis for the AquiferEx GIS. AVIS and Radar imagery is geometrically corrected, while the CHRIS images are only thought to provide a survey of the area.

The position of the sampling points and the results of the measurements are integrated into the GIS. The ARCGIS files and their corresponding Excel tables are located in subdirectories of AquiferEx\GIS\Groundtruth_data. Photographs of the measurements can also be found in these subdirectories.

The basic design of the AquiferEx GIS is based upon the setting of relative paths. The existing GIS is designed to run on CD, i.e. the main path is set on device E:\. Two ARCGIS projects were configured, one for each test site (AquiferEx\GIS\BenGardane.mxd and AquiferEx\GIS\Gabes.mxd).

If the CD device is not E:\ or the user wants to copy the GIS into another device, the path has to be changed once the project is opened. The path can be changed browsing the following folder of the project: File -> map properties -> Hyperlink base (see **Figure 4.14: relative path setting**)

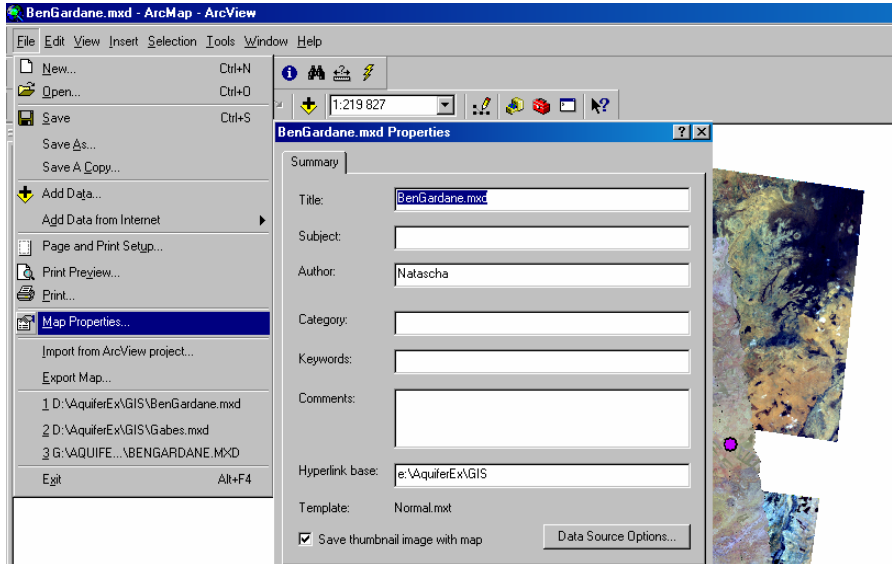


Figure 4.14: relative path setting

Figure 4-1 shows the presentation of the results for an example of the test site Ben Gardane. The sampling points are marked in the remote sensing images. When a specific sample point is chosen, the geographical position (UTM) is given in the attribute file as well as the date of the measurement and the corresponding ground truth result(s).

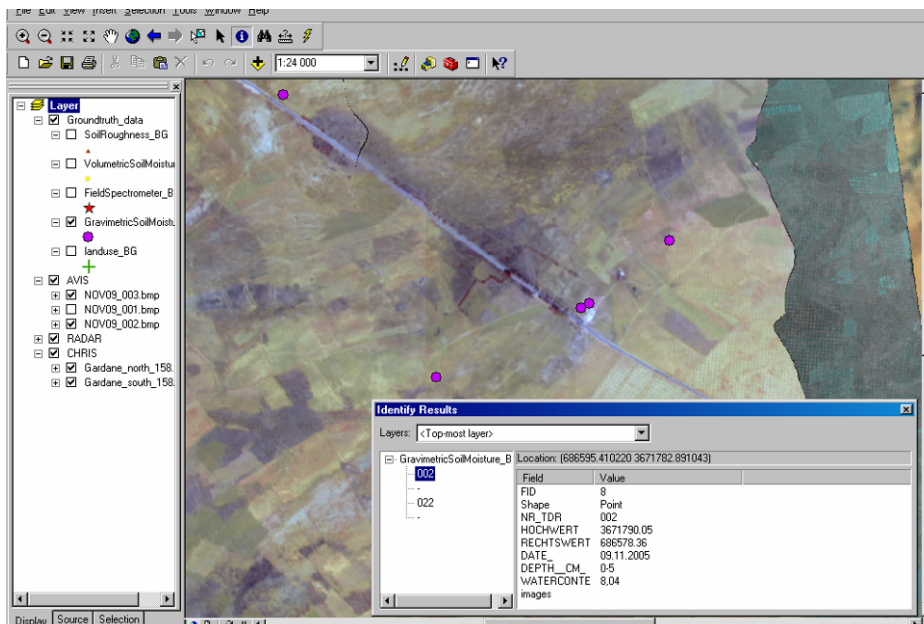


Figure 4-1: Exemplary result of gravimetric soil moisture measurement as shown in the GIS

The results of the measurements are also listed in Excel tables that are stored in the corresponding subdirectories. An example is given in Figure 4.16.

Nr_TDR	Hochwert	Rechtswert	date	time	depth [cm]	watercontent [%]
001	3673240.87	684444.05	09.11.2005	10:00:00	0-5	0,82
-	3673240.87	684444.05	09.11.2005	10:00:00	5-10	1,01
003	3670402.78	688471.05	09.11.2005	10:25:00	0-5	1,06
-	3670402.78	688471.05	09.11.2005	10:25:00	5-10	2,36
004	3670372.12	688479.41	09.11.2005	10:30:00	0-5	1,02
-	3670372.12	688479.41	09.11.2005	10:30:00	5-10	1,15
005	3670325.57	688462.17	09.11.2005	10:40:00	0-5	1,70
-	3670325.57	688462.17	09.11.2005	10:40:00	5-10	3,91
002	3671790.05	686578.36	09.11.2005	10:20:00	0-5	8,04
-	3671790.05	686578.36	09.11.2005	10:20:00	5-10	7,15
006	3671755.07	686522.02	09.11.2005	10:40:00	0-5	1,49
-	3671755.07	686522.02	09.11.2005	10:40:00	5-10	1,87
007	3672228.97	687132.31	09.11.2005	11:10:00	0-5	0,90
-	3672228.97	687132.31	09.11.2005	11:10:00	5-10	1,33

Figure 4.16: Presentation of measurement results in Excel sheets

Additional data such as the BBCH-codes for the estimation of the phenological stages of vegetation are stored in the subdirectory “additional_data”.

The results of the measurements are also listed in Excel tables that are stored in the corresponding subdirectories. An example is given in Figure 4.16.

Additional data such as the BBCH-codes for the estimation of the phenological stages of vegetation are stored in the subdirectory “additional_data”.

4.4.1 General Information:

- The AquiferEx GIS is based on ArcGIS (Version 9.1).
- The basic design of the AquiferEx GIS is based upon the setting of relative paths. The existing GIS is designed to run on CD, i.e. the main path is set on device E:\. Two ARCGIS projects were configured, one for each test site (AquiferEx\GIS\BenGardane.mxd and AquiferEx\GIS\Gabes.mxd). If the CD device is not E:\ or the user wants to copy the GIS into another device, the path has to be changed once the project is opened. The path can be changed by browsing the following folder of the project: File -> map properties -> Hyperlink base)
- The GIS is based on the UTM WGS 84 (Zone 32 N) coordinate system.
- Information about time is given in UTC; otherwise it is specified in the attribute table of a shape file.

4.4.2 Image data

- CHRIS, AVIS and Radar quicklooks form the basis for the AquiferEx GIS. AVIS and Radar imagery is geometrically corrected, while the CHRIS images are only thought to provide a survey of the area.
- The AVIS-2 shown are real colour composites with bgr = 477, 550, 660nm with a ground resolution of 5 m. The AVIS data format is described in the PDF-document “AquiferEx_FinalResults”. For further information please contact the AquiferEx technical officer (Remo Bianchi Remo.Bianchi@esa.int) or LMU Munich (Natascha Oppelt n.oppelt@lmu.de).
- The CHRIS data are real colour composites with bgr = 485, 565, 670 nm with a ground resolution of 16 m (at nadir). For further information please contact the AquiferEx technical officer (Remo Bianchi Remo.Bianchi@esa.int) or VISTA GmbH (Heike Bach bach@vista-geo.de).

- The ESAR data are composites of different polarisations of C-Band bgr = VV, HV, HH. The data are presented in two ground resolutions: 2 m and 5 m. For further information please contact the DLR (Rolf Scheiber Rolf.Scheiber@dlr.de).

4.4.3 Ground measurements

- The results of the ground measurements are implemented in the GIS as Shape files and their corresponding attribute tables. The position of the sampling points and the results of the measurements are integrated into the GIS. The ARCGIS files and their corresponding Excel tables are located in subdirectories of AquiferEx\GIS\Groundtruth_data. Photographs of the measurements can also be found in these subdirectories.
- The procedure of the various measurements is described in the PDF-document "AquiferEx_FinalResults".
- The entities of the measurement results are given in their corresponding attribute table or in the PDF-document "AquiferEx_FinalResults".
- The contributions of ITC are included into the GIS. A description of the measurements is given in the PDF-document "ITC".
- Photographs taken during the campaign are connected as hotlinks and can be found in the subdirectories corresponding to a specific measurement.

4.5 Ground measurements GIS (ArcExplorer)

An additional GIS on the basis of freely available software was built on demand of several users. The freeware GIS is based on ArcExplorer (Java edition for education).

Some restrictions do occur such as:

- Absolute path setting is required (E:/)
- Remote sensing data cannot be viewed as mosaic

5 SCIENTIFIC RADAR DATA ANALYSIS

The purpose of this chapter is to make a first assessment of the radar data collected during the campaign in November 2005 in Tunisia. Three topics are the main goal of investigation: polarimetric SAR analysis, the surface parameter estimation with C- and L-band and the generation of land cover maps. In the first section the radar data used will be described. A short analysis of the backscattering intensity is provided, then polarimetric ratios and coherence will be analysed. The difference between C- and L-band is highlighted. One surface model has been used for soil moisture parameter estimation, the inversion procedure is described and the problems using C- or L-band are discussed. As the soil is mainly composed of sand in the arid area, the penetration depth at L-band frequency was analysed. In addition, polarimetric classification algorithms were applied on a L-band data set.

5.1 Test site selection

For detailed investigation the Gabes flight stripe was chosen. The flight stripe has a length of around 20 km. For easier handling the stripe has been spit into two parts – west and east part (Figure 5.1 and 5.2). For further evaluation the volumetric soil moisture samples were selected for investigation. The gravimetrically taken measurements have a stronger standard deviation and some of the samples show 0 vol. %. In Figure 5.3 the volumetrically taken samples are plotted. The mean value is 15 vol. % with a mean standard deviation of 1 to 2 vol. %. Around 114 samples were taken by the gtc-ground measurement team at the Gabes test site. The samples were taken from vegetated and non vegetated fields. Some of the fields were irrigated and used for agricultural production. The non irrigated fields are very dry fields, where some of them are low or sparsely vegetated. The instrument used for soil moisture measurement was a TDR (time domain reflectometry) with a stick length of 10 to 15 cm.

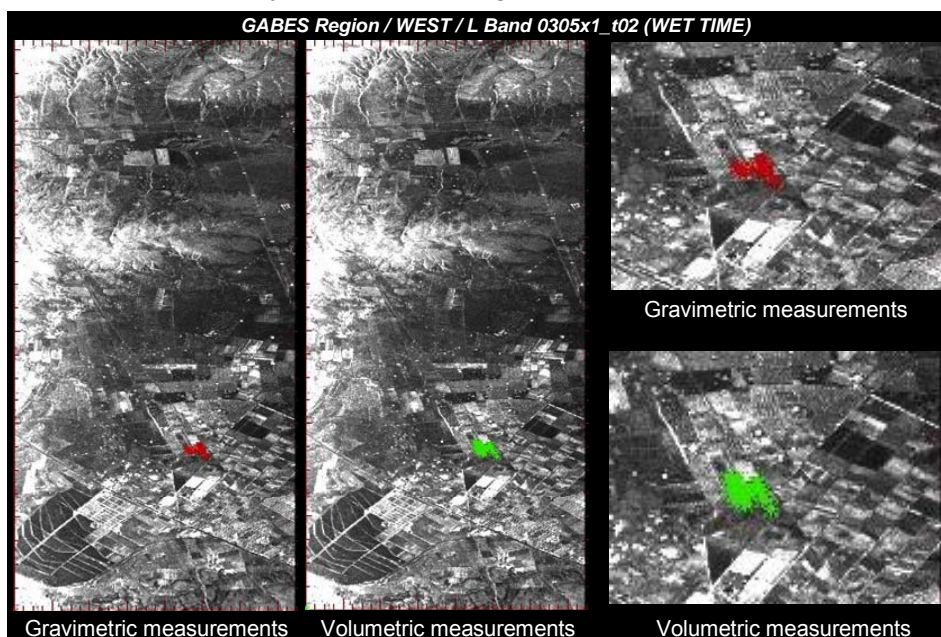


Figure 5.1: L-band images of the WEST part of the GABES test site and the gravimetric and volumetric soil moisture measurements estimated on the ground. The red/green aster symbols indicate where vol./grav. Measurements have been taken.

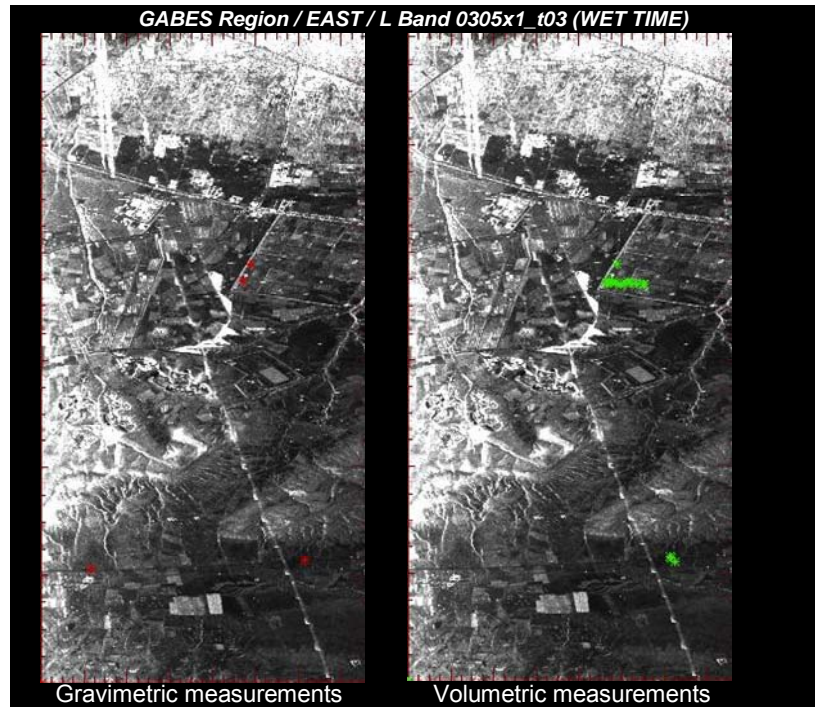


Figure 5.2: L-band images of the East part of the GABES test site and the gravimetric and volumetric soil moisture measurements estimated on the ground. The red/green aster symbols indicate where vol./grav. Measurements have been taken.

Polarimetric investigations were made with all taken sample points, whereas the surface parameters (soil moisture and roughness) can be only investigated using the samples from the non vegetated area.

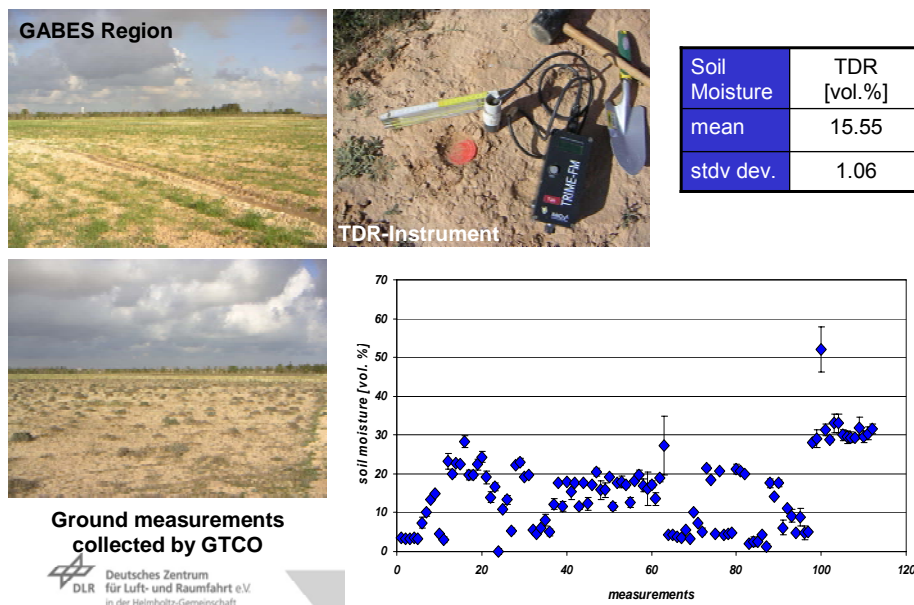


Figure 5.3: Ground measurements: Volumetric soil moisture estimated with TDR against the taken samples. Some images of non irrigated fields.

5.2 Polarimetric Analysis

Backscattering Intensities

The polarimetric analyses were made in C- and L-band. The backscattering intensities represented as sigma nought are varying for the different polarisations, as seen in figure 5.4. For L-band the mean value for HH is -26 dB, for VV -24 dB and for the cross polarisation -36 dB. The values are mean values over the whole Gabes scene, where within a scene agricultural fields exist and also smaller settlements can be seen. But still the highest value is observed for VV polarisation as it is expected for a dominant surface contribution. The second row of figure 5.4 shows the backscattering intensity over range, in this case with changing incidence angle from 25 to 55 degree. In principle, a higher backscattering in near range can be observed than in far range. The backscattering intensity is slowly decreasing with increasing incidence angle. Both trends can be observed for C- and L-band frequency and for all polarisations.

A special case could be investigated when by chance a rain event could be recorded between two days. The backscattering values show only small differences. The reason could be the composition of the soil. The sandy soil is very fast absorbing the rain and the humidity is transferred to deeper soil regions.

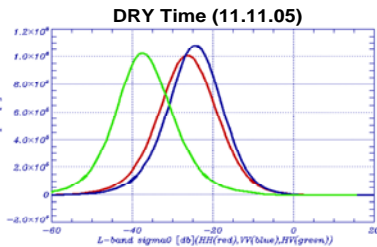
In C-band the backscattering values are much higher (up to 10 dB) as already expected, but also here the VV backscattering intensity is higher than for other polarisations.

In figure 5.5 the polarimetric SAR data displayed for each polarisation at L-band are shown. The bright areas represent high backscattering regions and the dark gray areas the low radar backscattering regions. In near range in the beginning and in the middle of the images very bright regions can be observed, these are mountainous areas. Only at the lower part of the image an agricultural area is present. The fields can be clearly recognised as very structured features. In Figure 5.6 an RGB image in the Pauli basis is presented. The different colours represent different scattering mechanisms: Bluish areas are characterised by surface scattering, reddish areas by dihedral scattering and greenish areas by volume scattering. White areas are composed of all three scattering mechanisms.

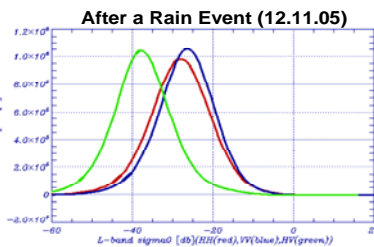
In Figure 5.7 the same RGB is presented for the C-band frequency. Differences in the colours are given over the same field areas. The differences are due to the smaller wavelength that interacts differently with the illuminated object.

L-Sigma-Nought HH / VV / HV

estimate over a whole scene



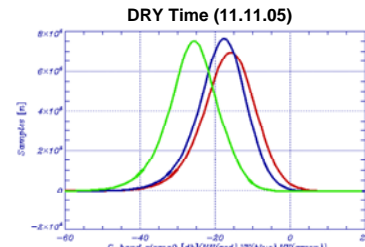
Polarisation	Sigma-Nought (mean) [dB]	Sigma-Nought (std) [dB]
HH	-25.89	7.84
VV	-24.18	7.37
HV	-35.69	8.12



Polarisation	Sigma-Nought (mean) [dB]	Sigma-Nought (std) [dB]
HH	-29.44	14.44
VV	-28.02	14.34
HV	-37.69	13.43

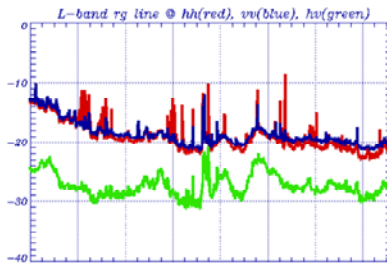
Sigma-Nought HH / VV / HV @ C-band

estimate over a whole scene



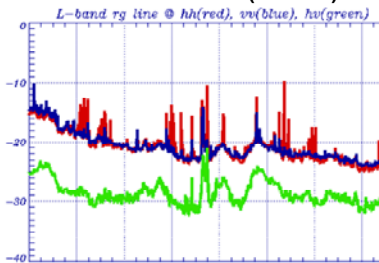
Polarisation	Sigma-Nought (mean) [dB]	Sigma-Nought (std) [dB]
HH	-16.00	7.32
VV	-17.99	6.88
HV	-25.59	7.05

DRY Time (11.11.05)



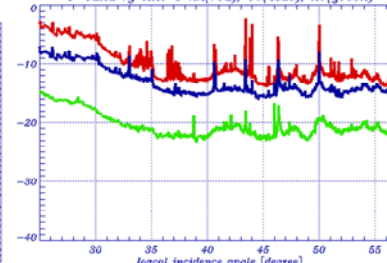
Sigma-Nought	min	max	diff
HH	-22.96	-8.41	14.55
VV	-21.47	-9.88	11.59
XX	-31.17	-20.71	10.36

After a Rain Event (12.11.05)



Sigma-Nought	min	max	diff
HH	-31.24	-9.65	21.59
VV	-31.35	-10.01	21.35
XX	-37.16	-21.01	16.15

C-band sigma-naught @ HH, VV, HV



Sigma-Nought	min	max	diff
HH	-13.88	-2.03	11.85
VV	-15.86	-6.98	8.88
XX	-23.25	-14.69	9.16

Figure 5.4: First row: Histogram of backscattering intensity for L- (two left) and C-band (one right) at different polarisations; second row: Backscattering intensity summed up in range for L- (two left) and C-band (one right) at different polarisations. The range variation corresponds to a variation of 25 to 55 degree in the local incidence angle.

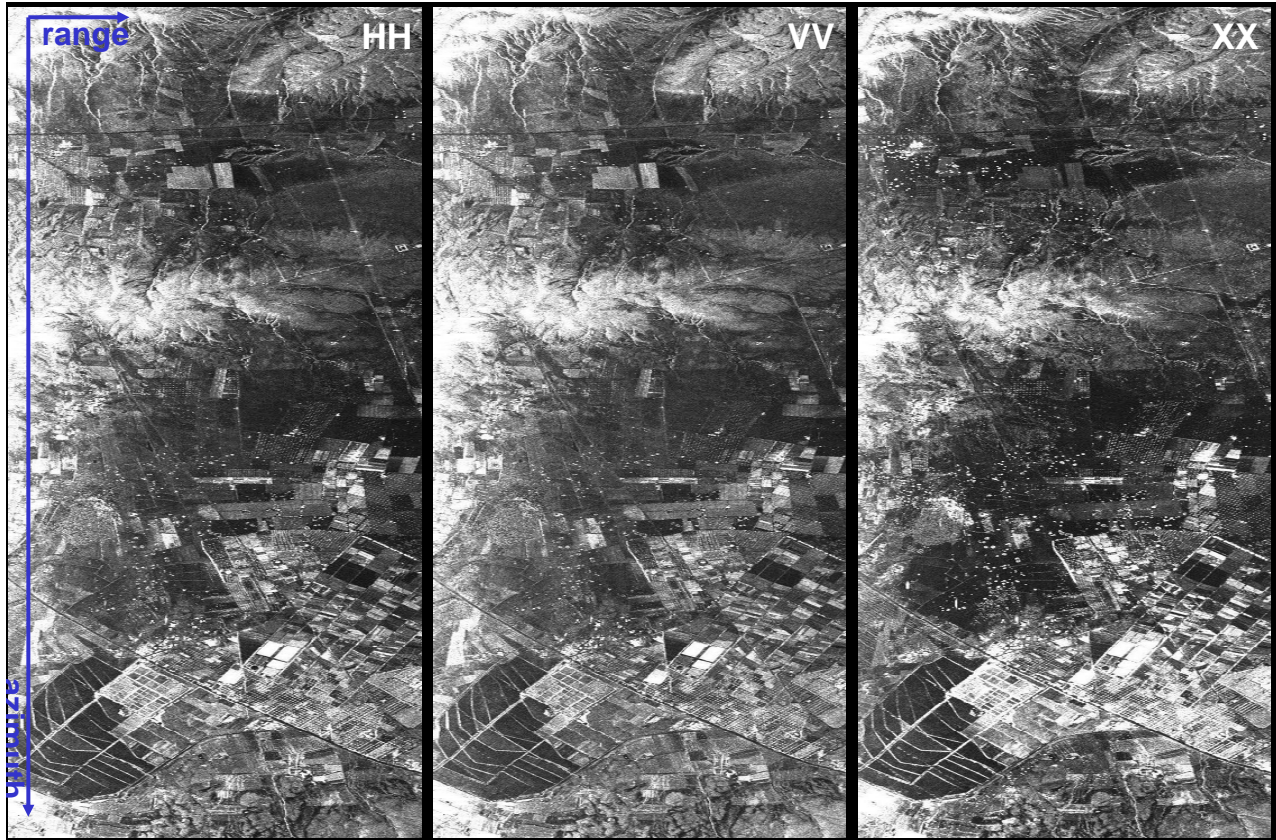


Figure 5.5: E-SAR acquired polarimetric SAR data at L-band frequency for the Gabes (west part) region. HH stands for horizontal transmitted and received, VV stands for vertical transmitted and received and XX stand as a normalised value between HV and VH.



Figure 5.6: RGB image in the Pauli representation in L-band frequency for the Gabes (west part) region – smaller part of the whole scene.

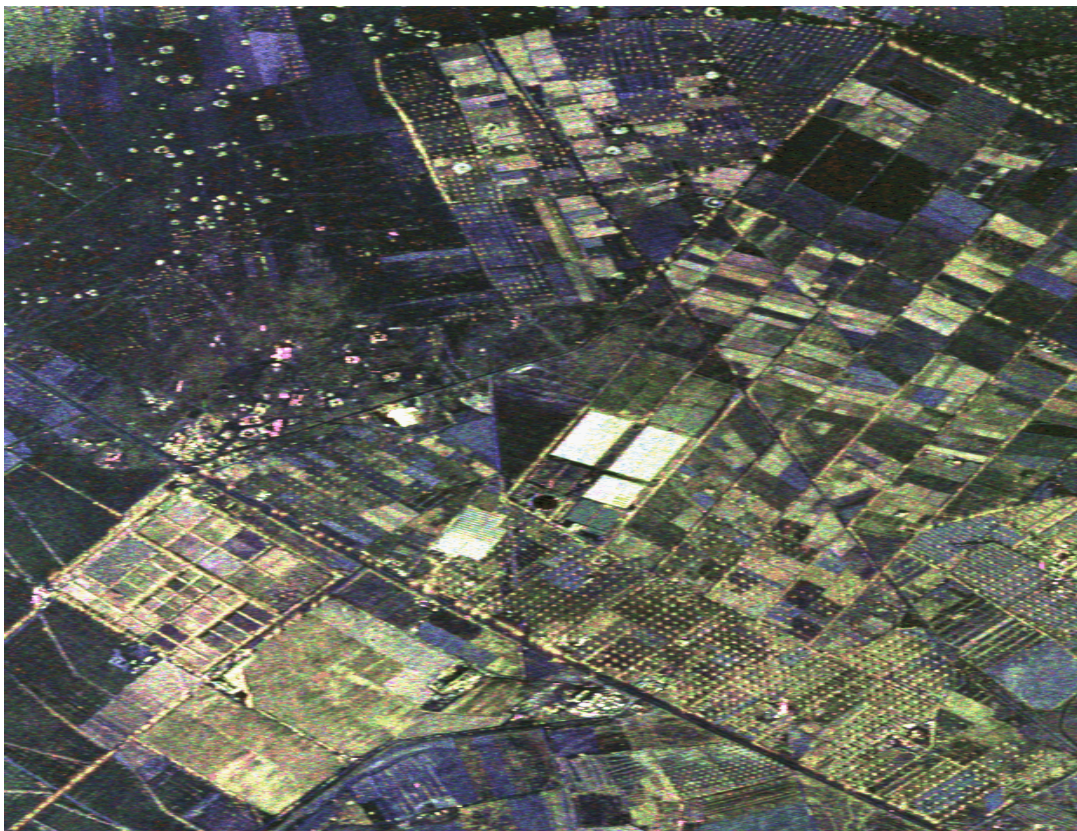


Figure 5.7: RGB image in the Pauli representation in C-band frequency for the Gabes (west part) region – smaller part of the whole scene.

5.3 Surface Parameter Estimation

In this section the main focus is the estimation of surface parameters using existing surface scattering models.

The main problem for the quantitative estimation of soil moisture and/or surface roughness from SAR data lies in the separation of their individual effects on the backscattered signal. Polarimetry plays here an important role as it allows either a direct separation or a parameterisation of roughness and moisture effects within the scattering problem. The scattering problem of electromagnetic waves from randomly rough surfaces has been research topic over decades and is still not satisfactorily solved due to the lack of an exact closed-form solution. However, for many practical applications, approximate solutions are sufficient. In the absence of any direct relationship between surface parameters and backscattering signal empirical models have been developed. In the field of radar remote sensing the most common approximation methods are based on the evaluation of backscattering amplitudes considering single or dual-channel SAR data. The choice of an appropriate scattering model is essential for the quantitative estimation of the surface parameters. On the one hand it must contain enough physical structure while on the other hand it should have a right balance between the amount of parameters needed for their description and available observables. As natural surfaces are complex stochastic objects a priori information and assumptions can be used to simplify the inversion problem. Hence, to obtain an accurate estimate of soil moisture, information about the surface roughness was required for some of the scattering models. Roughness has been considered as a disturbing effect and several conditions have been developed in order to minimise its influence (Hajnsek 2001). There are three main categories of surface scattering models: the theoretical, the empirical and semi-empirical, and the model based methods.

One frequently used theoretical model is the Small Perturbation Model (SPM), where the variation in surface height is assumed to be small compared to the wavelength and is therefore more appropriate for applications with long wavelengths, as at S-, L- or P-band. Although valid only within a limited range of rough surface parameters, it is one of the classical and most widely used solutions of the rough surface scattering. It has been used extensively in many practical applications and the analytic conditions for its validity have been investigated in detail in several studies (Beckmann & Spizzichino 1963, Chen & Fung 1988). A perfectly smooth surface has zero backscatter at oblique incidence. However, in the Bragg scattering region, where the variation of surface height is small relative to the wavelength (i.e., for the vertical surface roughness (k_s) values $\ll 0.3$) the presence of roughness can be seen as a perturbation of the smooth surface scattering problem. In this case, the backscatter coefficients are obtained by the small perturbation or Bragg scattering model which is derived directly from Maxwell's equations (Oh et al. 1992). According to this model, the random surface is decomposed into its Fourier spectral components, each one corresponding to an idealised sinusoidal surface. The scattering is mainly due to the spectral component of the surface which matches (i.e. is in resonance) with the incidence wavelength and angle of incidence (AOI). One of the most important statements of the SPM is that the co-polarised ratio R_s/R_p depends only on the complex permittivity and the local incidence angle, and is independent of surface roughness. For dry surfaces, the co-polarised ratio is high and decreases with increasing moisture content. A strong variation of the ratio for all incidence angles is observed for soil moisture values ranging from $0 < mv < 20$ vol. % which saturates for mv values > 20 vol. %. This indicates that the SPM is insensitive to very wet surfaces and therefore, its inversion yields prospectively to large uncertainties for moisture content estimates above the saturation level. Several studies have experimentally verified the sensitivity of R_s/R_p to soil moisture

content in the case of slightly rough surfaces as well at its saturation above $mv = 20$ vol % (Chen & Fung 1988). This model predicts zero cross-polarization and zero depolarisation effects leading to all polarimetric coherences equal to one. Because of these limitations, the applicability of the SPM on natural surfaces is restricted.

Applying simple polarimetric ratios on L-band and C-band AQUIFEREX data, the sensitivity to volumetric soil moisture, vegetation cover and/or the interaction between vegetation and surface contribution can be predicted. In Figure 5.8 different polarimetric ratios are presented as range profiles over the whole scene. The HH/VV ratio is an indicator for surface scattering in case for a ratio smaller than 1. For both cases we can see that the ratio is close to one but mostly > 1 . This means that HH is higher than VV and therefore surface scattering is not dominant in the scene. The same trend can be also observed in Figure 5.8 on the right side and in the middle. The cross polarised to co polarised ratios are both smaller than expected, but their contribution is still high. Even higher are the co polarised and the two cross/co polarised ratios at C-band.

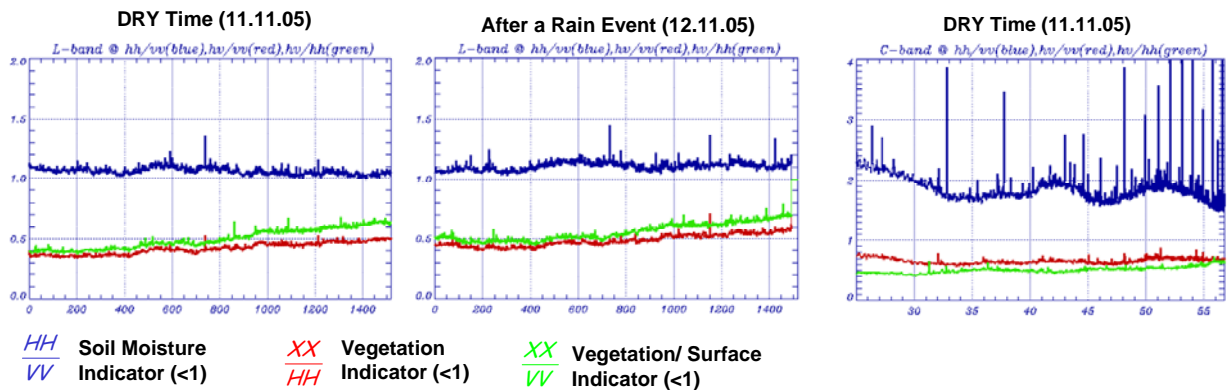


Figure 5.8: Polarimetric ratio in L-band and C-band as indicators for different scattering types derived for the whole scene. Left presented for the dry time, middle for the wet time in L-band and right for the dry time and in C-band.

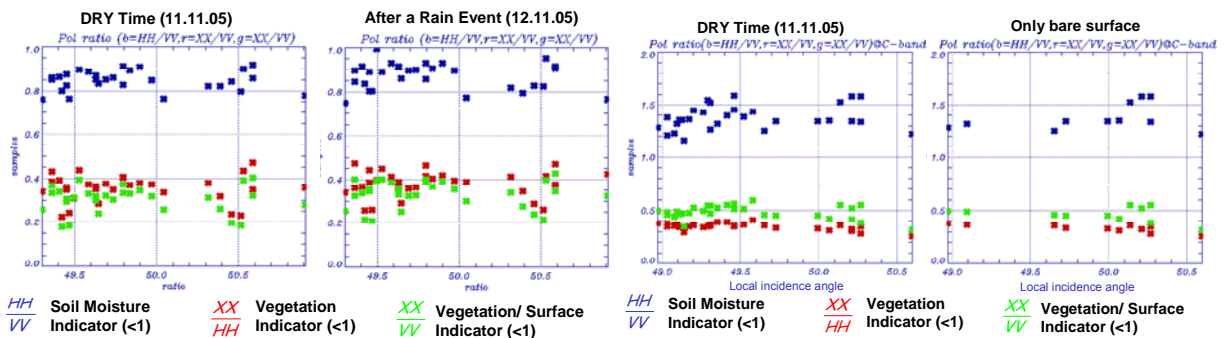


Figure 5.9: Polarimetric ratio in L-band and C-band as indicators for different scattering types derived from the 114 sample taken on the ground. Left two presented for L-band and right two for the C-band.

In Figure 5.9 the polarimetric ratios are given only for the areas, where the soil moisture samples were taken. On the two left plots the copolarised ratio at L-band is close but still smaller than one. This is an indication that VV is higher than HH and that the dominant scattering mechanism occurring is surface scattering. At the right side the same area is investigated in C-band. Here the ratio is still higher than 1 even if only fields or areas are considered that are pure bare surfaces.

The HHVV phase is known as a valuable parameter for the characterisation of vegetated and non vegetated agricultural fields. When the HHVV phase is close to zero, the fields can be considered as non-vegetated. Values higher than +/- 10 degrees could be considered as sparsely vegetated. In Figure 5.10 both plots on the left - presented only for bare surfaces - show values within +/- 10 degrees in L-band. The solid line represents the average value along azimuth plotted over in range. The dots are average mean values for areas, where ground measurements were taken. On the right side the values with vegetated and non vegetated areas are presented for C-band and they show exemplarily the differences between both agricultural field types. Also here the solid line represents the mean value over the azimuth area.

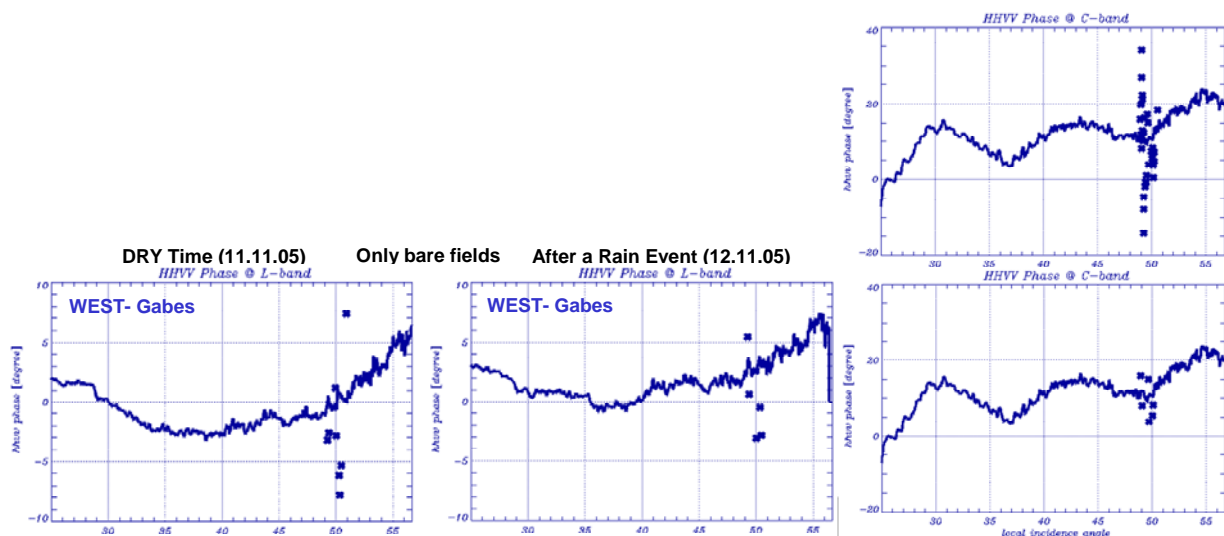


Figure 5.10: Left two plots: HHVV phase for the pure bare surfaces of the Gages area at L-band. Right two plots: HHVV phase for the Gages area for all 114 point and only for the pure bare surfaces at C-band.

An independent estimate of roughness conditions is not possible by using only a single polarisation and single- frequency SAR system. By increasing the amount of observables by using a fully polarimetric data set, both the amount of surface parameters and the estimation quantity increases. However, the main limitation for using models based on polarimetric backscattering amplitudes is their insufficiency to deal - at least in a practical way - with diffuse or secondary scattering processes, depolarisation effects caused by surface roughness, and the presence of multiplicative and / or additive noise components.

A large class of natural surface scatterers, is characterised by secondary and/or multiple scattering effects. With increasing surface roughness, relative to the wavelength the effect of multiple scattering becomes stronger, generating an adequate |HV| scattering component. Dihedral scattering due to small correlation lengths characterised by $|HH| > |VV|$, and/or diffuse scattering (|HV| contribution) affects the backscattered signal. Also, effects induced by the presence of vegetation cover can not be accounted for with surface scattering models. Both effects lead to a violation of the required conditions of most models and/or to biased estimation of the roughness and moisture parameters.

In order to extend the validity domain of the SPM, Hajnsek et al. (Hajnsek 2003) introduced a fully polarimetric coherent Extended Bragg scattering model (X-Bragg) to estimate both the cross-polarised scattering and the depolarisation effects. Assuming an azimuthally orientation angle induced by slope variations, the cross-polarized energy is obtained by applying a

rotation matrix on the Bragg coherency matrix [T] about β . As the depolarization effects are concerned, they are induced by a Bragg scattering slope distribution in the azimuth direction that assumes that the orientation angle presents a symmetrical distribution $p(\beta)$ of orientation angles about $\Theta = 0$ at the pixel-scale and which leads to the averaged Bragg coherency matrix [T]. In this type of model, it should be noticed that the roughness component introduced as an ancillary perturbation is given by the width of the distribution $p(\beta)$ which controls the polarimetric coherence as well as the amount of cross-polarized power. The simple model has been developed independent of any empirical relations and shows a good agreement between ground measured surface parameters and inverted parameters at L-band. Its simple handling and good inversion performance makes it a preferable model to be used for the estimation of soil moisture and surface roughness as input parameter for land surface process models.

In Figure 5.11 a simple sketch of the X-Bragg model is presented. The X-Bragg components are derived from the coherency matrix, where a uniform distribution of β is added in order to simulate the roughness component of a natural bare surface.

Polarimetric Surface Scattering Model Extended Bragg Model (X-Bragg)

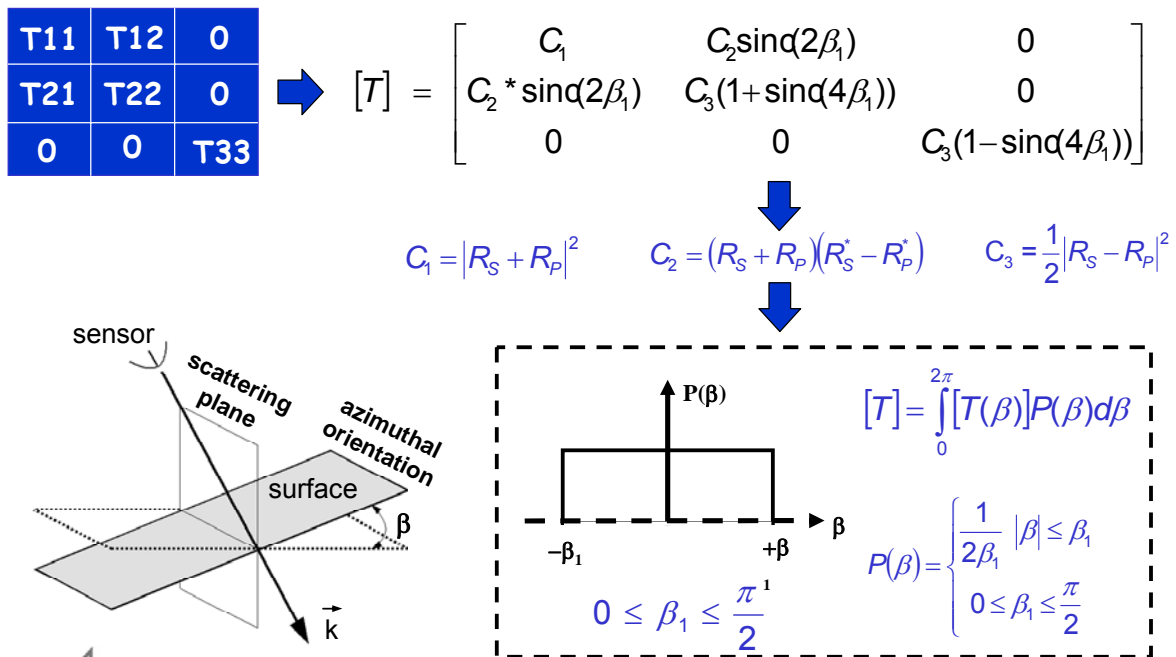
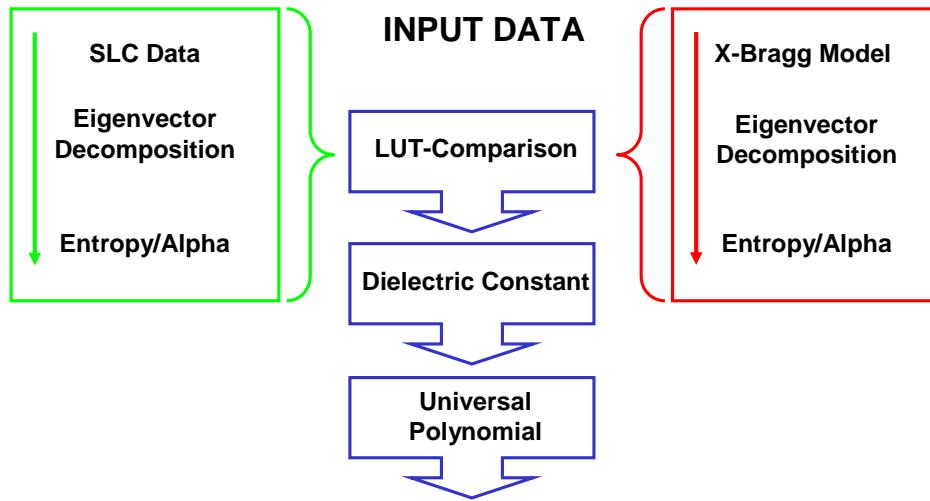


Figure 5.11: Simple sketch of the X-Bragg model.

The inversion of the X-Bragg model is done by introducing the eigenvector decomposition of the coherency matrix. In Figure 5.12 on the left side the experimental SAR data are processed to the polarimetric statistical parameters: the polarimetric entropy and alpha angle. On the right side also an eigenvector decomposition is performed on the coherency matrix of the X-Bragg model in order to derive the polarimetric parameters. The polarimetric parameters of the look up table and from the single look complex (SLC) data are compared, from which the dielectric constant is then derived. Using a uniform polynomial relation the dielectric constant can be converted to the volumetric soil moisture content.

Inversion Procedure X-Bragg



Soil Moisture Content

Figure 3.12: Workflow of the X-Bragg inversion procedure.

From the eigenvector decomposition three main statistical polarimetric parameters can be derived: the polarimetric entropy, the polarimetric alpha angle and the polarimetric anisotropy. The entropy and the alpha angle are used in a plot to distinguish different scattering regions. The most interesting region for surface parameter estimation is the low alpha angle area < 43 degrees and the low entropy region < 0.5 . In Figure 5.13 the entropy/alpha plot for the whole GABES scene is presented. The variation of the colours displays the intensity of pixels that are distributed within the scene. Red represents the highest intensity whereas blue the lowest intensity. In the left images the highest intensity is located at the lower entropy/alpha region in L-band. That means, that in the GABES scene a high contribution of surface scattering mechanisms is present. However, also high entropy/alpha areas can be observed. Which need to be excluded before the surface parameter estimation using the X-Bragg surface scattering model. On the right the contribution at the low entropy/alpha region is very small in C-band and therefore the amount of available areas, in which a surface parameter inversion can be performed, is very small. Hence, the inversion procedure described in figure 5.12 is applied on the GABES scene only in L-band.

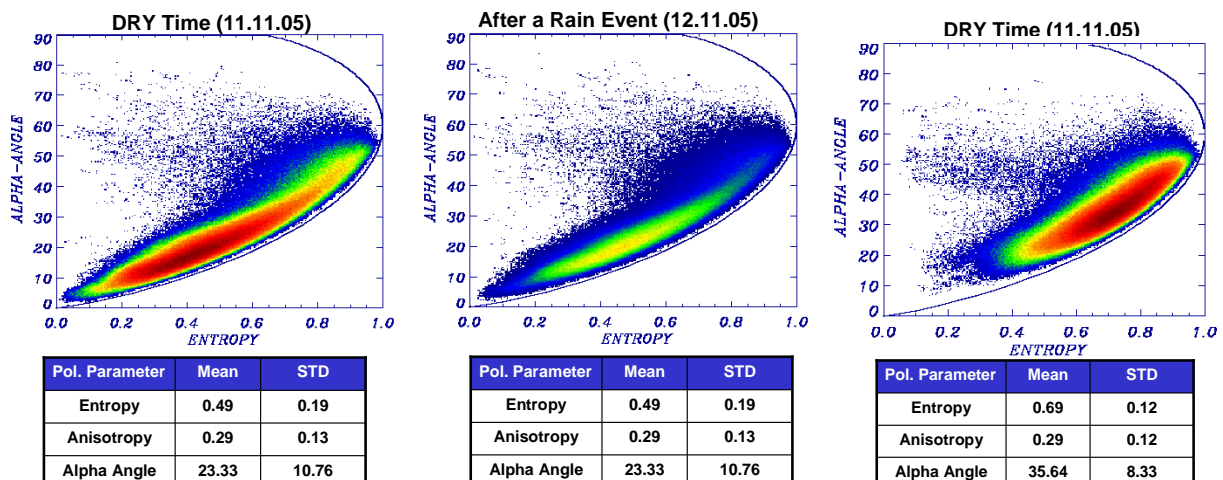


Figure 5.13: Entropy and alpha angle plot: Two left in L-band and right in C-band

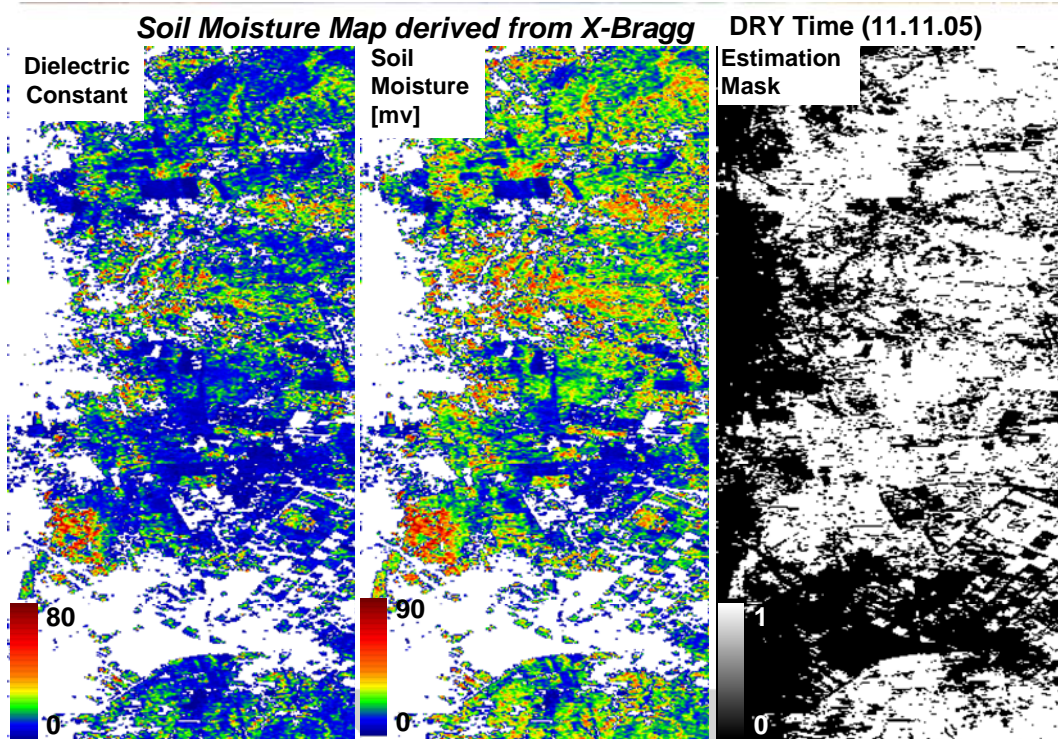


Figure 5.14: Inversion results of the X-Bragg model at L-band over the GABES scene (dielectric constant (real part), soil moisture (vol %), validity mask)

The inversion results of the GABES scene in L-band are presented in figure 5.14. A dielectric constant map, the soil moisture map and an estimation mask are displayed. The estimation map characterises the valid areas (white) that satisfy the validity range of the X-Bragg model and can be inverted. In figure 3.15 the same maps are displayed in C-band and the difference is clearly visible. Valid areas are much smaller and the derived soil moisture level seems higher.

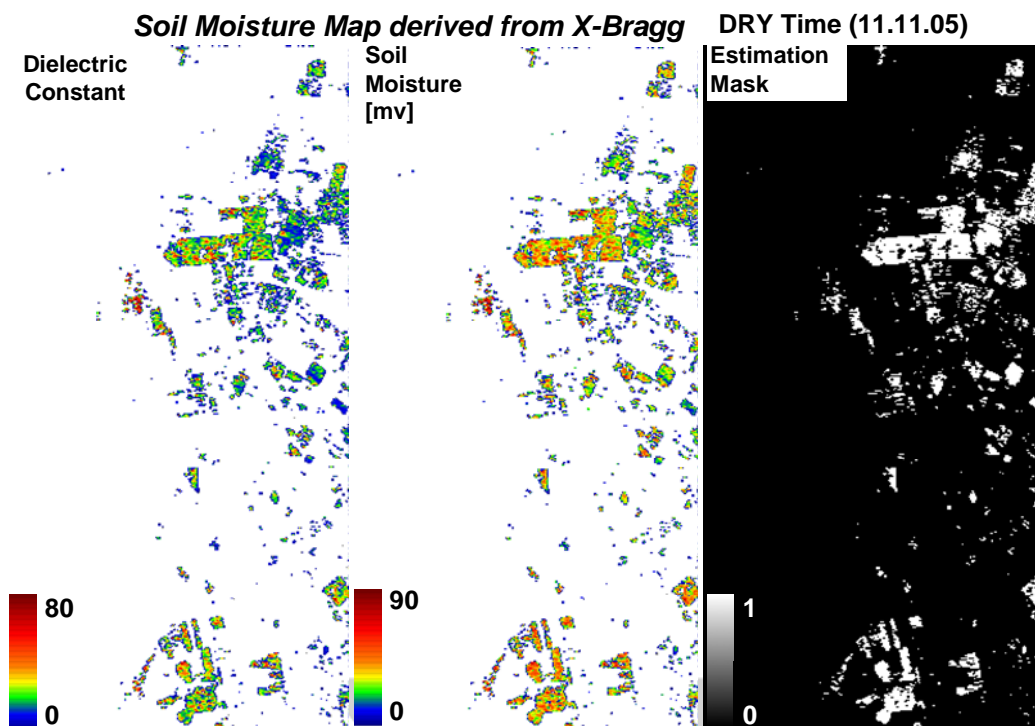


Figure 5.15: Inversion results of the X-Bragg model at C-band over the GABES scene.

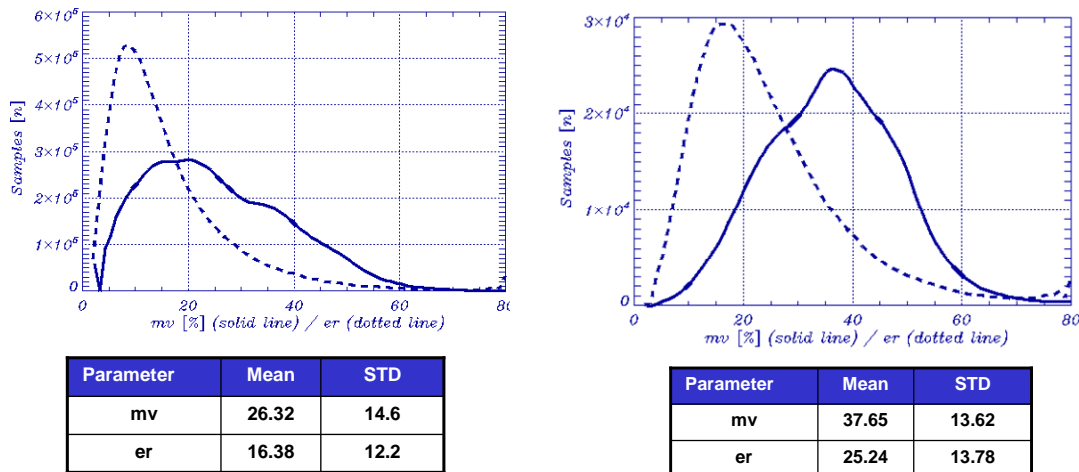


Figure 5.16: Histogram of the soil moisture distribution of the GABES scene – left in L-band and right C-band.

In Figure 5.16 the histogram of the dielectric constant and the soil moisture is presented: left for the inversion with L-band and right for the inversion with C-band. The mean value difference between both observations is around 10 vol %. The difference is high and arises probably from the fact that the amount of valid inversion points is much smaller for C-band to have a stable statistical observation.

Another aspect that has been observed and analysed is the rain event that appeared between two acquisitions. The difference in terms of soil moisture is displayed in figure 5.17, where on the right side the difference is derived. Blue areas represent a smaller difference, green, yellow or reddish areas with high soil moisture difference between two acquisition dates. Higher differences can be observed in the middle area of the scene either than on the lower part, where the main agricultural fields are present. This could mean that a small rain shower was located more in the upper part of the area, or that some fields, e.g. in the lower left, were irrigated.

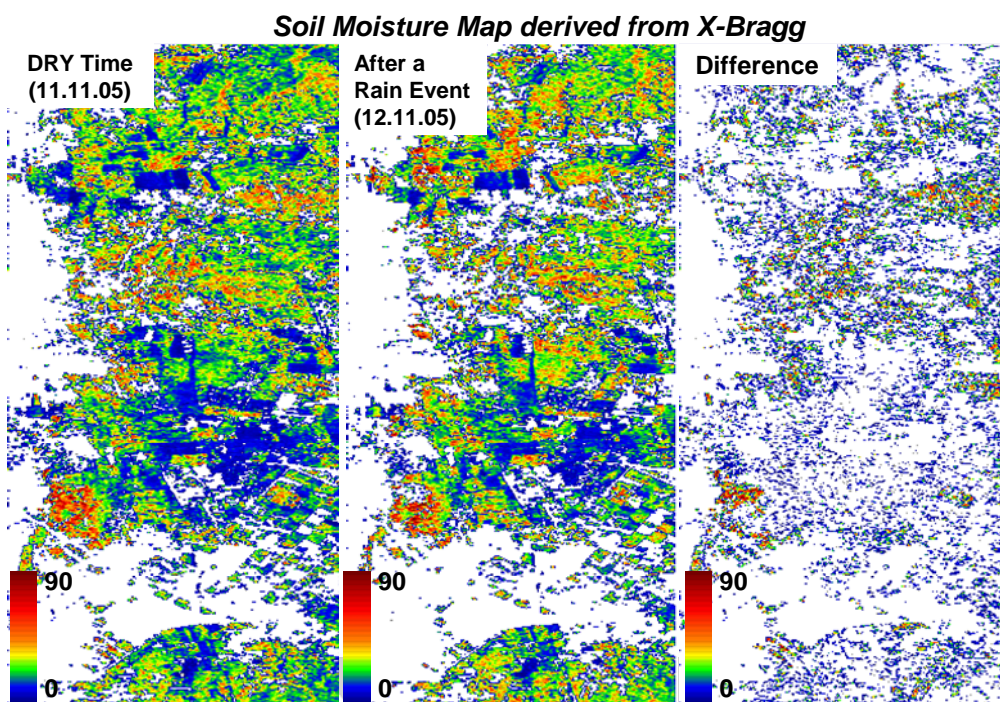


Figure 5.17: Soil moisture maps derived from the dry time and after the rain and the difference between both presented in terms of the soil moisture difference.

Inversion Result @ L-band – WEST - DRY

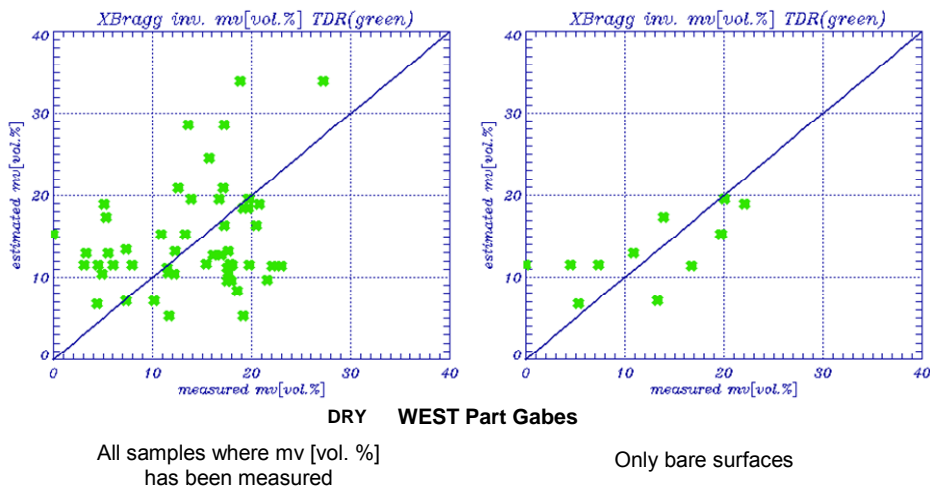


Figure 5.18: Comparison of estimated versus measured soil moisture (mv) – left: all 114 ground samples; right: only samples taken over the bare fields.

The validation of soil moisture estimates with ground measurements is an important task for the quantitative estimation and the accuracy of the model performance. The estimation accuracy, as an example for the GABES scene for all the 114 taken samples for vegetated and non vegetated fields is displayed in Figure 5.18 left plot. The standard deviation is high and some of the points do not match at all with the ground measurements. On the right side of Figure 5.18 only the samples taken over bare surfaces are displayed. Here a good agreement between the estimated with X-Bragg and the measured values is obtained. The standard deviation is very small and in the range of less than 5 vol. %. Only one sample is extremely out of range with measured soil moisture close to 0 vol. %. Here also a problem with the ground measured soil moisture can occur. Very low soil moisture values normally have higher error bars on the TDR measurement. In this case it could be that the soil moisture value is higher as presented. This reasoning has been confirmed by the ground team.

Overall it can be stated, that the soil moisture estimation shows a good agreement between the estimated and measured values over bare surface varying less than 5 vol. %.

Further investigations have been performed in order to be sure, that no influences are disturbing the validation results. Three main checks have been performed:

1. Noise level
2. Volume contribution over bare surfaces
3. Penetration depth

In principle, the noise level influences the soil moisture estimation in terms of increasing the level. The noise level was estimated using the cross polarisation difference (HV and VH) and was extracted from the last eigenvalues of the 4 dimensional coherency matrix. Then the polarimetric entropy, alpha angle and anisotropy were derived and plotted against the non filtered polarimetric parameters, see figure 5.19. The difference between both for all the three parameters is very small. The highest difference can be observed for anisotropy, which is mostly affected by noise due to the very low signal values. The same investigation was also made in C-band and here the difference is higher for all parameters, again being highest for anisotropy. In summary, the data used for investigation are not significantly affected by noise and therefore the noise correction can be neglected.

**Entropy / Alpha / Anisotropy
after noise filtering**

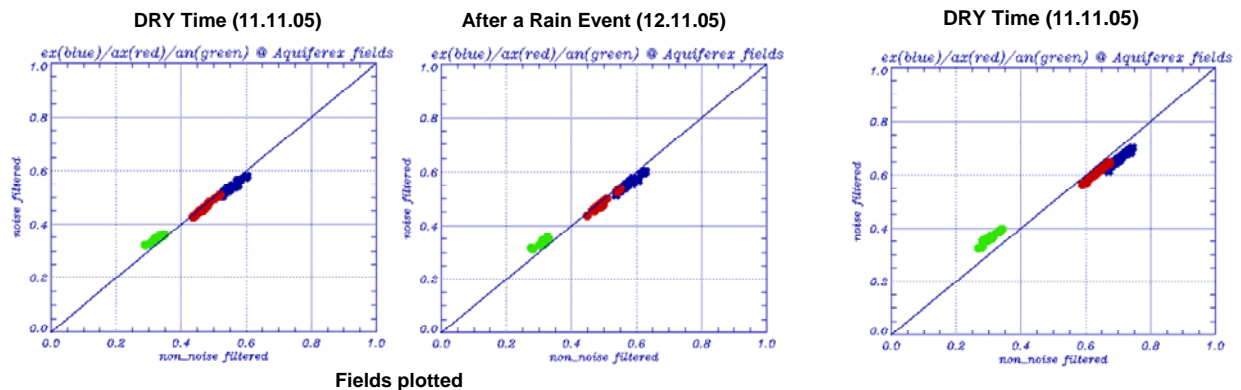


Figure 5.19: Statistical polarimetric parameters entropy, alpha angle and anisotropy over bare surfaces – left for L-band and right for C-band

The second investigation is going towards the idea, that volume contribution could disturb the inversion performance. The volume contribution is investigated that is introduced due to the bare surface. The very dry soil and its sandy composition potentially causes longer wavelengths to penetrate deeper into the soil as it has been measured with the Time Domain Reflectometry, where the deepest soil moisture measurements were made in 15 cm depth. The check is to investigate the cross polarisation contribution in dB. In figure 5.20 the level of cross polarisation is for some field lower than -20 dB which is already an indication of volume contribution.

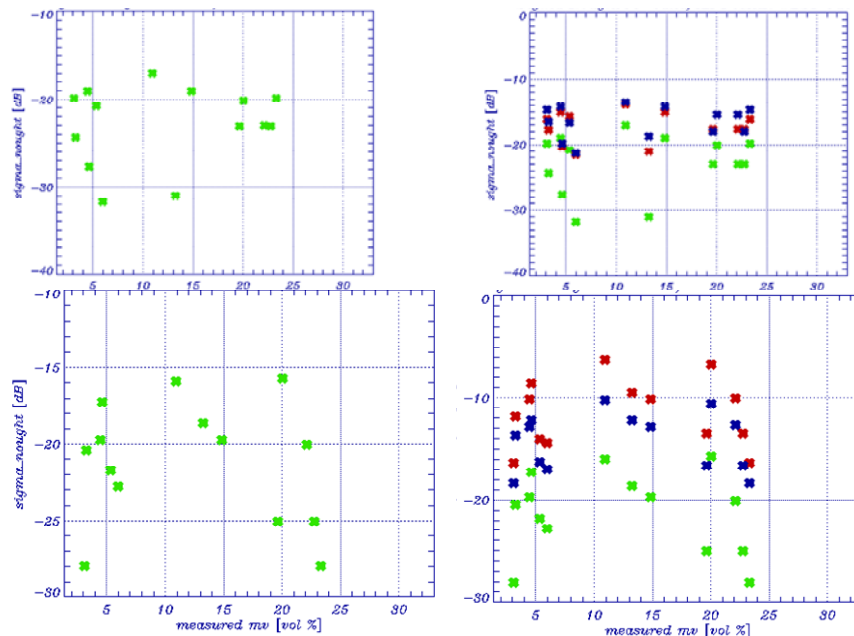


Figure 3.20: Backscattering intensity [dB] of the normalised cross polarisation (left: green (HV) only cross polarisation; right: blue (VV) and red (HH)) – first row in L-band and second row in C-band

The third step was to have a look to the penetration depth. It is expected that the penetration of the electromagnetic waves into the dry soil causes a volume scattering contribution. There are two methods how to estimate the penetration depth: One is to use the soil properties and calculate the imaginary part of the dielectric constant – corresponding to the absorption of the soil -in order to derive the penetration depth (Hallikainen et al. 1985). The results of this calculation are shown in Figure 5.21 for the L-band frequency. In Figure 5.22 the real part of

the dielectric constant and the derived penetration depth are presented. The results show that there are some fields where the penetration depth can reach values up to 36 cm and this mainly at the lower part of the GABES scene where ground measurements are available. This is already an indication, that L-band is penetrating deeper into the dry soil as ground measurements have been performed.

er' real part calculated with X-Bragg	ϵ'
er'' imaginary part calculated after Hallikainen	$\epsilon'' = 0.007 * er^2 + 0.858 * er - 0.0283$
penetration depth	$\delta\rho = \frac{\lambda\sqrt{\epsilon'}}{2\pi * \epsilon''}$

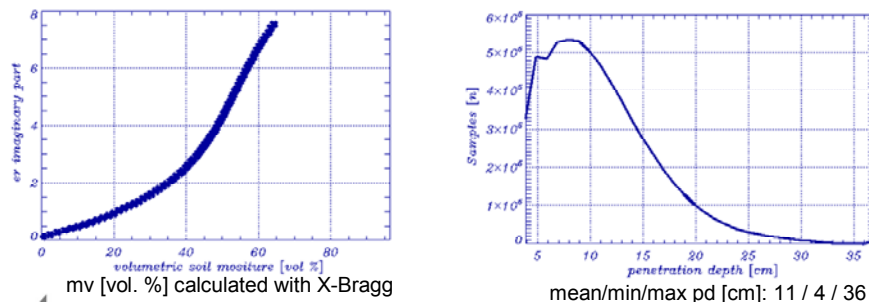


Figure 5.21: Penetration depth derivation after Hallikainen et al. at L-band

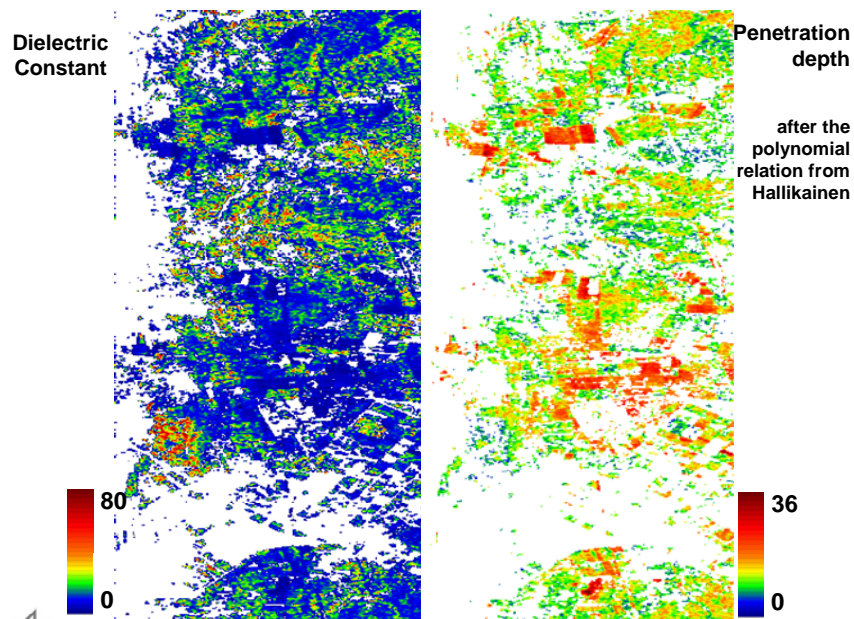


Figure 5.22: Penetration depth (left) dielectric constant and (right) penetration depth in [cm] after Hallikainen et al. of the GABES scene in L-band.

The other method to check the penetration depth is using the interferometric phase in order to observe height differences. For the GABES scene a small baseline was available for the estimation of the interferometric coherence and the interferometric phase using a corner reflector. The corner reflector is used as a reference estimate for the ground phase. If the ground phase is known the phase difference in the surrounding of the corner reflector has been estimated. Here four areas were selected, assigned with P1 to P4, as displayed in Figure 5.23. The phase difference is varying from 17 cm to 1.3 m. The location of the corner reflector is in the middle of the GABES scene and this means not very close to the agricultural fields. But still the phase difference values estimated give a good estimate of the soil condition

in this area.

L band (HH) InSAR Phase Difference

Frequency/ Polarisation (VV)	L Band Part1	L Band Part2	L Band Part3	L Band Part4
InSAR Coherence	0.88	0.88	0.93	0.91
Phase Difference	5.6	0.7	1.2	5.9
Phase Difference [m]	1.3	0.17	0.28	1.35

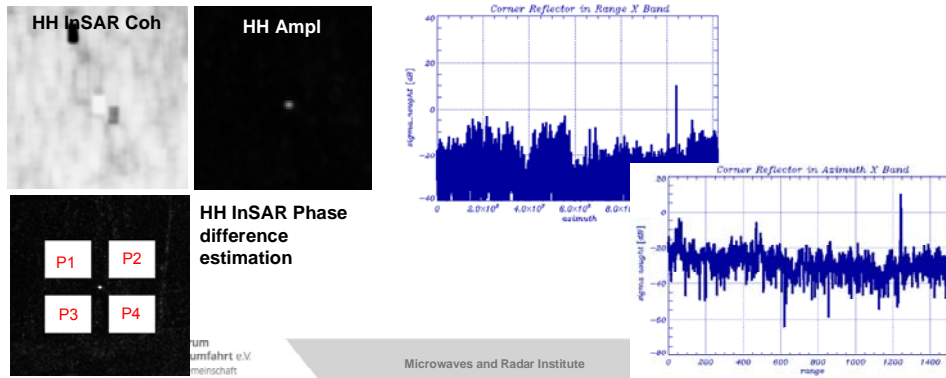


Figure 5.23: Results of the phase difference investigation using the interferometric observables in L-band close to a corner reflector, where the ground phase is known.

The dry sandy soil allows deeper penetration than areas in central Europe and this also needs to be accounted for. Because of the penetration higher volume contributions are obtained and in this case other models need to be used if the dielectric constant is the main propose of investigation. The good performance on the validation points is attributed to the fact that these measurement points are located within the validity region for the X-Bragg model (see Fig. 5.9). The final result in terms of a soil moisture map derived from L-band can be displayed in a geographical information tool, as for example in Figure 5.24 where it has been done in ARC MAP.

Visualisation of Soil Moisture Map in ARC MAP

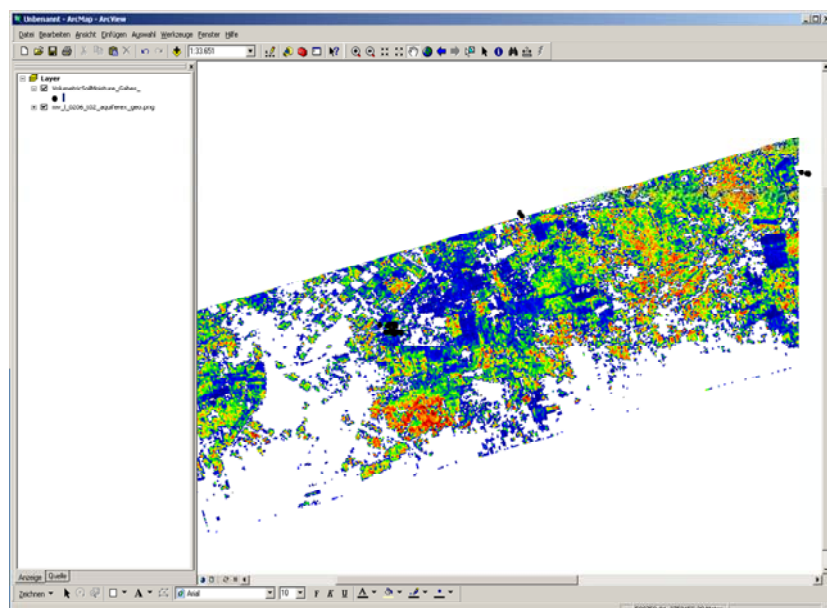


Figure 5.24: A geocoded soil moisture map represented in GIS tool – ARC MAP.

5.4 Polarimetric Classification

The polarimetric unsupervised classification is a good tool to differentiate features within a scene. In this chapter we used already existing tools for classification purposes in order to test their ability for feature discrimination.

One of the established tools for classification of polarimetric SAR data is the Wishart classifier based on second order statistics of the coherency matrix, where the polarimetric statistical parameters (entropy/alpha/anisotropy) are used to initialise the maximum likelihood classification procedure. The classification procedure is a part of the POLSARPRO 2.0 software that ESA distributes free of charge to scientists. This tool has been used to generate the classification result shown in Figure 5.25. In forehand of the classification the polarimetrically refined Lee filter has been applied with a window size of 7.

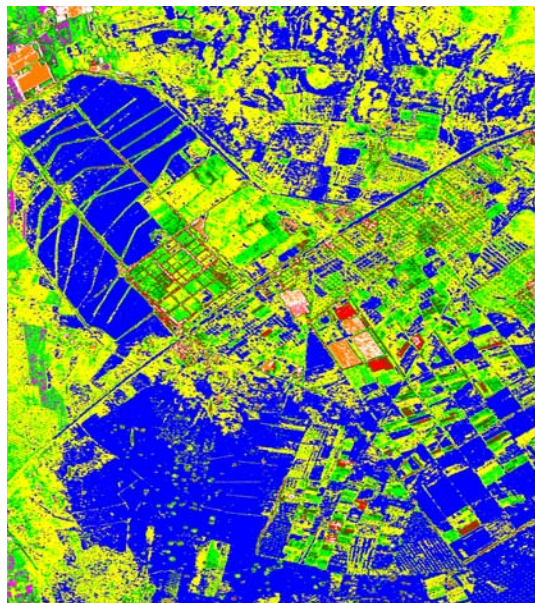


Figure 5.25: H/alpha angle Wishart classification of South-West Gabès area based on polarimetric L-band data using POLSARPRO 2.0.

Comparison with land use data acquired during the campaign and documented in the Ground Measurement GIS revealed the land use classes given in Table 5.1.

Table 5.1: Land cover /land use classes for Gabès.

Colour	Land cover / land use
	non cultivated bare soil
	ploughed or harvested fields & alfalfa
	fresh cultivated fields & alfalfa
	mature crops (carrots & gombo), trees
	high vegetation, trees
	no ground truth
	no ground truth
	ploughed fields

Land use protocols were taken in the lower middle part of Figure 5.25. Note that due to the high change of incidence angle within an airborne SAR acquisition the same land use may map into different classes/colours in this classification. For example the yellow and green areas on the left of Fig 5.25. (steep incidence angle) may not be cultivated land. The

consideration of changing incidence angles in the classification of airborne SAR images is not solved satisfactorily at present. However, for a spaceborne geometry the incidence angle changes only slightly and negligible effects are expected. This will allow reliable polarimetric classification over much wider areas compared to the airborne case.

5.5 References

- Beckmann, P. & Spizzichino A., 'The Scattering of Electromagnetic Waves from Rough Surfaces', Oxford: Pergamon, Reprinted 1978 by Artech House Inc., Norwood, Massachusetts, USA, p. 503, 1963.
- Chen, K.S., Wu, T.D., Tsay, M.K. & Fung, A. K., 'A Note on the Multiple Scattering in an IEM Model', IEEE Transactions on Geoscience and Remote Sensing, vol. 38, no. 1, pp. 249-256, 2000.
- Chen, M. F. & Fung, A. K., 'A Numerical Study of the Regions of Validity of the Kirchhoff and Small-Perturbation Rough Scattering Models', IEEE Transactions on Geoscience and Remote Sensing, vol. 23, no. 2, pp. 163-170, 1988.
- Dubois, P.C., J. J. van Zyl, and T. Engman, 'Measuring soil moisture with imaging radars,' IEEE Trans. Geosci. Remote Sensing, vol. 33, pp. 915-926, 1995.
- Fung, A.K., 'Microwave Scattering and Emission Models and their Application,' Norwood, MA Artech House, Remote Sensing Library, 1994.
- Fung, A.K., and K. S. Chen, 'Dependence of the surface backscattering coefficients on roughness, frequency and polarization states,' International Journal of Remote Sensing, vol. 13, pp. 1663-1680, 1992.
- Hallikainen, M.T.; Ulaby, F.T.; Dobson, M.C.; El-Rayes, M.A.; Lil-Kun Wu; Microwave Dielectric Behavior of Wet Soil-Part 1: Empirical Models and Experimental Observations IEEE Transactions on Geoscience and Remote Sensing, Volume GE-23, Issue 1, Jan. 1985
Page(s):25 - 34
- Hajnsek, I. & Cloude, S., 'The Potential of InSAR for Quantitative Surface Parameter Estimation' Can. J. Remote Sensing, vol. 31, no.1, pp. 85-102, 2005
- Hajnsek, I., 'Inversion of Surface Parameters Using Polarimetric SAR', DLR-Science Report, vol. 30, ISSN 1434-8454, p. 224, 2001.
- Hajnsek, I., Alvarez-Perez, J.L., Papathanassiou, K.P., Moreira, A. and Cloude, S.R., 'Surface Parameter Estimation Using Interferometric Coherences at Different Polarizations', ESA/ESRIN Workshop on PolinSAR, January 2003, p.6, 2003.
- Hajnsek, I., E. Pottier, and S. R. Cloude, 'Inversion of surface parameters from polarimetric SAR,' IEEE Trans. Geosci. Remote Sensing, vol. 41, pp. 727-744, 2003.
- Hajnsek, I., Papathanassiou, K. P. & Cloude, S. R., 'Surface Parameter Estimation Using fully polarimetric L- and P-band Radar data', Proc. 3rd International Symposium, 'Retrieval of Bio-Geophysical Parameters from SAR Data for Land Applications', 11-14 Sept. 2001, Sheffield, UK, ESA SP-475, January 2002, pp. 159-164
- Hajnsek, I., Papathanassiou, K. P. & Cloude, S. R., 'Surface Parameter Estimation Using fully polarimetric L- and P-band Radar data', Proc. 3rd International Symposium, 'Retrieval of Bio-Geophysical Parameters from SAR Data for Land Applications', 11-14 Sept. 2001, Sheffield, UK, ESA SP-475, January 2002, pp. 159-164
- Hajnsek, I., S. Cloude, 'Differential Extinction Estimation over Agricultural Vegetation from Pol-InSAR', Proceedings of ESA Workshop on Applications of SAR Polarimetry and Polarimetric Interferometry, PolinSAR 2005, Frascati, p. 6.
- Lee, J. S., D. L. Schuler & T. L. Ainsworth, 'Polarimetric SAR Data Compensation for Terrain Azimuth Slope Variation', IEEE Transactions on Geoscience and Remote Sensing, vol. 38, no. 5, part I, pp. 2153-2163, 2000.
- Oh, Y., 'Quantitative retrieval of soil moisture content and surface roughness from multipolarized radar observations of bare soil surfaces,' IEEE Trans. Geosci. Remote Sensing, vol.42, pp. 596-601, 2004.
- Oh, Y., K. Sarabandi, and F. T. Ulaby, 'An empirical model and an inversion technique for radar scattering from bare soil surfaces,' IEEE Trans. Geosci. Remote Sensing, vol. 30, pp. 370-381, 1992.

- Oh, Y., K. Sarabandi, and F. T. Ulaby, 'An inversion algorithm to retrieve soil moisture and surface roughness estimation from polarimetric radar observation,' Proceedings of IGARSS94, Pasadena, pp. 1582-1584, 1994.
- Oh, Y., K. Sarabandi, and F. T. Ulaby, 'Semi-empirical model of the ensemble-averaged differential Mueller matrix for microwave backscattering from bare soil surfaces,' IEEE Trans. Geosci. Remote Sensing, vol. 40, pp. 1348-1355, 2002.

6 SUMMARY & CONCLUSIONS

With the AquiferEx project a data base of high resolution optical (hyperspectral) and radar (multi-frequency and polarisation) data has been acquired, for areas typical of semi-arid regions covering a huge variety of land use and irrigation practise. This data base is complemented by a variety of ground measurements and several satellite data acquisitions. Initial soil moisture and classification results demonstrate that high resolution radar sensors are able to provide relevant information for national authorities to help the management of water resources in arid regions, which is one of the most challenging tasks in African countries. The further use of the acquired airborne data and the synergy with satellite data will further be investigated in the frame of Aquifer and follow-on projects.

In the following specific conclusions are summarised:

Campaign Preparation & Data Acquisition

Almost one year was allocated for campaign preparation. Besides successful integration, certification & test of AVIS-2 in the DLR aircraft, a-priori visits were conducted to Tunisian organisations (DGRE, OSS) and to local authorities and institutes (CRDA & IRA) working in the areas where the test sites were located. The a-priori harmonization with the in-situ partners and the close cooperation with the Aquifer project team (especially GAF & VISTA) paved the way for a smooth campaign, without any delays in data acquisition. Thus a high quality data set could be acquired for both test sites – Ben Gardane (clear sky) & Gabès (with some clouds) -, accompanied by time synchronous ground measurements.

Data Processing

Data processing and calibration has been performed without difficulties. The georeferencing for E-SAR and AVIS data was performed onto the same grid to allow exact reference (overlay) of the two data sets. Auxilliary information (DEMs derived from the X-band SAR data and incidence angle maps) complement the data set. The ground measurements (including the soil moisture samples of ITC) were compiled into a GIS including browse images of the acquired optical and radar data. A full featured version for ArcGIS 9.1 and a version for the free ArcExplorer 2.2 were generated.

With respect to E-SAR processing two points can be highlighted:

- Extension of the E-SAR processor to accomodate variable AGC settings along azimuth (as operated for Gabes test site). This ensured good SNR even in areas of high contrast backscatter within a scene. This feature proved important for surface parameter extraction as described in section 5.
- Combination of 2 dual-polarized data sets in C-band to generate a synthetic quad-pol product. This is possible because of the precise repeat-pass processing chain implemented for E-SAR data. In the context of AquiferEx it allowed for the first time (at least with E-SAR data) the investigation of surface parameter retrieval from C-band polarimetric data in comparison with L-band.

Radar Data Investigations for Surface Parameters

The GABES scene was investigated for surface parameter estimation with the main focus on volumetric soil moisture estimation. Polarimetric investigation has been done for L- and C-band in terms of the sensitivity to soil moisture estimation. Then the polarimetric SAR data were used and inverted with the X-Bragg model and the results were discussed. The best results have been obtained using L-band data over pure bare surfaces. The validation to ground measurements showed a high correlation with a deviation of less than 5 vol. %.

However, despite of the good results some data checks were performed in order to

understand the high percentage of not valid areas that could not be inverted. For this reason the SNR of the data were investigated. The SNR of the data showed high quality even over low backscattering signal regions. This is attributed to the manual receiver gain adjustments performed during data acquisition (see section 4.1.2). The penetration depths were investigated using the Hallikainen approach and the interferometric phase difference. Both indicated that penetration into the dry sandy soil occurs. The conclusion of this is that the soil moisture measured on ground for validation purposes was probably not measured deep enough. The interferometric phase difference indicated the location of the phase center being up to 1.2 m deep in the soil. The deepest ground measurements were made at 15 cm. A comparison or validation in this case is not necessarily possible. It is suggested for dry sandy soil to measure soil moisture in higher depths. For convenience it is suggested to use ground penetrating radars for soil moisture estimation. Therefore the data acquired by the ITC team in the frame of AquiferEx (GPR data and further soil moisture measurements) should further be used to push the research in this area.

Polarimetric Classification with POLSARPRO

To exemplify the power of recent SW developments performed at ESA, a classification based on polarimetric L-band data has been performed for the SW part of Gabes test site. As the POLSARPRO SW is available free of cost to the geoscience community, other AquiferEx data sets can similarly be investigated.

Practical considerations for future investigations

As only limited investigations of the acquired data could be performed within the AquiferEx contract there are several other analysis currently being performed or waiting to be addressed in the frame of further research:

- Combined use optical and radar data: This is an ongoing task in the frame of the Aquifer project. Refined Land-Use maps were generated by VISTA and presented to Tunisian project partners.
- Use of optical and radar data for desertification studies - Subject of a diploma thesis at the University of Munich (LMU).
- Combined use of soil moisture samples, GPR and airborne SAR measurements. This topic has been suggested by ITC team and research is in progress.
- Investigation on parameter retrieval by Pol-InSAR data. Suitable repeat-pass data tracks have been acquired in L-band for both test sites, and their information content has not been explored yet.
- Comparison and combination with space-borne data. This task has partially been performed in the frame of Aquifer, especially relative to CHRIS and AVIS, but additional investigations relative to the dual-polarimetric data sets acquired by ASAR and E-SAR could be addressed.

One of the interesting practical outcomes is that there is a strong indication that regular high resolution data taken combined with soil moisture estimated from this data could be used to monitor land use and irrigation practice, even on a field level. However, present day satellite sensors do not provide this high resolution (especially for the small scale field sizes experienced in Tunisia) and concerning SAR, they are also restricted in terms of polarimetric characteristics. In this sense the AquiferEx data set is a first demonstration of the future potential of high resolution remote sensing for semi-arid regions. It is a base data set to develop new applications to better meet the local user needs.

7 ACKNOWLEDGEMENTS

The project team acknowledges the support of Tunisian authorities for campaign approval and preparation (embassy & involved ministries, especially DGRE, CNT, CERT, OSS), Djerba airport handling agency KARS for logistics matters, as well as DGRE and the local institutions (CRDA in Gabès and Medenine, & IRA in Medenine) for providing support to ground measurements. Special thanks to the Aquifer project (especially GAF and VISTA) for supporting the project in all respects and for providing the satellite data for the campaign preparation.

8 ANNEX 1: AIRBORNE RADAR DATA SUMMARY

The AquiferEx project acquired, processed, and delivered the following airborne radar data products of the E-SAR sensor of DLR-HR (RGI – radar geometry images incl. single-look-complex; GTC- geocoded terrain corrected data, **DEM – digital elevation model**)

Ben Gardane (Data acquisition on November, 9)

Name	Band	Pol.	Segm.	RGI	GTC	RP Interf.	Remarks
Northern Part							
05aqifer0101x1_t02	C	vh/vv	NE	x	x	-	
05aqifer0102x1_t02	C	vh/vv	NW	x	x	-	
05aqifer0103x1_t02	C	hv/hh	NE	x	x	-	
05aqifer0104x1_t02	C	hv/hh	NW	x	x	-	
05aqifer0105x1_t02	L	full	NE	x	x	Master, NE	
05aqifer0106x1_t02	L	full	NW	x	x	Master, NW	
05aqifer0107x1_t02	L	full	NE	x	-	Slave, 0m, NE	
05aqifer0108x1_t02	L	full	NW	x	-	Slave, 0m, NW	
05aqifer0109x1_t02	X	VV	NW	x	x	-	
05aqifer0110x1_t02	X	VV	NE	x	x	-	
Southern Part							
05aqifer0101x1_t03	C	vh/vv	SE	x	x	-	
05aqifer0102x1_t03	C	vh/vv	SW	x	x	-	
05aqifer0103x1_t03	C	hv/hh	SE	x	x	-	
05aqifer0104x1_t03	C	hv/hh	SW	x	x	-	
05aqifer0105x1_t03	L	full	SE	x	x	Master, SE	
05aqifer0106x1_t03	L	full	SW	x	x	Master, SW	
05aqifer0107x1_t03	L	full	SE	x	-	Slave, 0m, SE	
05aqifer0108x1_t03	L	full	SW	x	-	Slave, 0m, SW	
05aqifer0109x1_t03	X	VV	SW	x	x	-	
05aqifer0110x1_t03	X	VV	SE	x	x	-	

Gabès test site (Data acquisition on November, 11 and 12)

Name	Band	Pol.	Segm.	RGI	GTC	RP Interf.	Remarks
Western Part							
05aqifer0201x1_t02	C	vh/vv	NW	-	-	-	sub-optimum AGC
05aqifer0202x1_t02	C	vh/vv	SW	x	x	-	
05aqifer0203x1_t02	C	vh/vv	NW	x	x	-	
05aqifer0204x1_t02	C	hv/hh	SW	x	x	-	
05aqifer0205x1_t02	C	hv/hh	NW	x	x	-	
05aqifer0206x1_t02	L	full	SW	x	x	Master, SW	
05aqifer0207x1_t02	L	full	NW	-	-	Master, NW	raw data corrupt
05aqifer0208x1_t02	L	full	SW	x	-	Slave, 60m, SW	
05aqifer0209x1_t02	L	full	NW	-	-	Slave, 15m, NW	needs 0207
05aqifer0210x1_t02	L	full	SW	x	-	Slave, 0m, SW	
05aqifer0301x1_t02	X	VV	SW	x	x	-	redundancy
05aqifer0302x1_t02	X	VV	NW	x	x	-	
05aqifer0303x1_t02	X	VV	SW	x	x	-	
05aqifer0304x1_t02	C	hv/hh	NW	x	x	-	
05aqifer0305x1_t02	L	full	SW	x	-	Slave, 0m, 1 Day, SW	75m vertical bl
05aqifer0306x1_t02	L	full	NW	-	-	Slave, 0m, 1 Day, NW	needs 0207 75m vertical bl
05aqifer0307x1_t02	L	full	SW	x	-	Slave, 15m, 1 Day, SW	75m vertical bl
Eastern Part							
05aqifer0201x1_t13	C	vh/vv	NE	-	-	-	sub-optimum AGC
05aqifer0202x1_t13	C	vh/vv	SE	x	x	-	
05aqifer0203x1_t13	C	vh/vv	NE	x	x	-	
05aqifer0204x1_t13	C	hv/hh	SE	x	x	-	
05aqifer0205x1_t13	C	hv/hh	NE	x	x	-	
05aqifer0206x1_t13	L	full	SE	x	x	Master, SE	
05aqifer0207x1_t13	L	full	NE	-	-	Master, NE	raw data corrupt

05aqifer0208x1_t03	L	full	SE	x	-	Slave, 60m, SE	
05aqifer0209x1_t03	L	full	NE	-	-	Slave, 15m, NE	needs 0207
05aqifer0210x1_t03	L	full	SE	x	-	Slave, 0m, SE	
05aqifer0301x1_t13	X	VV	SE	x	x	-	redundancy
05aqifer0302x1_t13	X	VV	NE	x	x	-	
05aqifer0303x1_t13	X	VV	SE	x	x	-	
05aqifer0304x1_t13	C	hv/hh	NE	x	x	-	
05aqifer0305x1_t03	L	full	SE	x	-	Slave, 0m, 1 Day, SE	75m vertical bl
05aqifer0306x1_t03	L	full	NE	-	-	Slave, 0m, 1 Day, NE	needs 0207 75m vertical bl
05aqifer0307x1_t03	L	full	SE	x	-	Slave, 15m, 1 Day, SE	75m vertical bl

Note:

Data sets 0201 and 0301 were not processed, whereas data set 0207 is delivered because it is the MASTER for two other data sets, although part of this data set 0207 is not polarimetric.

Due to manual receiver gain changes during data acquisition, the Gabès data sets have different calibration offsets. These offsets are summarized in the table below (see next page).

Gabès data radiometric calibration offsets

Scene Id	Frequency-Band	Cal. Offset	confirmed on CR	Remarks
0201	C (VH-VV)	4	ne	NW + NE
0202	C (VH-VV)	- 1	- 3	SW + SE
0203	C (VH-VV)	+ 1	+1	NW + NE
0204	C (HV-HH)	- 4	- 5	SW + SE
0205	C (HV-HH)	+ 7	+ 7	NW + NE
0206_t02	L - PM	0	-1	SW + SE
0206_t13	L - PM	2	+2	SW + SE
0207_t02(*)	L - PM	0	0	NW + NE
0207_t13(*)	L - PM	-8	0	NW + NE
0208_t02	L - PM	0	- 2	SW + SE
0208_t13	L - PM	0	- 2	SW + SE
0209_t02	L - PM	10	+10	NW + NE
0209_t13	L - PM	0	-1	NW + NE
0210_t02	L - PM	0	??	SW + SE
0210_t13	L - PM	0	??	SW + SE
0301	X - VV	+ 9	+ 11	SW + SE
0302	X - VV	- 2	- 2	NW + NE
0303	X - VV	+ 6	+ 9	SW + SE
0304	C (HV - HH)	+ 7	+ 7	NW + NE
0305_t02	L - PM	0	0	SW + SE
0305_t13	L - PM	2	+3	SW + SE
0306_t02	L - PM	11	+11	NW + NE
0306_t13	L - PM	0	??	NW + NE
0307_t02	L - PM	0	0	SW + SE
0307_t13	L - PM	2	ne	SW + SE

The cal-offset must be added to the data!!

Example: For 0209_t02 the calibration factor becomes -50dB instead of the nominal -60dB.

cal_offset=-dAGC(range_lines_skip) (for L-band)

Cal_offset=-dAGC_end (for X- and C-band)

(*) Data take 0207 is with errors (partly single channel acquisition only). Radiometry & Polarimetry are not reliable in this case.

9 ANNEX 2: AIRBORNE AVIS DATA SUMMARY

The AquiferEx project acquired, processed, and delivered the following airborne hyperspectral data products of the AVIS-2 sensor of the University of Munich (LMU/gtco).

Aquisition Area:	BEN GARDANE			
Filename	BG11_091105	BG-12_091105	BG10_091105	
Flight Line	11	-12	10	
Acquisition date	09.11.2005	09.11.2005	09.11.2005	
Acquisition time [UTC]	11:07 - 11:13	11:20 - 11:26	11:31 - 11:37	
Aircraft altitude [m MSL]	3020	3020	3020	
Coordinate Upper left corner (middle of the pixel)	RW	685408.75558	682133.02135	683272.86073
	HW	3681458.11898	3681010.13566	3684686.57922
Number of lines	3675	4266	4252	
Number of columns	984	1077	1077	

Aquisition Area:	GABES I (first flight)			GABES II (second flight)	
Filename	GA-12_111105M	GA11_111105M	GA-10_111105M	GA-10_121105M	
Flight Line	-12	11	-10	-10	
Acquisition date	11.11.2005	11.11.2005	11.11.2005	12.11.2005	
Acquisition time [UTC]	10:32 - 10:37	10:43 - 10:48	10:55 - 11:00	14:03 - 14:08	
Aircraft altitude [m MSL]	3230	3230	3230	3160	
Coordinate Upper left corner (middle of the pixel)	RW	575157.82713	579611.66075	575479.18156	575554.96310
	HW	3759215.31077	3757228.49796	3757395.18106	3757468.66793
Number of lines	1671	1662	1575	1618	
Number of columns	4031	4142	4037	4024	

The corresponding incident angle-files have the same size and the extension *_IA.LIN (incident angle). AVIS data are provided as binary and in *.bmp format. A freelook-program is also included.

10 ANNEX 3: SPACEBORNE DATA SUMMARY

During the time frame of AquiferEx data acquisition, also space-borne data have been ordered by the Aquifer consortium, covering the AquiferEx test sites. ASAR data are available via GAF, whereas CHRIS data via VISTA.

Mission (Sensor)	Acquisition Dates / Orbit / Track / Frames	Acquisition Mode	Remarks
ENVISAT (ASAR)	18. 11. 2005 / 19443 / 351 / 2925	Swath I2; AP (HH-HV)	Inc. angle 19.2° - 26.7°
ERS-2 (SAR)	18. 11. 2005	VV-pol.	Inc. angle 23°
ENVISAT (ASAR)	28. 11. 2005 / 19586 / 494 / ...	Swath I7; AP (HH-VV)	Inc. angle 42,5° - 45,2°
ENVISAT (ASAR)	30. 12. 2005 / 20044 / 451 / 2943-2961	Swath I7; AP (HH-HV)	Inc. angle 42,5° - 45,2°
Proba (CHRIS)	23. 10. 2005	Mode 3	10x10km; north part
Proba (CHRIS)	31. 10. 2005	Mode 3	10x10 km; south part
AlSat-1	17. 10. & 02. 11. 2005		~600x600km footprint

Table A9.1: Scheduled satellite data acquisition for Ben Gardane test site (all radar data descending)

Mission (Sensor)	Acquisition Dates / Orbit / Track / Frames	Acquisition Mode	Remarks
ENVISAT (ASAR)	15. 11. 2005 / 19400 / 308 / 2943	Swath I2; AP (HH-HV)	Inc. angle 19.2° - 26.7°
ERS-2 (SAR)	15. 11. 2005	VV-pol.	Inc. angle 23°
ENVISAT (ASAR)	25. 11. 2005 / 19543 / 451 / ...	Swath I7; AP (HH-VV)	Inc. angle 42,5° - 45,2°
ENVISAT (ASAR)	02. 01. 2006 / 20087 / 494 / 2925-2943	Swath I7; AP (HH-HV)	Inc. angle 42,5° - 45,2°
Proba (CHRIS)	01. 11. 2005	Mode 3	10x10km; east part
Proba (CHRIS)	09. 11. 2005	Mode 3	10x10km; west part
AlSat-1	17. 10. & 02. 11. 2005		~600x600km footprint

Table A9.2: Scheduled satellite data acquisition for Gabes test site (all radar data descending)



11 CONTACTS

<p>ESA Technical Officer Remo Bianchi European Space Agency/Agence Spatiale Européenne Mission Experts Division ESRIN. Italy phone: +39 (06) 9418 0405 fax: +39 (06) 9418 0402 email: remo.bianchi@esa.int Web: http://www.esa.int</p>	<p>Project Lead & Radar Data Processing Rolf Scheiber German Aerospace Center Microwaves and Radar Institute (HR) Department SAR Technology PO Box 1116. 82230 Wessling. Germany Phone:+49 (0)8153 28 23 19 Fax: +49 (0)8153 28 14 49 Email: rolf.scheiber@dlr.de Web: http://www.dlr.de/HR</p>
<p>Project Partner GTCO – Ground Measurements Natascha Oppelt University of Munich LMU Dept. for Earth and Environmental Sciences. Section Geography Luisenstraße 37. 80333 München. Germany Phone.: +49 89 2180 6694 Fax.: +49 89 2180 6675 Email: N.Oppelt@iggf.geo.uni-muenchen.de Web: http://www.geographie.uni-muenchen.de/gtco/Produkte/produkte1.htm</p>	<p>Project Partner GTCO Wolfram Mauser University of Munich LMU Dept. for Earth and Environmental Sciences. Section Geography Luisenstraße 37. 80333 München. Germany Phone.: +49 89 2180 6674 Fax.: +49 89 2180 6675 Email: W.Mauser@iggf.geo.uni-muenchen.de Web: http://www.geographie.uni-muenchen.de/gtco/Produkte/produkte1.htm</p>
<p>HR Coordinator - E-SAR System Operator Ralf Horn German Aerospace Center Microwaves and Radar Institute (HR) Department SAR Technology Phone:+49 (0)8153 28 23 84 Faxsimile: +49 (0)8153 28 1449 Email: ralf.horn@dlr.de Web: http://www.dlr.de/HR</p>	<p>Scientific Radar Data Evaluation Irena Hajsek German Aerospace Center Microwaves and Radar Institute (HR) Department SAR Technology Phone:+49 (0)8153 28 23 63 Faxsimile: +49 (0)8153 28 1132 Email: irena.hajsek@dlr.de Web: http://www.dlr.de/HR</p>

<p>GAF AG Stefan Saradeth Project manager "Aquifer" Arnulfstr. 197 80634 München. Germany Tel.: +49 (0)89 121528-39 Fax: +49 (0)89 121528-79 Email: saradeth@gaf.de Web: http://www.gaf.de</p>	<p>VISTA Geowissenschaftliche Fernerkundung GmbH Heike Bach "Aquifer" project partner Gabelsbergerstr. 51 80333 München. Germany Tel.: +49 (0)89 523 89 802 Fax: +49 (0)89 523 89 804 Email: bach@vista-geo.de Web: http://www.vista-geo.de</p>
<p>CNT - TUNISIA Bacha SINAN Sous-Directeur des Applications des Techniques Nouvelles Centre National de Télédétection BP 200 - 1080 Tunis Cédexdirection Siège: Route de la Marsa (km9) 2040 El Aouina Tel.: +216 71 761 333 Fax: +216 71 760 890 Email: cnt.dg@cnt.nat.tn Web : http://www.cnt.nat.tn/</p>	<p>Ministry - TUNISIA Mekki HAMZA Directeur Général & Brahim Ben Baccar Directeur Eaux Souterraines Direction Générale des Ressources en Eau Ministère de l'Agriculture 43 rue de la Manoubia 1008 Tunis. Tunisie Tel: + 216 71 493452 Fax : + 216 71 391549 Email: Ben_Baccar@yahoo.fr http://www.ministeres.tn/html/ministeres/agriculture.html</p>
<p>OSS Djamel Latrech User Coordinator Regional Coordinator / Coordinator SASS Observatoire du Sahel et Sahara Boulevard de l'environnement BP 31 - 1080 Tunis Cedex - Tunisie Tel : + 216 71 96 10 28 Tel : Oss : +216 71 206 636 Mobile: + 216 97 193 780 Email: sass@oss.org.tn</p>	<p>ITC Maciek Lubczynski Water Resources Department ITC - International Institute for Geo-Information Science and Earth Observation Hengelosestraat 99. P.O.Box 6; 7500 AA Enschede; The Netherlands Tel: +31-53-4874277; Fax: +31534874336; e-mail: lubczynski@itc.nl http://www.itc.nl</p>